Study on Atmospheric and Terrestrial Water Circulation Processes Using Stable Water Isotopes

(水の安定同位体比情報を利用した大気と陸面の水循環過程の解明に関する研究)

WEI ZHONGWANG
魏　忠旺

Department of Natural Environmental studies
Graduate School of Frontier Sciences
The University of Tokyo
自然環境学専攻　新領域創成科学研究科　東京大学大学院

February 2016

© 2016 WEI ZHONGWANG. All rights reserved.

Abstract

We observed stable isotopes in precipitation and atmospheric water vapor over a humid subtropical rice paddy field in Tsukuba, Japan, from June 2013 to May 2014. We used observed isotope ratios, in combination with an isotope-enabled general circulation model (GCM; Isotopes-incorporated Global Spectral Model: $IsoGSM$) to improve our understanding of the impacts of moisture sources and transport on the variability of water vapor isotopes. The isotopic measurements of water vapor and precipitation suggested that vapor isotopes in the study area were controlled by not only air-rain isotopic exchange, but also other kinetic effects associated with land evapotranspiration and large scale atmospheric circulation at the seasonal time scale. The contribution of land evapotranspiration to local water vapor content (F_{ET}) was approximately 16.0±12.3% as an annual average, with a summer maximum of 20.5±12.9%. Our results show that large-scale atmospheric circulation is the primary control on the variability of near surface water vapor isotope. An $IsoGSM$ tagging simulation experiment demonstrated that the large temporal variation of surface water vapor isotopes can primarily be attributed to advection and mixing of moisture from different oceanic source regions.

By using high-frequency isotope measurements and continuous surface water measurements, we investigated the isotope ratios in soil-vegetation-atmosphere transfer and the physical mechanisms involved over a paddy field for a full growing season. The isotopic signals (δ) of evapotranspiration(ET) transpiration (T) and evaporation (E) were determined by the Keeling plot method, surface water isotopic measurements, and the Craig-Gordon model, respectively. The fraction of transpiration in evapotranspiration (T/ET) ranged from 0.2 to 1, with an almost continuous increase in the early growing season and a relatively constant value close to 1 later in the year. The result was supported by T/ET derived from simulated T and eddy correlation measured ET. The seasonal change in the transpiration fraction could be described quite well as a function of the leaf area index (LAI) ($T/ET = 0.67LAI^{0.25}$, $R^2 = 0.80$), implying that transpiration plays a dominant role in the soil-vegetation-atmosphere continuum during the growing season. The two end-member uncertainty analysis suggested that further improvement in the estimation of δ_T and δ_{ET} is necessary for partitioning evapotranspiration using the iso-

topic method. In the estimation of δ_{ET}, the assumptions underlying Keeling plot method were rarely met and the uncertainty was quite large. A high frequency of precise isotopic measurements in surface water was also necessary for δ_T estimation. Furthermore, special care must be taken concerning the kinetic fractionation parameter in the Craig and Gordon Equation for δ_E estimation under low-LAI conditions. The results demonstrated the robustness of using isotope measurements for partitioning evapotranspiration.

Recently isotopic method provides an unprecedented opportunity for ET partitioning across a variety of spatial and temporal scale which is unattainable by conventional technique. However, most of isotope-based studies show that T generally contributes more than 70% to the ET, while non-isotopic measurement generally leads to considerably smaller transpiration fractions. As a summary, quantitatively understanding of ET partitioning is somewhat arbitrary and remains the necessary of a theoretical and technical change, in both in-situ measurement and global scale. Considering the above tasks and background, we developed an ET partitioning algorithm, combining ET estimated by remote sensing, land surface models and LAI regression documented by 64 previous studies. The algorithm was used to understand spatial patterns and global average T/ET. Our global mean transpiration ratio (50%-60%) is smaller than the literature complication studies [*Wang et al.*, 2014; *Schlesinger and Jasechko*, 2014] but in good agreement with the value reported in GCMs (47%). On the other hand, it was significantly smaller than that reported in isotopic approaches [e.g., *Jasechko et al.*, 2013; *Good et al.*, 2015a]. Although further validation is required, our measured provided a new inspiration for partitioning global evapotranspiration and suggested vegetation plays a major role in driving the contribution of T/ET. Moreover, a further study about canopy interception is also required because canopy interception loss at various regions of the globe was few reported in the literature.

Acknowledgements

I would like to thank to my supervisor Prof. Kei Yoshimura for his considerable support throughout my PHD studies. He has provided me with a lot of help, support and encouragement. Thanks to his patience, kindness, encouragement and good advice, I can finish writting my PHD disertation. Thanks also to Prof. Taikan Oki and Prof Kazuo Oki, who have contributed with his expertise during seminar and lecture. Thanks to Prof Wang, Prof.Yamanaka, Prof. Zhongfang Liu, Prof. Chun-Ta Lai, Prof. Toshihiko Sugai and Prof. Ryoichi Imasu for their valuable suggestion and encouragement for my research.

Thanks are also extended to my friends and colleagues in Oki Lab and Yoshimura Lab, Kim-Sensei, Noda-san, Utsumi-san, Yano-san, Nishijima-san, Nitta-san, Satoh-san, Okazaki-san, Yoshikane-san, Nomoto-san, Fukubayashi-san, Kanazawa-san, Kakehashi-san, Cherry-san, Mehwish-san, Okaneya-san, Saya-san, Ronald-san, Hatono-san, Takahashi-san, Suzuki-san, Hamada-san, Yoshida-san, Fukuda-san, Makino-san, Watanabe-san and so on. I appreciate them a lot not only for their help on my research, but also for their kindness to make me feel welcome. Special thanks are given to Okazaki-san. I am so glad to know you and I will never forget your continuous quick, friendly and good help. In addition, I really appreciate the guidance from Dr. Eun-Chul Chang and Dr. Suryun Ham, who are so patient to give me help to settle the problem regarding modeling studies.

I am very grateful to researchers in National Institute for Agro-Environmental Sciences, Tsukuba, Ibaraki, Japan. Kim-san and Ono-san, thank you provided us abundant high quality data. Thanks to Masaharu Yokoi from Sanyo Trading Co., Ltd., Tokyo, Japan. With their help in field work and care in many practical matters such as instruments, measurements and data analysis. I would like to thank my Chinese friends, Xiaogang He, Yaping Liu, Pei Wang, who always lends me courage and we fighted together shoulder by shoulder. They make my daily life full of joy.

At last, thanks also to all my other friends who gave me unforgettable experience in my life. Thanks to my brother, without his help, I could not imagine how I can live through the last there years. At the same time, I would like to thank my parents. They gave me life, and spent countless love on me.

List of symbols Variables

CBL Convective Boundary Layer, m

CLM Community Land Model

$d - excess$ Deuterium excess , ‰

E Evaporation, mm day $^{-1}$

E_c Canopy interception, mm day $^{-1}$

E_s Soil evaporation, mm day $^{-1}$

ET Evapotranspiration,mm day $^{-1}$

F_{ET} Fraction of evapotranspiration to near surface water vapor content

F_v Vegetation Type %

$ISI - MIP1$ Inter-sectoral impacts model inter-comparison project 1

$IsoGSM$ Isotopes-incorporated Global Spectral Model

$GLEAM$ Global Land surface Evaporation: the Amster- dam Methodology

$GRACE$ NASA's Gravity Recovery and Climate Experiment

$GPCC$ Global Precipitation Climatology Centre

$GSWP - 2$ Global Soil Wetness Project 2

H Sensible heat flux, W m^{-2}

$IGBP$ International Geosphere-Biosphere Programme

JPL Jet Propulsion Laboratory

LAI Leaf area index, m^{-2} m^2

LE Latent heat flux, W m^{-2}

$MODIS$ Moderate Resolution Imaging Spectroradiometer

NSS isotopic non-steady state

P Precipitation amount

Q_v water vapor mixing ratio at 2-m

Q_{bg} background air vapor mixing ratio

R Runoff, mm day $^{-1}$

RH Relative humidity

S_i The evaporative stress and is computed combining observed vegetation water content and estimates of root-zone soil moisture from a multilayer soil module driven by observed precipitation and surface soil moisture.

SSA isotopic steady-state

$STEAM$ Simple Terrestrial Evaporation to Atmosphere Model

T Transpiration, mm day $^{-1}$

T_a Air temperature

T_d dew temperature

T/ET Fraction of transpiration to evapotranspiration

$TWSC$ Terrestrial Water Storage Changes

vt Vegetation type

ϵ_K The Kinetic fractionation factor

α_{eq} Temperature dependent equilibrium fractionation factor.

σ Std of isotopic ratios

β A constant to account for declines in transpiration when the canopy is wet.

δ Isotope composition of sample water relative to a standard, ‰

$\delta D_{v,e}$ δD of precipitation predicted water vapor, ‰

δD_v δD of water vapor, ‰

δD Stable isotope composition of hydrogen in water, ‰

$\delta^{18}O$ Stable isotope composition of oxygen in water, ‰

δ_E δ of soil evaporation flux, ‰

δ_{ET} δ of evapotranspiration flux, ‰

δ_T δ of transpiration flux, ‰

δ_{sw} δ of surface water, ‰

δ_v δ of water vapor, ‰

δ_P δ of precipitation, ‰

δ_{bg} δ of background air, ‰

Contents

Abstract **i**

Acknowledgements **iii**

1 Introduction **1**

1.1 Stable isotopes approach: theory and measurement 1

1.2 Variability of near-surface water vapor isotopes 3

1.3 Partitioning ET using stable isotopes 5

1.4 Global ET estimation and its partitioning 8

1.5 Objective and outline of this dissertation 11

2 Methods **16**

2.1 Site description 16

2.2 In-situ observation 17

2.2.1 Isotopic measurement system 18

2.2.2 Calibration protocol 19

2.2.3 δ_E, δ_T and δ_{ET} estimation 20

2.3 $IsoGSM$ simulation and water tagging experiments 23

2.3.1 $IsoGSM$ simulation 23

2.3.2 Water-tagging experiments using $IsoGSM$ 24

2.4 Global ET estimation and its partitioning 25

2.4.1 Global synthesis of LAI control on dry canopy ET partitioning . . 25

2.4.2 ET estimated from LSM, RS and $GRACE$ 26
2.4.3 Global ET partitioning 28

3 Understanding the variability of δ_v 42

3.1 Characteristics of observation and simulation 42
3.2 Effect of precipitation on the δD_v variability 44
3.3 Effect of local ET on the the δD_v variability 45
3.4 Remote controls on the δD_v variability 47

4 ET partitioning over a paddy field 67

4.1 Estimation of δ_{ET}, δ_T, and δ_E 67
4.2 ET partitioning and its environmental control 69
4.3 The error analysis 71
4.4 Comparison with other studies 75

5 Global ET partitioning 87

5.1 Global synthesis of LAI control on dry canopy ET partitioning 87
5.2 ET and E_c estimation from CLM, $GLEAM$ and $GRACE$ 89
5.3 Global ET partitioning 90
5.4 The uncertainties in our partitioning 90

6 Conclusions and Future Plan 105

Appendix 107

A Previous studies used in LAI regerssion estimation. 108

B Water tagging experiments for SON, DJF and MAM. 111

C ET partitioning based on Two layer method. 115

References 117

List of Tables

1.1 Previous studies of ET partitioning. 15

2.1 The dataset used in global T/ET estimation. 39

2.2 Data used in estimation of $GRACE$-inferred ET. 40

2.3 Land cover type codes and definitions and $IGBP$ and this study. 41

3.1 The linear correlation coefficient R and p-value (a: p-value < 0.001; b: $0.001 <$ p-value < 0.05 and none: p-value>0.05) of hourly isotope ratios (δD, $\delta^{18}O$, and $d-excess$) with observed weather variables (water vapor mixing ratio Q, Relative humidity RH, surface air temperature T_a) for all observed data in each month from June 2013 to May 2014. 64

3.2 Monthly mean values of observed δD, $\delta^{18}O$, and $d-excess$ for atmospheric water vapor, precipitation, and the vapor in Equilibrium with precipitation in Mase, Japan. Meteorological variables (Temperature T_a, Humidity RH, Precipitation amount P and water mixing ratio Q) are also listed. All isotope parameters were presented in ‰. 65

3.3 The contribution of evapotranspiration (F_{ET}) to that of the ABL water vapor estimated from monthly water vapor δD, background isotope ratio δ_{bg} and evapotranspiration isotope ratio δ_{ET}. Data from rainy days, data of latent heat $LE < 50$ W/m^2 and daily $F_{ET} < 0$ data were excluded. All isotope parameters presented in ‰. 66

5.1 Global systhesis of LAI control on ET partitioning. 102

5.2 Comparison of measured and simulated E_c/ET 103

5.3 T/ET estimated based on Equation 2.13 with different ET and E_c. 104

A.1 Previous studies used in LAI regerssion estimation. 109

A.2 Previous studies used in LAI regerssion estimation (continue). 110

List of Figures

1.1 Objective and outline of this dissertation. 14

2.1 (a). Location of the study site in Mase, Japan (closed blue circle). (b). A photo about measurement site. (c). A photo about water vapor isotopic measurement system (Picarro L2120-i). (d) A photo about Automatic rain sampler (Eigenbrodt NSA181). 30

2.2 Linearly interpolated measurements of leaf area index (LAI, blue filled circle) and Vegetation height (z_v, red filled square) throughout the whole growing season in 2013. LAI and z_v was measured by the National Institute for Agro−Environmental Sciences ($NIAES$). Field management of the study site in 2013 is also summarized. 31

2.3 The measurement content schematic in this study. 32

2.4 Comparison of dew temperature (T_d) and air temperature (T_a). 33

2.5 Calibration of water vapor and precipitation data (a). An example of correction procedure [*van Geldern and Barth*, 2012] to reduce memory effect in precipitation isotopic analysis. All the injections of a sample can be used after correction and the number of rejections per unknown can be reduced to 4. Four injections of each sample were averaged and normalized to the $VSMOW/SLAP$ scale by using a two-point linear calibration. (b). Evaluation of the dependency of the measured isotopic value on water vapor concentration by injecting different amounts of standard water into the vaporizer. Three tests have been done in field conditions, during 2013/09/01−2013/09/02 ($Q = 15200 \pm 200$ ppmv, $\delta D = 183.1 \pm 1.1$‰, Total number, $n = 1516$), 2014/09/16−2014/09/17 ($Q = 6500 \pm 700$ ppmv, $\delta D = 184.3 \pm 3.3$‰, $n = 2109$) and 2015/03/31−2015/04/01 ($Q = 3700 \pm 100$ ppmv, $\delta D = 183.2 \pm 3.2$‰, $n = 1136$). 34

2.6 Comparison of dew temperature (T_d) and air temperature (T_a). 35

2.7 An example of δ_{ET} estimation using Keeling plot. 36

2.8 Mean precipitation in mm/month (2004−2010), 1.0 degree, obtained from *GPCC* full data product version 7. 37

2.9 *GRDC* composite annual runoff (mm/year). 38

3.1 Time series of daily observation in precipitation amount (P), vapor mixing ratios (Q), water vapor and precipitation $\delta^{18}O$, δD and $d-excess$ (blue line for water vapor, green square for precipitation). The red lines represent the simulated Q and δ by $IsoGSM$. 51

3.2 Monthly averaged relative humidity (RH, dash), Temperature (T_a, solid), isotope ratio δD, $d - excess$ of water vapor (diamond)and precipitation (circle). Water vapor isotope $\delta D_{v,e}$ and $d_{v,e} - excess$ predicted from precipitation (square) are also plotted. 52

3.3 Diurnal averaged water vapor mixing ratio, isotope ratio $\delta^{18}O$, δD, $d - excess$ of water vapor. 53

3.4 Comparison between the observed water vapor δD_v and precipitation predicted $\delta D_{v,e}$. Each point represents a rainy day. 54
3.5 Day time CBL height simulated using $IsoGSM$. 55
3.6 Daily variation of isotope ratios of evapotranspiration (green filled square, excluded rainy days), water vapor (blue unfilled circle, excluded rainy days) and background derived from $IsoGSM$ simulation. 56
3.7 $IsoGSM$ simulated seasonal mean latent heat fluxes. Black dot shows the study site. 57
3.8 The atmospheric column precipitable water contributed from tagged boxes in JJA. Source regions for tagging experiments of water vapor tagged within 10×10 degree boxes (contour): a, 25°N−35°N, 120°E−130°E; b,35°N−45°N, 120°E−130°E; c, 25°N−35°N, 130°E−140°E; d, 35°N−45°N, 130°E−140°E; e, 25°N−35°N, 140°E−150°E; f, 35°N−45°N, 140°E−150°E. 58
3.9 The contribution fraction from tagged boxes in JJA, SON, DJF and MAM. 59
3.10 850 hpa isotope ratios documented based on the wind direction (0° to 90°, Area f; 90° to 180°, Area e; 180° to 270°, Area a+c; 270° to 360°, Area b+d). 60
3.11 The variation of hourly water vapor δD as a function of q for JJA, SON, DJF and MAM. Rayleigh distillation curves representing a pseudoadiabatic process based on oceanic temperatures with an initial δD values of -80‰ (approximate value of vapor in equilibrium with ocean, shown as blue dash line) are shown as green solid line (15 °C) and blue solid line (25 °C). The red line called Evaporation line represents a special case where the source water is the infinite reservoir of vapor that is in thermodynamic equilibrium (i.e., saturated) with the ocean surface. 61
3.12 $IsoGSM$ simulated the wind field and water vapor δD at 850 hpa. 62
3.13 Relationship between daily $d - excess$ and RH at SST from the source regions (10 × 10 degree). Different symbols present water vapor from different source shown in Figure 3.8. 63

4.1 Hourly variation in the isotope ratios of ET from June to August 2013 and May to June 2014. Blue circles (filled, 2013; un-filled, 2014) indicate daytime data (8:00−17:00), and green squares (filled, 2013; un-filled, 2014). indicate nighttime data. 78

4.2 Observed δD in surface water from June to August 2013 (blue line) and May to June 2014 (red line). Filled squares with error bars indicate the spatial average values and their standard deviations. Unfilled squares represent the measurement of only one point in 2014. Vertical bars denote daily precipitation amount from June to August 2013 (green bar) and May to June 2014 (yellow bar). 79

4.3 Comparison of the ensemble mean diurnal variation in the evapotranspiration δD signal during the growing season (July and August 2013, blue squares) and non-growing season (September and October 2013, red circles). Vertical bars denote the standard deviation for each hour. Green dash line indicates the mean irrigation water δD (-47.46‰). 80

4.4 Daily averaged variation in isotope ratios of ET (blue circles), T (red squares), and E (pink diamonds). Two points of δ_E, which were less than -300‰, are not shown in this figure. 81

4.5 Transpiration faction determined by the isotope-based method and eddy correlation based method. Blue circles represent isotope-based daily averaged T/ET. Green triangles represent the simulated T and measured ET based daily averaged T/ET. Vertical bars denote the standard deviation for each day. The red line with filled squares represents the isotope based monthly average T/ET excluding unreliable values ($T/ET > 1.2$ or $T/ET <$ -0.2). Pink line with filled squares represents the simulated T and measured ET based monthly averaged T/ET. 82

4.6 The fractional contribution to the partitioning uncertainty of uncertainty δ_{ET} (blue circle) and end-member uncertainty (δ_T (green square) and δ_E (red diamond)) as a function of the transpired fraction of evapotranspiration, T/ET. The fractional contribution was calculated from Equation 2.8. Data where $T/ET > 1.2$ or $T/ET <$ -0.2, with only one point measurement of δ_T and with less than 3 hours of highly accurate δ_{ET} estimation in each day excluded. 83

4.7 Relationship between the 0.5−bin averaged LAI and the daily averaged transpiration fraction (T/ET). $T/ET > 1.2$ or $T/ET <$ -0.2 data are excluded. Two regression lines (green, agricultural system; blue, natural system) derived from a global observation data set *Wang et al.* [2014] are also plotted. 84

4.8 Comparison of the ensemble mean diurnal variation in uncertainty of δ_{ET} (a) and standard deviation of water vapor of mixing ratio (b) during the growing season (July and August 2013, blue circle) and non-growing season (September and October 2013, red square). Vertical bars denote the standard deviation for each hour. 85

4.9 Impact of using different parameters for δ_E estimation in the T/ET estimation. Data with $T/ET > 1$ or $T/ET < 0$ are excluded. 86

5.1 Global systhesis of LAI control on ET partitioning. 94

5.2 Comparison of ET derived from $GLEAM$ (a), CLM (b) and $GRACE$ (c). 95

5.3 Comparison of canopy interception derived from $GLEAM$ (a) and CLM (b). 96

5.4 LAI control on ET partitioning based on different methods. 97

5.5 Global T/ET derived from LAI regression: (a) $GRACE$ derived ET with GLEAM E_c (b) $GRACE$ derived ET with CLM E_c). 98

5.6 Global T/ET estimated from land surface models, isotopes, satellites, site measurements and LAI regression. 99

5.7 Comparison of simulated E_c/ET and measured E_c/ET. The measured data was obtained from *Mitchell et al.* [2009], *Mitchell et al.* [2012], *Lee et al.* [2010], *Oishi et al.* [2008] and *Jian et al.* [2015] 100

5.8 Hourly averaged latent heat observed at night time. 101

B.1 The atmospheric column precipitable water contributed from tagged boxes in SON. Source regions for tagging experiments of water vapor tagged within 10×10 degree boxes (contour): a, 25°N−35°N, 120°E−130°E; b,35°N−45°N, 120°E−130°E; c, 25°N−35°N, 130°E−140°E; d, 35°N−45°N, 130°E−140°E; e, 25°N−35°N, 140°E−150°E; f, 35°N−45°N, 140°E−150°E. 112

B.2 The atmospheric column precipitable water contributed from tagged boxes in DJF. Source regions for tagging experiments of water vapor tagged within 10×10 degree boxes (contour): a, 25°N−35°N, 120°E−130°E; b,35°N−45°N, 120°E−130°E; c, 25°N−35°N, 130°E−140°E; d, 35°N−45°N, 130°E−140°E; e, 25°N−35°N, 140°E−150°E; f, 35°N−45°N, 140°E−150°E. 113

B.3 The atmospheric column precipitable water contributed from tagged boxes in MAM. Source regions for tagging experiments of water vapor tagged within 10×10 degree boxes (contour): a, 25°N−35°N, 120°E−130°E; b,35°N−45°N, 120°E−130°E; c, 25°N−35°N, 130°E−140°E; d, 35°N−45°N, 130°E−140°E; e, 25°N−35°N, 140°E−150°E; f, 35°N−45°N, 140°E−150°E. 114

Chapter 1

Introduction

1.1 Stable isotopes approach: theory and measurement

The stable isotopologues $^{2}H^{1}H^{16}O$ and $^{1}H_{2}{}^{18}O$ are powerful tools to trace hydrological processes. Compare to the most abundant water $^{1}H_{2}{}^{16}O$, their slightly different masses affect their thermodynamic (e.g., differences in latent heat as a result of different hydrogen bonds between molecules) and kinetic properties (e.g., difference in the molecular diffusivity of water vapor when water evaporates into unsaturated vapor or when condensation occurs from supersaturated vapor)[*Yoshimura*, 2015; *Rothfuss et al.*, 2013; *Jouzel and Merlivat*, 1984]. As a result, differences in the rates of evaporation and condensation between heavy and light isotopologues of water is able to create spatial and temporal variability in the isotopic composition of water in the air and also on the land surface such as lakes, rivers, soils, and plants [*Welp et al.*, 2012]. These variability can help to address the origin and movement of atmospheric water [*Craig*, 1961; *Dansgaard*, 1964], partition water flux in terrestrial water cycle, reconstruct the past climate [*Liu et al.*, 2014] and understand groundwater dynamic [*Liu and Yamanaka*, 2012].

Since *Dansgaard* [1964], global isotopic datasets (such as Global Network of Isotopes in Precipitation ($GNIP$)) developed over the past 60 years have enabled continental-scale

assessments of transpiration/evaporation ratios, oceanic water vapor source tracing and the recycling of rainfall back into the atmosphere [*Evaristo et al.*, 2015]. Recently, Global Network of Isotopes in Rivers ($GNIR$) database contained around 21,000 stable water isotope records from 750 sites in 35 countries was developed for better understanding of the resilience of our major global river systems to environmental and human perturbations [*Halder et al.*, 2015]. However, few water vapor study was conducted because trandition-ally the water vapor have to be collected using cryogenic method, which is less practical and less accurate [*Yoshimura*, 2015]. Before ten years ago, mass spectrometry is often used for measuring the composition of stable water isotopes such as ice core and precipitation, or isotopes storage in speleothems, coral skeletons and tree cellulose. Recent development in high frequency laser spectrometer in-situ technology and remote sensing retrieval has made it possible to measure the vapor isotopic ratios at high temporal resolution and on a continuous basis [e.g., *Lee et al.*, 2006; *Frankenberg et al.*, 2013]. Such measurements offer unique opportunities to examine the temporal variation in water vapor isotopic ratios and gains insights into mechanisms involved. For example, it is possible to use in-situ stable isotope measurement to partition long-term evapotranspiration [*Wei et al.*, 2014, 2015]. It is also used to study vertical mixing process [*Benetti et al.*, 2014; *Wei et al.*, 2016] or rain-precipitation interaction [*Laskar et al.*, 2014]. Not long ago, the in-situ leaf water and continuous in-situ liquid water measurement were also developed (Picarro L2140-i and L2130-i Analyzer). These provide powerful tools towards a detailed quantitative understanding of air-precipitation exchange processes, ground water-underground water interaction and vegetation activity dynamic. Moreover, new remote sensing techniques allows us to measure water vapor isotope in global scale. For example, Using the Tropospheric Emission Spectrometer (TES), *Worden et al.* [2007] investigated evaporation and continental convection in the tropical water cycle. After that, several improved sensors (such as Scanning Imaging Absorption Spectrometer for Atmospheric Chartography ($SCIAMACHY$) [*Frankenberg et al.*, 2009], Greenhouse gases Observing SATellite ($GOSAT$) [*Frankenberg et al.*, 2013; *Risi et al.*, 2013] and Infrared Atmospheric Sounding

Interferometer ($IASI$) [*Lacour et al.*, 2015]) were also used for to investigate aspects of the atmospheric hydrological cycle that are not well constrained by observations of precipitation or atmospheric vapor content. Stable isotope method has been become one of the most useful tools for quantifying water-cycle components and the linkages between plant ecology, physical hydrological and atmospheric dynamic.

1.2 Variability of near-surface water vapor isotopes

Water vapor isotopic measurement have been used in many studies to trace the origin and movement of atmospheric water [e.g., *Craig*, 1961; *Dansgaard*, 1964; *Strong et al.*, 2007; *Gat*, 1996; *Samuels-Crow et al.*, 2014a,b; *Lai and Ehleringer*, 2011; *Steen-Larsen et al.*, 2013, 2014a; *Tremoy et al.*, 2012, 2014; *Worden et al.*, 2007]. Most of these studies have focused on condensed phases (i.e., precipitation), with fewer studies considering the vapor phase. Despite a wide range of applications, water isotope in the condensed phase is too coarse to determine the dynamical and microphysical processes involved in atmospheric moisture evolution. Water vapor observation is not limited to rainy days, but can be done continuously over synoptic events and seasons [*Angert et al.*, 2008]. Water vapor isotopic composition is also a useful tool to investigate land vegetation activity and to understand vegetation-atmosphere exchange processes [e.g., *Good et al.*, 2014; *Wei et al.*, 2015].

Recently, water vapor isotopic measurements were shown to be useful for constraining state variable simulations in general circulation models (GCMs) [e.g., *Bonne et al.*, 2014; *Steen-Larsen et al.*, 2014b]. *Yoshimura et al.* [2014] conducted the first ideal observation system simulation experiment, through the combination of a local transform ensemble Kalman filter and an isotope-enabled GCM simulation. The authors showed that by incorporating a synthetic global dataset of Satellite-based water vapor isotope measurements and near surface water vapor isotopic measurements, model simulations were significantly improved in both the vapor isotopic and meteorological fields. Satellite-based water vapor isotope measurements have been used for validating GCMs and partitioning the global

hydrologic water flux [e.g., *Frankenberg et al.*, 2009; *Good et al.*, 2015b,a]. However, their inherent uncertainties are likely too large to quantify sub-grid scale hydrological processes.

Previous studies have identified the factors that control the isotopic signatures of water vapor over oceans [e.g., *Benetti et al.*, 2014, 2015; *Steen-Larsen et al.*, 2014a, 2015], ice sheets [*Steen-Larsen et al.*, 2013], plateaus [e.g., *Galewsky and Samuels-Crow*, 2014a,b; *Samuels-Crow et al.*, 2014a,b], and land surfaces under various climatic conditions [e.g., *Welp et al.*, 2012; *Berkelhammer et al.*, 2013; *Tremoy et al.*, 2012, 2014; *Lee et al.*, 2006; *Noone et al.*, 2013; *Wen et al.*, 2010; *Huang and Wen*, 2014; *Laskar et al.*, 2014]. Common findings of these studies are large variability of the oberved atmospheric water vapor isotopic composition from daily to seasonal time scales, irrespective of geographical conditions. Such variation is related to specific hydrological processes. For example, during precipitation events, water vapor isotopes are significantly affected by air-precipitation isotopic exchange [e.g., *Huang and Wen*, 2014; *Lawrence et al.*, 2004; *Wen et al.*, 2010; *Tremoy et al.*, 2014]. Thus, some studies have suggested that it is possible to estimate the monthly water vapor isotope ratio from the precipitation isotope ratio [e.g., *Jacob and Sonntag*, 1991; *Lee et al.*, 2006; *Wen et al.*, 2010]. This method is fascinating because information regarding the liquid phase (such as surface water and precipitation isotope ratios) is readily available [*Lee et al.*, 2006]. A number of studies have concluded that land evapotranspiration play a important role on the isotopic variability of near surface water vapor in well-vegetated areas [e.g., *Welp et al.*, 2008; *Noone et al.*, 2013] or the sea surface [e.g., *Benetti et al.*, 2014].

Some studies have also confrimed the significance of other factors, such as the advection of large-scale moisture sources. *Strong et al.* [2007] used water vapor isotopes to diagnose moisture paths transported from three different oceans. They reported a low deuterium isotope ratio when moisture advection originated from the Gulf of Mexico (warmer than the Pacific Ocean) and a high ratio if water vapor is originated from the Pacific Ocean. By investigating the relationship between meteorological variables and water vapor isotope ratios, *Lee et al.* [2006], *Wen et al.* [2010] and *Huang and Wen*

[2014] suggested the dominant effect of Rayleigh distillation during large scale moisture transport.

The use of high frequency water vapor isotopes has a great potential to improve our understanding of the mechanisms that control stable isotope variability in hydrological processes. Despite these advances, there are several problems when using high frequency water vapor isotope measurements: 1) continuous measurements that cover multiple seasons are scarce [e.g., *Farlin et al.*, 2013; *Noone et al.*, 2013]; 2) very few study has yet been conducted at sites with changing vegetation cover over multiple seasons [*Bastrikov et al.*, 2014]; and 3) it is difficult to understand how large scale moisture transport controls the isotopic variability of water vapor observed at a single tower. Studies investigating the exact cause(s) of what controls long-term isotopic variability are rare.

1.3 Partitioning ET using stable isotopes

To elucidate eco-hydrological processes and their underlying mechanisms, detailed knowledge of the relative contribution of different sources of water, such as soil evaporation and vegetation transpiration over land surfaces, is required. Although the total contribution of the land surface ET has been widely measured (e.g., $FLUXNET$), its partitioning into plant transpiration (T) and surface evaporation (E) is still subject to debate [e.g., *Coenders-Gerrits et al.*, 2014; *Jasechko et al.*, 2013; *Schlaepfer et al.*, 2014; *Schlesinger and Jasechko*, 2014; *Sutanto et al.*, 2014]. A quantitative relationship between ET partitioning and vegetation cover index (e.g., LAI) for different systems (i.e., agricultural versus natural systems) in global scale was established by *Wang et al.* [2014]. However, large variations in the fraction of transpiration in evapotranspiration (T/ET) occurred across all LAI ranges with wider variability at lower LAI. It is still not clear to what extent that T/ET is controlled by vegetation and what are the additional factors that could further explain the T/ET variations at a global scale. The partitioning of ecosystem ET and its controlling factors are therefore crucial to better understand hydrological

processes at the landscape scale.

Various methods have been developed for *ET* partitioning which have been well documented in several review studies [e.g., *Kool et al.*, 2014; *Sutanto et al.*, 2014]. The most widely used among these methods is the combination of the eddy correlation method to measure *ET* with other measurements (e.g., lysimeters [*Agam et al.*, 2012], sapflow [*Williams et al.*, 2004], chambers [*Daikoku et al.*, 2008], or model simulations based on aerodynamic and biophysiological theories (e.g., the Penman Equation [*Penman*, 1948]). A complementary method of partitioning *ET* using isotopic biogeochemistry has been successfully applied in different vegetation types [e.g., *Dubbert et al.*, 2013, 2014a; *Good et al.*, 2014; *Moreira et al.*, 1997; *Rothfuss et al.*, 2010; *Wang and Yakir*, 2000; *Wang et al.*, 2010, 2013; *Williams et al.*, 2004; *Yepez et al.*, 2003] and at the global scale [e.g., *Coenders-Gerrits et al.*, 2014; *Jasechko et al.*, 2013; *Schlaepfer et al.*, 2014; *Schlesinger and Jasechko*, 2014]. To apply this method, detailed knowledge of isotopes in the different phases of water in soil, vegetation, and the atmosphere is required. Historically, because of the practical experimental difficulties in collecting and quantifying ground-based water vapor isotope samples, very few studies have reported successful implementation of the isotopic methodology [*Scanlon and Kustas*, 2012]. Recent development in high-frequency laser spectrometer in-situ technology has made it possible to measure water vapor isotopic ratios at a high temporal resolution and on a continuous basis [*Lee et al.*, 2006]. Such measurements provide a unique opportunity to examine temporal variation in water vapor isotopic ratios and to determine the mechanisms involved [*Lee et al.*, 2006]. The number of isotope-based studies therefore has been increasing dramatically in recent years [e.g., *Rothfuss et al.*, 2010; *Wang et al.*, 2012, 2013; *Dubbert et al.*, 2013, 2014b,a; *Good et al.*, 2014; *Hu et al.*, 2014].

Partitioning *ET* is specifically important for high water consuming agricultural products such as rice, which is widespread in the monsoon Asia. Although some other model-based studies have been conducted [e.g., *Kondo and Watanabe*, 1992; *Maruyama and Kuwagata*, 2010], no direct long term experiment has been reported in a rice paddy field

yet, mainly because of the experimental difficulties in the measurement of sapflow or leaf transpiration. The isotopic method offers an easy way to investigate the fraction of transpiration in evapotranspiration and its controlling factors in rice paddy fields. The long-term water vapor isotope-based partition technique has been used in a series of studies as mentioned above, however, no study has been performed over a wetland such as rice paddy. To the best of our knowledge, this study is the first report of long-term evapotranspiration partitioning using high-frequency continuous water vapor isotope observations over a paddy field. Due to significantly different surface condition (flooded) from that of other studies, the isotope characteristic of each composition in rice paddy field ET partitioning is not clear.

Although it has been addressed by many studies [*Braud et al.*, 2005, 2009a,b; *Dubbert et al.*, 2013; *Good et al.*, 2012; *Rothfuss et al.*, 2010, 2012], the uncertainties of the isotope-based method is still not well known. At the global scale, the isotope-based method shows a higher T/ET than the hydrometric method [*Sutanto et al.*, 2014]. To partition ET using the isotopic method, the isotopic signals of ET, T, and E must be quantified first. However, estimation of these three terms has a degree of uncertainty [*Good et al.*, 2012; *Hu et al.*, 2014]. The isotopic composition of ET (δ_{ET}) is traditionally measured by a Keeling plot approach [*Keeling*, 1958], underlying which the assumptions used to calculate δ_{ET}, as described in sect. 2.2.3, are rarely met perfectly in nature. On time scales from hours to days, much of the variation in the levels of water vapor isotopes δ_v is caused by the advection of air masses in varying stages of rainout and has little to do with ET. Therefore, the intercept parameter in a Keeling plot depends on which part of the weather cycle is measured and not on ET [*Lee et al.*, 2006]. Usually, δ_T is assumed to be equal to that of root uptake, maintaining a condition referred to as the isotopic steady-state assumption (SSA) [e.g., *Flanagan et al.*, 1991; *Yakir and Sternberg*, 2000]. However, many previous studies showed that the steady state is approached only at midday [e.g., *Lai et al.*, 2006; *Lee et al.*, 2007; *Peters and Yakir*, 2010], mainly because of the non-steady state (NSS) induced by changes in humidity and leaf energy balance [e.g.,

Farquhar and Cernusak, 2005; *Lai et al.*, 2006]. Furthermore, the isotopic composition of soil evaporation (surface water in our case) is commonly estimated from the Craig-Gordon model [*Craig and Gordon*, 1965]. However,the kinetic effect in the model depends on the relative roles of molecular and turbulent diffusion [e.g., *Dubbert et al.*, 2013; *Cappa et al.*, 2003; *Craig and Gordon*, 1965; *Gat*, 1996; *Kim and Lee*, 2011]. Recently, the methods coupling the laser spectrometer and the gas-exchange chamber have been used for directly estimating these three isotopic components [e.g., *Dubbert et al.*, 2013, 2014b,a; *Good et al.*, 2014; *Rothfuss et al.*, 2013; *Wang et al.*, 2012, 2013]. However, well-trained operators are needed and the installment and maintenance of the chamber are difficult.

1.4 Global ET estimation and its partitioning

Quantifying the global terrestrial water budget and energy cycles is essential for improving our understanding of the availability of water resources, the potential for hydrologic extremes, and the interactions of the land surface with the atmosphere and climate, and thus improving our predictions of large scale weather and climate, helping us make a robust water resource managements, estimating the risk of floods and droughts, and understanding of the land-air water exchange [e.g., *Sheffield et al.*, 2009; *Sahoo et al.*, 2011]. Therefore, it becomes one of main object of recent and ongoing projects such as the Coupled Model Intercomparison Project ($CMIP$), Global Energy and Water Experiment ($GEWEX$), Moderate Resolution Imaging Spectroradiometer project ($MODIS$), Global Earth Observing System of Systems ($GEOSS$). The terrestrial water budget can be defined as the balance between the change in water storage and the difference between the incoming water fluxes of precipitation and outgoing fluxes of evapotranspiration and discharge at the Earth's surface [*Sahoo et al.*, 2011]. Among these components, land evapotranspiration is the second largest component (after precipitation) of the terrestrial water flux and returns more than 60% of precipitation at global scale [*Mu et al.*, 2011]. ET uses up more than half of the total solar energy absorbed by the land surface

[*Jasechko et al.*, 2013]. Especially, ET typically accounts for over 90% of water losses in semi-arid and arid areas [*Zhang et al.*, 2001]. Accurate evapotranspiration estimates therefore are critical for understanding the mechanism of water cycling and evaluating the impacts of climate change, providing an important linkage between the land surface and the atmosphere.

To quantify global land surface evapotranspiration, many datasets including remote sensing-based estimations, reanalysis, land surface model driven with observations-based forcing [*Miralles et al.*, 2011a,b], vegetation coupled land surface model ([*Lawrence et al.*, 2011]), water balance based estimation [*Oki and Kanae*, 2006], have been derived in recent years. Although having being calibrated by local scale evapotranspiration measurements such as $FLUXNET$ eddy correlation dataset (`http://fluxnet.ornl.gov`), the analyzed reference datasets displayed large uncertainty in spatial and temperal variability [*Mueller et al.*, 2011, 2013]. These datasets are somewhat arbitrary, because they are all based on some degree of modeling assumption but not the direct measurement. Although some datasets showed similar results, they may share common biases related to common calibration or forcing dataset, and/or common model assumption. These leave a open question about whether it could be verified by independent methods or experiments.

It is more important that the understanding of mechanism of T/ET has been a fundamental challenge since more over 70 years ago. The contribution of T to ET is a prerequisite for understanding changes in carbon assimilation and water cycling in a changing environment. On local scale, evapotranspiration partitioning can be achieved by a combination of in-situ measurements, such as eddy covariance systems, Bowen-ratio systems, weighing lysistem, sap flow meters, leaf conductance upscaling, chamber measurement and isotopic measurements. On global scale, dozens of datasets including satellite-based estimations, reanalysis, land surface model driven by observations-based forcing, upscaling of point observation and water balance based estimation can be used for quantifying the contribution of each component in evapotranspiration (Table 1.1). For example, by combining a wide range of remotely-sensed observations, *Miralles et al.*

[2011b] found 80% annual land evapotranspiration corresponds to transpiration. Recently, isotope approach has been used for partitioning ET in both global and local scale. Based on isotopic mass and water balance, some quantities difficult to be measured such as transpiration can be easily obtained. Basing on isotopic analysis of a global data set of large lakes and rivers, *Jasechko et al.* [2013] used the lake isotopic information to show that transpiration represents 80 to 90% of the terrestrial evapotranspiration. *Good et al.* [2015b] suggested the transpired fraction of evapotranspiration is estimated a mean of 64% based on satellite isotopic measurements, which is much lower than previous studies. Although these results suggested that plant transpiration is a majority of terrestrial water fluxes, the uncertainties were significant. Potential uncertainties derives from:

1. The concept of total evapotranspiration sometimes is confusing. In general, the total evapotranspiration is the combination of soil evaporation (E_s), canopy transpiration (T) and canopy interception evaporation (E_c). However, due to measurement difficulty, E_c was rarely measured in field based partitioning studies. Thus in a lot of field studies, the total evapotranspiration was the combination of E_s and T. On the other hand, except very few study (e.g. *Yang et al.* [2015]), E_c is generally included in global or regional studies. Due to lack of observation in ET partitioning studies, E_c remains large uncertainty in global simulation.

2. Quantification of contribution of transpiration in large scale have long been associated with large uncertainties due to no reliable, benchmarking or good-quality forcing data sets for the evaluating the various products. The local scale ET partitioning techniques remain difficult to be implemented at large scale (such as regional or continental scale). Some studies directly compared several site measurement results with global simulation [*Wang et al.*, 2014; *Schlesinger and Jasechko*, 2014]. However, field based observation is still rare and only for point scale (also see Table 1.1). Global coverage by such point measurements is not feasible and the representativeness of such local-scale observation remains challenging. *Wang et al.* [2014] reviewed the published studies (48 individual publications) that measured at least

two of the three components (E, T, and ET) and LAI simultaneously in an attempt to establish a quantitative relationship between ET partitioning and LAI and extent the in-situ observation to global scale. However, the relationship between T/ET and LAI was not well constrained in his study.

3. The different methods generally yield different results. Isotopic method provides an unprecedented opportunity for ET partitioning across a variety of spatial and temporal scale which is unattainable by conventional technique. However, as cautioned by several studies, isotope-based T/ET partitioning studies show that T generally contributes higher than 70% to the ET. On the other hand, non-isotopic measurement generally leads to considerably smaller transpiration fractions. Thus they argued that the isotopic measurement may overestimate the contribution of T. Moreover, global isotopic partitioning is sensitive to bulk flux estimates (such as precipitation and interception amount).

As a summary, quantitative understanding of ET and its partitioning are somewhat arbitrary and remains the necessary of a theoretical and technical change, in both in-situ measurement and global scale.

1.5 Objective and outline of this dissertation

The research presented in this dissertation focuses on the development and application of a stable isotope method to investigate the key factors affecting the water cycling including raindrops-air isotopic interaction, land-atmosphere water exchange and large scale moisture circulation. Specifically, based on our observation, we develop a new approach to quantitatively understanding of ET and its partitioning in global scale. The dissertation is organized into papers destined for publication in peer-reviewed journals and paper in preparation [*Wei et al.*, 2014, 2015, 2016; *Wei and Yoshimura*, 2016]. The flow chart of this study is presented in Figure 1.1. The introduction and methods are presented in Chapter 1 and 2. Each chapter from 3-5 within the main body is organized to investigate

a specific objective as:

1. In Chapter 3, we conduct a long-term water vapor isotopic study that uses in-situ isotopes and meteorological measurements along with an isotope-enabled GCM, to explore the impact of oceanic water sources on water vapor isotopic variability from daily to seasonal time scales over a rice paddy field in Tsukuba, Japan. We use isotopic information to partition water vapor content into contributions from local and remote-source components. Tagging experiments using the Isotopes-incorporated Global Spectral Model ($IsoGSM$) are conducted to understand the role of large scale moisture transport in the observed isotopic variability.

2. In Chapter 4, we use high-frequency water vapor isotope measurements and surface water measurements to investigate isotopic variation in soil-vegetation-atmosphere transfer and to determine the physical mechanisms involved in a paddy field throughout a full growing season, which is the first observation-based long term ET partitioning study over wetland surface. The main objectives are: 1) to identify the temporal characteristics of isotopic variation in soil, vegetation and evapotranspiration over the paddy field; 2) to partition evapotranspiration into evaporation and transpiration and to investigate its relation with the vegetation growth; and 3) to explore the potential uncertainties in δ_{ET}, δ_T, δ_E and their impact on ET partitioning. We examine the capability of the Keeling plot method to estimate the isotopic signals of the ET flux and the steady state assumption for transpiration. We also estimate T/ET and compare it to water flux based partitioning results.

3. In Chapter 5, by combining our isotopic T/ET observation and the published observation based T/ET studies (64 individual publications), we investigated global synthesis of LAI control on ET partitioning. T/ET is estimated as different functions of LAI with different vegetation types. We estimated the ET from remote sensing ($GLEAM$), land surface model ($CLM4.5SP$) and water balance approach based on $GRACE$ satellite. We develop a new approach to quantitative estimation

of T in global scale and further compare the global T/ET results with previous studies.

The conclusion and outlook in the papers are appended to this dissertation (Chapter 6) as a summary of the methods we used, the most significant results, the limitation and its future orientation in each papers.

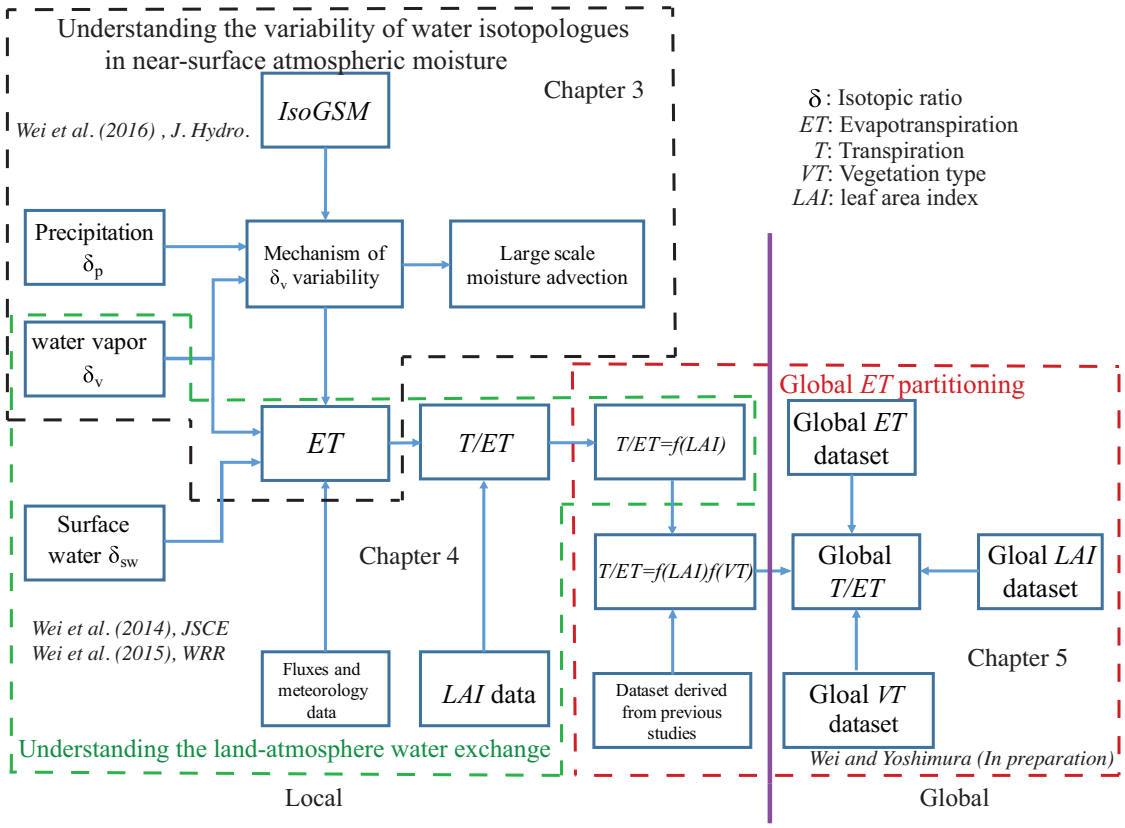

Figure 1.1: Objective and outline of this dissertation.

Table 1.1: Previous studies of ET partitioning.

Methods	E_c/ET	T/ET	$T/(ET-E_c)$	Scale	Source
Land surface models					
$GSWP-2$	16%	48%	57%	Global	*Dirmeyer et al.* [2006]
$ISI-MIP1$	27%	36%	49%	Global	Calculated from ISI-MIP1 models
$STEAM$	21%	59%	74%	Global	*Wang-Erlandsson et al.* [2014]
$IsoMatsiro$	36%	31%	49%	Global	*Yoshimura et al.* [2006]
$LCM3$	17%	41%	49%	Global	*Lawrence et al.* [2007]
$LCM3.5$	18%	43%	52%	Global	*Lawrence et al.* [2011]
$LCM4CNb$	21%	56%	70%	Global	*Lawrence et al.* [2011]
$LCM4SP$	20%	48%	60%	Global	*Lawrence et al.* [2011]
$LCM4CNEc$	22%	56%	71%	Global	*Lawrence et al.* [2011]
Isotopes					
Lakes isotope	10%d	85%	94%	Catchment	*Jasechko et al.* [2013]
Lakes isotope	29%e	67%	94%	Catchment	*Coenders-Gerrits et al.* [2014]
Global isotope budget	27%e	64%	88%	Global	*Good et al.* [2015b]
Satellite					
$GLEAM$	11%	80%	89%	Global	*Miralles et al.* [2011b]
Site measurements					
Isotope+hydrometric+model		61%		Site averaged	*Schlesinger and Jasechko* [2014]
Isotope+hydrometric		60%		Site averaged	*Wang et al.* [2014]
Other					
LAI regression		55%	70%	Global	This study

Chapter 2

Methods

2.1 Site description

The study site (36° 03' 14.3" N, 140° 01' 36.9"E, a.s.l. 12 m) was located in a rectangular 100 m×50 m cultivated plot near the center of a 150-ha rice paddy field in Tsukuba (Figure 2.1). The location of the measuring instrument provided a sufficient fetch of uniform land cover for flux and isotope measurements. Cultivation activity influenced the land cover in different seasons. The field was sparsely covered by weeds in spring (March-April), and by a canopy of rice seedlings from May until harvesting at the end of August. The field was flooded during the growing season and allowed to drain in the rest of the year. The maximum canopy height was about 1.1 m and the maximum leaf area index was 6.2±1.4. The site has participated in AsiaFlux activities since 1999. Detailed information regarding meteorological and flux measurements can be found on the AsiaFlux website (`http://asiaflux.net/index.php?page_id=83`).

During our study period, irrigation started on April 23, 2013 and April 24, 2014. Rice was sown on May 2, in both 2013 and 2014, at a density of about 16 hills/m^2 (each hill contains a group of transplanted rice). The crop was harvested at the end of each August. Harvest residuals remained on site, and ratoon (re-sprouting young rice plants) continued to grow. Field management of the study plot in 2013 is summarized in Figure

2.2. During the full growing season, the field was flooded to a mean water depth of 3.0 cm [*Ono et al.*, 2013]. Periodic measurements of the LAI and vegetation height z_v undertaken in 2013 are plotted in Figure 2.2. Our study area is located near the western Pacific Ocean, which is under the influence of a tropical to subtropical climate, with a monsoon period in both summer and winter. In different seasons, this region potentially receives moisture from different oceans. Furthermore, our study was conducted in a large paddy field. Cultivation and irrigation activities influenced the surface cover; thus, we expected significant differences in the evapotranspiration isotopic pattern among seasons.

2.2 In-situ observation

The study site is part of the AsiaFlux Network. As Figure 2.3 showed, data in this site is available from (i) regular meteorology measurements, (ii) eddy covariance measurements, and (iii) isotopic measurements (also see photos in Figure 2.1). For (i) and (ii), data have been collected since 1999 by the National Institute of Agro-Environmental Sciences ($NIAES$). For (iii), new measurements began in June 2013, a month after the rice was planted. (i) and (ii) are briefly summarized here with a detailed description given in *Saito et al.* [2005]. The eddy covariance instruments, consisting of an open path infrared gas analyzer (LI-7500, Li-cor) and a sonic anemometer thermometer (DA-600, Kaijo), were mounted at 3.0 m above the ground. Air temperature (T_a) and relative humidity (RH) were measured at two heights, 3.8 and 1.1 m, with the temperature-humidity sensors (HMP-45A, Vaisala Helsinki, Finland). For (iii), water vapor and precipitation data measured from June 2013 were collected. All isotope measurements are presented as the ratio of heavy to light isotopologues and are relative to the normalized delta notation in per mil (‰),

$$\delta = \left(\frac{R_{sample}}{R_{standard}} - 1 \right) \times 1000 \tag{2.1}$$

where R_{sample} and $R_{standard}$ are the oxygen mass 18 to mass 16 ($^{18}O/^{16}O$) or deuterium to hydrogen (D/H) ratios of a sample and the Vienna standard mean ocean water ($V-SMOW$), respectively. $d-excess$, defined as $\delta D - 8\delta^{18}O$ [*Dansgaard*, 1964], was also calculated to provide further insight into the kinetic effects associated with evaporation processes.

2.2.1 Isotopic measurement system

The 1 Hz water vapor isotopic measurement system consisted of a Cavity Ring-down Spectrometer (L2120-i), Standard Delivery Module (A0101), High-Precision Vaporizer (A0211) and 16-port Distribution Manifold (A0311) (Picarro, Sunnyvale, CA, USA). Measurements were made evry 2 seconds and the results were averaged into 1-minute. Air sampling was undertaken using a distribution manifold. A shielded air intake was installed at a height of 2.0 m and was connected to the distribution manifold with a 14-m, 1/8-inch Teflon inlet tube (Du Pont-Mitsui Fluorochemicals, Tokyo, Japan) at a rate of about 40 mL min^{-1}. The flushing time was about 2 min. Because the observed Ta was higher than the dew point temperature (Figure 2.4), it is not necessary to heat the tubing.

Precipitation samples were collected every six hours using an Eigenbrodt NSA181 rain sampler, which is a wet-only automatic sampling system. The closure system is designed to prevent evaporation of the sample water or potential exchange with the atmosphere. The equipment guaranties automatic all year operation, possible through the use of heating at temperatures of 0°C and below. This collector contains a permanent cooling and sample-changing system, allow samples to be changed every 6-hours. Daily and monthly averages of δD and $\delta^{18}O$ were weighted by the precipitation amount and calculated as follows:

$$\delta_p = \frac{\sum_{k=1}^{n} \delta_{p,k} \times P_k}{\sum_{k=1}^{n} P_k} \tag{2.2}$$

where n is the number of observations for each day, and $\delta_{p,k}$ and P_k are the δ value and

the total amount of the kth precipitation, respectively. Assuming that water vapor and precipitation are in isotopic dynamic equilibrium, the equilibriumed water vapor isotopic ratio $\delta_{v,e}$ can be calculated from δ_p by incorporating a temperature-dependent equilibrium fractionation factor α_{eq} [*Majoube*, 1971]:

$$\delta_{v,e} = \left(\frac{1 + \delta_p/1000}{\alpha_{eq}} \right) \times 1000 \tag{2.3}$$

Water vapor isotopic measurements are briefly summarized here and a detailed measurement information was conducted in *Wei et al.* [2015]. Unfortunately, there was a data gap from 22 October to 23 December 2013, due to a pump failure. Surface water was sampled 1.5 days per week in the growing season of 2013 and increased to 3 days per week on average for 2014. Seven sampling locations were chosen to provide a general distribution of surface water isotopes.

2.2.2 Calibration protocol

The collected liquid water samples were transferred into high-density glass storage bottles and stored in a refrigerator at 15 °C in the laboratory until analysis. The laboratory room temperature was kept at 25 °C to prevent condensation during the analysis process. The samplers were analyzed using Cavity Ring-down Spectrometer (L2120-i). A new technique proposed by *van Geldern and Barth* [2012] was performed as a correction procedure for liquid water isotopic measurement. This technique required modifications to the hardware for liquid water injection, an optimized sequence layout, and a simple post-run correction procedure to remove memory effects. Three standard waters which were referenced against Vienna standard (i.e., KW: -0.3‰, -1.2‰; AW: -26.0‰, 197.9‰; SW: -9.6‰, -64.8‰ for $\delta^{18}O$ and δD, respectively) were included in each analysis batch to correct raw data for memory effects caused by the influence of the previous sample. The correction results showed that the final mean values agreed very well with the true values (Figure 2.5a). To check the correction performance, we also measured the same

sample several times (after each 8 unknown samples) in one measurement event (Figure 2.6). The carry-over from the different previous samples were virtually removed. Our method reduced the number of injections per sample to four (compared to six in the manufacturer's recommended method) with similar precision and accuracy (std ±0.2‰ for $\delta^{18}O$ and ±0.5‰ for δD). After memory correction, four injections of each sample were averaged and normalized to the Vienna Standard Mean Ocean Water-Standard Light Antarctic Precipitation ($VSMOW - SLAP$) scale using a two-point linear calibration generated from reference waters.

The air samples were analyzed with a cavity ring-down spectrometer and were carefully calibrated with a standard delivery module. The calibration was performed using a self-calibration program provided by Picarro CO. LTD. Two in-house water standards (SW and AW) were vaporized by the standard delivery module, mixed with dry room air and transferred to the analyzer. Each standard sample was measured continuously for 10 min with a dry air cleanup of about 15 min every 9 hours during the whole measurement period. The results showed a high precision with std ±0.3‰ for $\delta^{18}O$ and ±1.3‰ for δD. The standard water was changed every 6 months. We also evaluated the concentration dependence of our instrument by injecting different amounts of standard water into the vaporizer. We did not correct the concentration dependence effect because the measurements generally worked well within the range of water vapor concentration encountered during our study period (Figure 2.5b). However, the large measurement uncertainty under low water vapor concentration suggested that the correction of the raw measurements using the humidity-isotope response functions [*Steen-Larsen et al.*, 2014a] might be required. Unfortunately, there was a data gap from 22 October to 23 December 2013, due to a pump failure.

2.2.3 δ_E, δ_T and δ_{ET} estimation

Considering water vapor as a mixture of ET (including E and T) from local surfaces and that in the background air, water vapor isotopic variations can be influenced by isotopic

variations in either of the components [*Yakir and Sternberg*, 2000]. Based on water and isotope mass balance, the isotopic composition of water can be directly used to partition ET. It should be noted that only δD-based results are presented here, as variation in δD largely mimics that in $\delta^{18}O$.

The Keeling plot method, in combination with water vapor isotope ratios, has been successfully used to investigate the variation in δ_{ET} [e.g., *Moreira et al.*, 1997; *Wang and Yakir*, 2000; *Yepez et al.*, 2003; *Williams et al.*, 2004; *Lee et al.*, 2006; *Good et al.*, 2012, 2014]. Based on the mass conservation of water vapor and isotopes, the isotopic composition of water vapor can be determined by

$$\delta_v = a \times \frac{1}{Q_v} + \delta_{ET} \tag{2.4}$$

where $a = (\delta_{bg} - \delta_{ET})\, Q_{bg}$, Q is the water vapor mixing ratio. The subscripts bg and v represent the background atmosphere and atmospheric water vapor at the measurement height, respectively. Our Keeling plot was based on 1-hr Q_v and δ_v measurement. Two assumptions must be satisfied [e.g., *Lee et al.*, 2006; *Wen et al.*, 2010] here: (i) δ_{bg}, Q_{bg} and δ_{ET} are constant over the observation period, which means that a should be constant; (ii) temporal variations in δ_v (in our case, water vapor δD) are caused by evapotranspiration only. An example is given in Figure 2.7.

Several experiments have been conducted in controlled experiments [e.g., *Cappa et al.*, 2003; *Kim and Lee*, 2011; *Rothfuss et al.*, 2010] or over bare soil [e.g., *Dubbert et al.*, 2013, 2014a] to understand isotopic compositions of soil evaporation, although it is still rare because of the technology limitations. Generally, the Craig and Gordon Equation [*Craig and Gordon*, 1965] is used to quantify the evaporative enrichment

$$\delta_E = \frac{\alpha_{eq}^{-1}\delta_w - h\delta_\nu - \varepsilon_{eq} - (1-h)\,\varepsilon_K}{(1-h) + 10^{-3}\,(1-h)\,\varepsilon_K} \tag{2.5}$$

where $\alpha_{eq} = (24840/T^2 - 76.25/T + 0.0526)$ is the equilibrium fractionation factor [*Majoube*, 1971], and $\varepsilon_{eq} = (1 - 1/\alpha_{eq}) \times 1000$, δ_w is the isotopic composition of surface water,

h is RH normalized by the saturation vapor pressure at the water surface. The Kinetic fractionation factor ε_K is defined by

$$\varepsilon_K = n\,(1 - D_i/D) \times 10^3 \tag{2.6}$$

where the ratio of the molecular diffusion coefficients of water vapor in dry air D_i/D is taken as 0.9839 from *Cappa et al.* [2003]; $n = 0.67$ is taken from *Kim and Lee* [2011] and is used to understand the isotopic enrichment of liquid water during evaporation from a water surface.

The chamber-based direct measurements of transpired water vapor isotopic composition (δ_T) have been developed recently [e.g., *Wang et al.*, 2010, 2012, 2013; *Dubbert et al.*, 2014a]. Such chamber measurement is a challenge for our study. It is difficult to ensure good air tightness of air chamber because of hollow stems of rice. Moreover, it requires changing the size of chambers frequently since rice is a fast growing crop. The flooded condition also increases the difficulty of the installation and maintaince of chamber. Practically, δ_T can be assumed the same as pone water δ_{sw}, although some bias might be produced by non-steady state isotopic enrichment especially during early morning and late afternoon [e.g., *Dongmann et al.*, 1974; *Lai et al.*, 2006, 2008; *Dubbert et al.*, 2014a,b]. Based on the water balance ($ET = T + E$) and isotope mass balance ($ET\delta_{ET} = T\delta_T + E\delta_E$), without considering rainfall interception evaporation, T/ET is then estimated as

$$\frac{T}{ET} = \frac{\delta_{ET} - \delta_E}{\delta_T - \delta_E} \tag{2.7}$$

The key point in this study is to precisely determine the isotope ratio of ET (δ_{ET}), T (δ_T), and E (δ_E) using isotopic measurements. To identify the principal uncertainties, we quantify the T/ET uncertainties through a first-order Taylor series expansion of the uncertainty in the final partitioned value [*Good et al.*, 2014; *Phillips and Gregg*, 2001]

$$\sigma_{T/ET}{}^2 = \frac{\sigma^2_{\delta_{ET}}}{(\delta_T - \delta_E)^2} + T/ET\frac{\sigma^2_{\delta_T}}{(\delta_T - \delta_E)^2} + (1 - T/ET)\frac{\sigma^2_{\delta_E}}{(\delta_T - \delta_E)^2} \tag{2.8}$$

The three terms on the right-hand side of the equation represent the contribution of uncertainties in δ_{ET}, δ_T, and δ_E to the total variance.

2.3 *IsoGSM* simulation and water tagging experiments

2.3.1 *IsoGSM* simulation

To investigate the impact of large-scale moisture transfer on the isotopic variability of near surface water vapor, we used *IsoGSM*, a global spectral model that incorporates water isotope tracers [*Yoshimura and Kanamitsu*, 2009]. *IsoGSM* simulations have been validated by ground-based isotope observation [e.g., *Farlin et al.*, 2013; *Uemura et al.*, 2008] and satellite observation [e.g., *Frankenberg et al.*, 2009]. These studies showed that *IsoGSM* is capable of reproducing the daily averaged variability in δD of near-surface water vapor associated with synoptic weather cycles. The model in this study had a horizontal scale of about 200 km (T62) and 28 vertical levels (L28), with six-hour intervals. *IsoGSM* was nudged by the spectral nudging technique [*Yoshimura et al.*, 2008] to include the actual atmospheric thermodynamic situation. The default land surface scheme in *IsoGSM* is the Noah model [*Ek et al.*, 2003]. In *IsoGSM*, isotopic fractionation takes place whenever phase transition occurs. *IsoGSM* assumes a constant isotopic value (0‰) for the ocean water and no isotopic fractionation occured in land surface evapotranspiration (i.e.,100% T/ET is assumed). Readers are directed to *Yoshimura et al.* [2008], *Yoshimura et al.* [2014] and *He et al.* [2014] for a detailed description of the model setup. Over a long time period (such as monthly time scale), the planetary boundary layer can be effectively assumed as a one dimension model, with input (evapotranspiration) and output (air from the free atmosphere) only from the top and bottom. Near surface hor-

izontal advection impact is small and can be cancelled out by the temporal averaging [*Helliker et al.*, 2004; *Angert et al.*, 2008]. Therefore, the water vapor source over this site was considered to originate from: 1) air from the background atmosphere (convective boundary layer (hereafter CBL) water vapor, represented by $IsoGSM$ simulated water vapor and its associated δD_v output (δ_{bg}) at CBL height); and 2) water vapor supplied from local land evapotranspiration (estimated by a Keeling plot). The relative contribution of evapotranspired water to surface water vapor was evaluated as follows [e.g., *Yakir and Sternberg*, 2000]:

$$F_{ET} = \frac{\delta_v - \delta_{bg}}{\delta_{ET} - \delta_{bg}} \tag{2.9}$$

where F_{ET} is the contribution of ET to the atmospheric boundary layer (ABL) water vapor. We further quantified uncertainties through a first-order Taylor series expansion of all the uncertainty in the final partitioned value [*Phillips and Gregg*, 2001].

2.3.2 Water-tagging experiments using $IsoGSM$

In addition to local evapotranspiration, water vapor isotopes are also affected by original oceanic sources. To understand the origin of near-surface water vapor and its impact on the isotopic variability, we conducted a tagging simulation using $IsoGSM$. The mechanism of our water-tagging experiments was very similar to that of *Yoshimura et al.* [2004], *Frankenberg et al.* [2009] and *Risi et al.* [2010]. By running $IsoGSM$ in tracer mode, it is possible to track a given moisture mass back to its last time at sea level, within a certain time span. This was achieved by setting the surface evaporative fractionation factor to 1 for the target region and 0 for the other regions in the model, and by turning off all the other isotopic fractionation in the atmosphere. For each of these simulation, the evaporated water is marked by its origin with a tag. Once this tagged vapor is added to the atmosphere, it undergoes exactly the same processes as normal vapor (It is allowed to advect, mix, condense and rainout in the atmosphere. Therefore, it has influence neither on the hydrological cycle nor on isotopic processes.), except it is not factored into

energy budget calculations. The method used here allows a direct quantification of the amount of water adverted from tagging region. Similar experiments were conducted to understand the cause of the seasonal precipitation isotopic variation along the western U.S. coast [*Buenning et al.*, 2012]. In our study, vapor was tagged within a 10°×10° boxed sub-region. The atmospheric column perceptible water derived from tagged boxes was used to identify the source region of the water vapor.

2.4 Global ET estimation and its partitioning

2.4.1 Global synthesis of LAI control on dry canopy ET partitioning

In order to understand global synthesis of LAI control on ET partitioning, we collected article searches in Google scholar and Web of Science and evaluate the relationship between LAI and T/ET. To select datasets of high quality, the following data screening criteria were used:(1) under dry canopy condition or soil evaporation is known. (2) at least two out of the three members (E, T, and ET for non-isotopic methods or δ_E, δ_T and δ_{ET} for isotopic method) were measured independently; (3) LAI was quantified during the measurement period; and (4) Vegetation types were recorded.

As a result, 64 individual publications (Among these studies, 31 individual publications shown in *Wang et al.* [2014] were adopted.) before 30 November 2015 were included in our analysis (Appendix A). Similar with *Wang et al.* [2014], the end members in ET partitioning and LAI values directly from tables or text in original papers are summarized. Some indirect data from figures was extracted using GraphClick software (Arizona software, USA). Based on vegetation types, we classified all the studies into 6 species: Broad leave forests, Needle leave forests, Mixed forests, Shrubs and grasses, crops and wetlands. To reduce systematic error, the data were averaged into 0.5-bin average of LAI. The relationship between LAI and T/ET for each piece of vegetation was inverstigated using power regression ($T/ET = aLAI^b$, where a and b depend on vegetation

type).

2.4.2 ET estimated from LSM, RS and $GRACE$

Three different ET products were used in this study (Table 2.1), i.e., (1) land surface modelling (LSM) estimated ET (Community Land Model 4.5, *Lawrence et al.* [2011]), (2) remote sensing (RS) based ET (Global Land surface Evaporation: the Amsterdam Methodology ($GLEAM$), *Miralles et al.* [2011a,b]) and (3) $GRACE$-inferred ET. $GRACE$ satelite-derived total water storage change ($TWSC$) can be used to estimate ET as a residual in the water balance equation:

$$ET = P - R - TWSC \tag{2.10}$$

where P is precipitation and R is runoff [*Ramillien et al.*, 2006; *Long et al.*, 2014]. $GRACE$ satellite provides information on changes in the gravity field which are controlled primarily by variations in water distribution and are used to derive $TWSC$ at a spatial resolution of 1 degree. To estimate $TWSC$, we used GRCTellus land data based on the Level-1 $GRACE$ observations, processed at JPL [*Watkins et al.*, 2015]. The spatial resolution is 1× degree. Because of the sampling and post-processing of $GRACE$ observations, $TWSC$ at small spatial scales tends to be attenuated. Therefore, $TWSC$ was corrected by multiply the GRCTellus land data by the scaling coefficient provided by Community Land Model 4 [*Landerer and Swenson*, 2012; *Wiese*, 2015; *Watkins et al.*, 2015]. Detailed information can be addressed in `http://grace.jpl.nasa.gov/data/get-data/monthly-mass-grids-land/`. $TWSC$ includes mass changes in groundwater storage, surface water and soil moisture and [*Long et al.*, 2014]. For runoff evaluation, monthly mean of composite runoff from Global Runoff Data Centre ($GRDC$) were used (Figure 2.9). $GRDC$ composite runoff was corrected by observed inter-station discharge [*Fekete et al.*, 2002]. Moreover, Global Precipitation Climatology Centre ($GPCC$) monthly precipitation dataset was also used (Figure 2.8). A detail data description can be found in

Table 2.2.

$GLEAM$ is designed to maximize the use of satellite-based observations to create a spatially coherent estimate of the evaporative flux over land [*Miralles et al.*, 2011a]. Global maps of evapotranspiration from land-surface are available with a daily resolution on a 0.25×0.25-degree grid. $GLEAM$ relies on a Priestley-Taylor ($P-T$) approach [*Priestley and Taylor*, 1972] to derive daily potential ET based on satellite observed surface net radiation (Rn), T_a and a Gash's analytical model based on observed precipitation (P) and different vegetation's characteristic was used to derived E_c. As a result estimates of ET for day j are derived from

$$ET_j = E_{P,i}S_i + (1-\beta)E_{c,i} \tag{2.11}$$

where E_p is derived through $P-T$ approach. S_i denotes the evaporative stress and is computed combining observed vegetation water content and estimates of root-zone soil moisture from a multilayer soil module driven by observed precipitation and surface soil moisture. β is a constant to account for declines in transpiration when the canopy is wet. A full description of $GLEAM$ was conducted in *Miralles et al.* [2011a,b] and the data can be download from `http://foofoo.ugent.be/satex/GLEAM/`.

The Community Land Model versions 4.5 (hereafter CLM) are the latest in a series of land models developed through the Community Earth System Model ($CESM$) project. CLM is a physically based model having a more complex ET computation for turbulent heat transfer based on Monin-Obukhov similarity theory, which is solved numerically to account for atmospheric stability [*Choi and Liang*, 2010]. In the case of a vegetated surface, ET is partitioned into vegetation and ground fluxes that depend on canopy temperature (T_c) and ground temperature T_s in addition to air temperature T_a and specific humidity q_a. Newton-Raphson iteration is used to solve for T_c, H and ET from vegetation simultaneously using the ground temperature from the previous time step. E_c in CLM is derived through a simple model based on observed P, LAI and stem area index

(SAI). Detailed information can be found in Technical Description of version 4.5 of the Community Land Model [*Oleson et al.*, 2013].

2.4.3 Global ET partitioning

A global LAI product (`http://globalchange.bnu.edu.cn/research/lai/#usage`), released by the Land-Atmosphere Interaction Research Group at Beijing Normal University, was used in this study (Table 2.1). This LAI product was generated by reprocessing the $MODIS\ LAI$ products which is available from 2000 to 2014 is generated in 8-days intervals. In this dataset, $MODIS\ LAI$ products were improved by using a two-step integrated method. This improved $MODIS\ LAI$ data are more accurate, spatiotemporally continuous and consistent than current $MODIS\ LAI$ data, and can be considered as input for LSM and GCM modelling [*Yuan et al.*, 2011].

The International-Geosphere-Biosphere-Program ($IGBP$) land cover dataset over the period 2000-2001 with 1×1 degree resolution [*Friedl et al.*, 2010; *Hall et al.*, 2006] was also used in our study (Table 2.1). This products describe the geographic distribution of the 17 land cover classification scheme proposed by $IGBP$ (Table 2.3). In each grid cell, Fraction of each land cover class (F_v) was also involoved. In this study, these 17 land cover classification scheme is re-classified into 6 land cover classifications, to match global synthesis of LAI control on ET partitioning analysis.

Based on estimated ET, fraction of each land cover class (F_{v_j}, a value of 0 to 1 for each vegetation class and 0 for non-vegetation type) and LAI regression for each class of vegetation ($aLAI^b$), T in each grid can be calculated as:

$$T = \sum_{j=1}^{n} \left[(ET - E_c) \times F_{v_j} \times aLAI^b \right] \tag{2.12}$$

where canopy interception E_c is taken from $GLEAM$ dataset or CLM dataset. As a

result, T/ET in each grid or in global is given by:

$$\frac{T}{ET} = \frac{1}{ET} \sum_{i=1}^{n} \left[(ET - E_c) \times F_{v_j} \times aLAI^b \right] \tag{2.13}$$

.

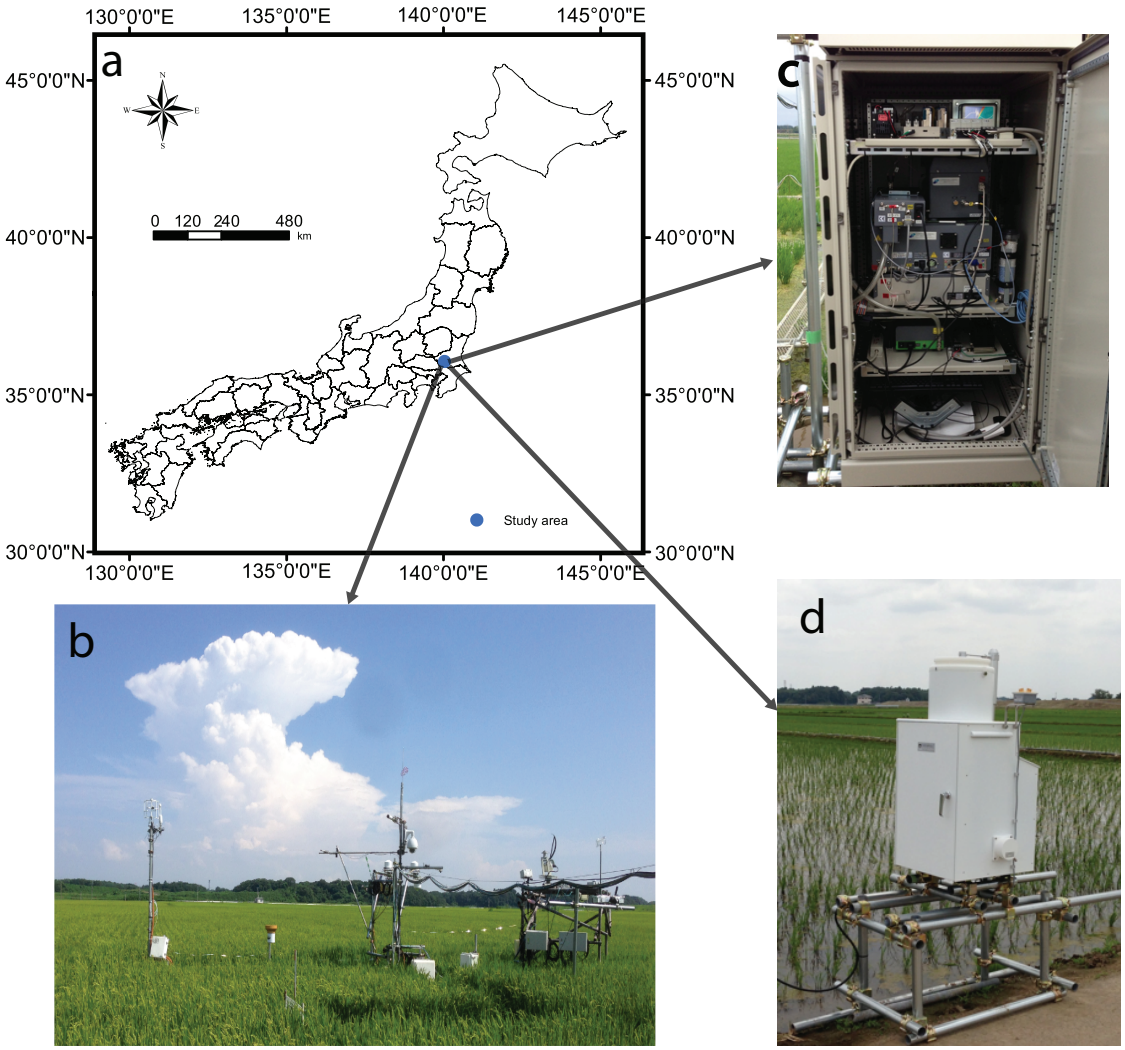

Figure 2.1: (a). Location of the study site in Mase, Japan (closed blue circle). (b). A photo about measurement site. (c). A photo about water vapor isotopic measurement system (Picarro L2120-i). (d) A photo about Automatic rain sampler (Eigenbrodt NSA181).

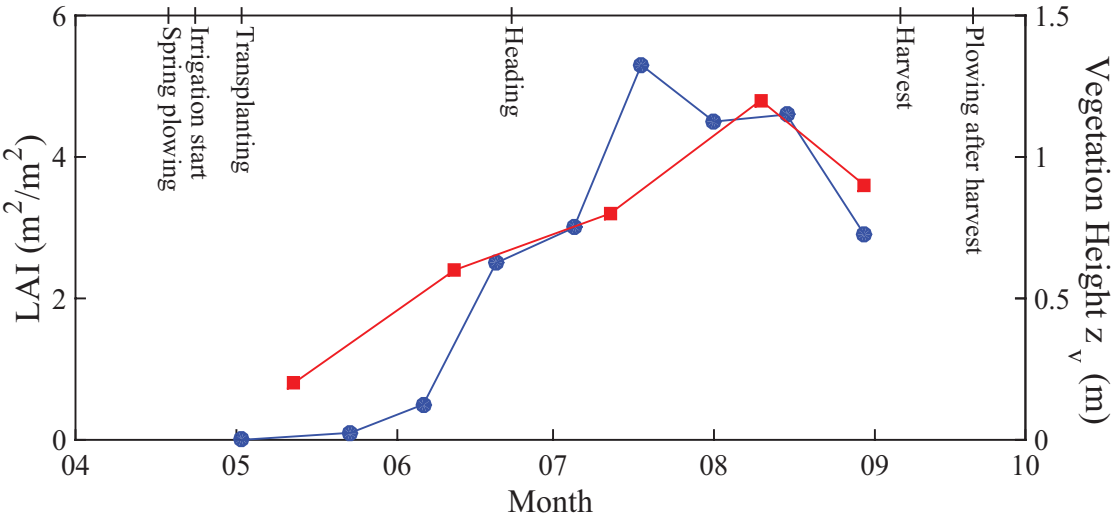

Figure 2.2: Linearly interpolated measurements of leaf area index (LAI, blue filled circle) and Vegetation height (z_v, red filled square) throughout the whole growing season in 2013. LAI and z_v was measured by the National Institute for Agro−Environmental Sciences ($NIAES$). Field management of the study site in 2013 is also summarized.

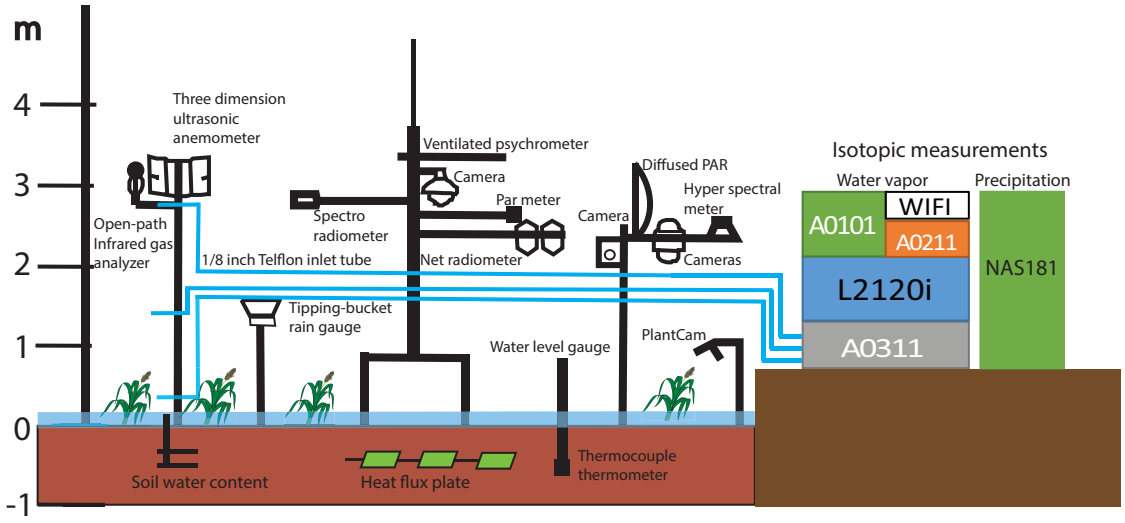

Figure 2.3: The measurement content schematic in this study.

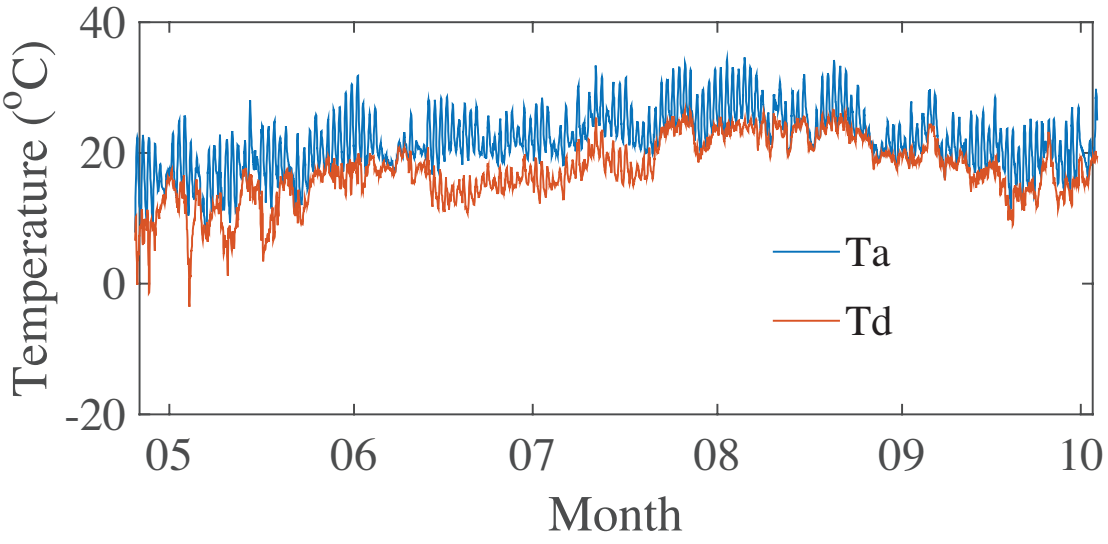

Figure 2.4: Comparison of dew temperature (T_d) and air temperature (T_a).

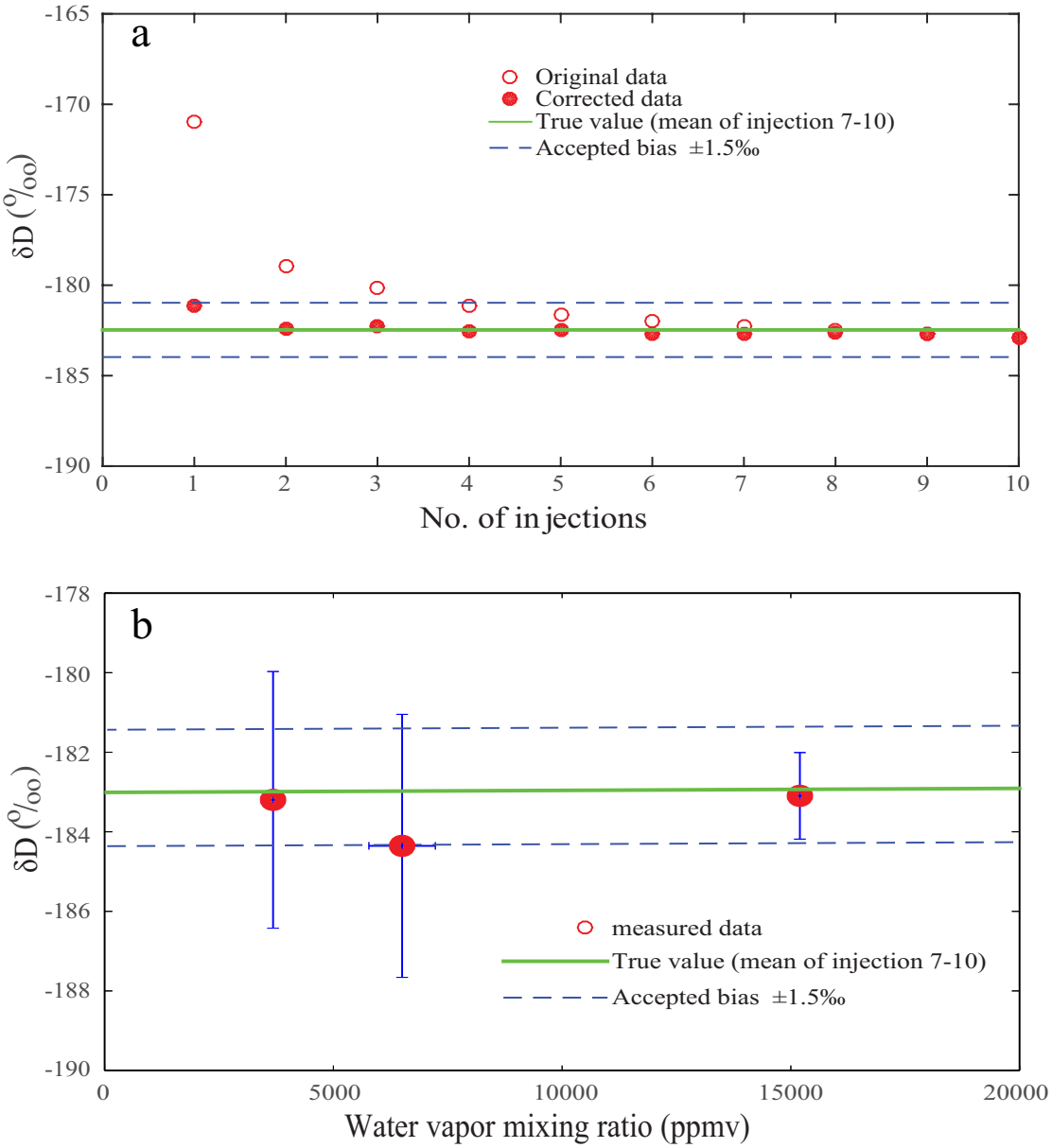

Figure 2.5: Calibration of water vapor and precipitation data (a). An example of correction procedure [*van Geldern and Barth*, 2012] to reduce memory effect in precipitation isotopic analysis. All the injections of a sample can be used after correction and the number of rejections per unknown can be reduced to 4. Four injections of each sample were averaged and normalized to the $VSMOW/SLAP$ scale by using a two-point linear calibration. (b). Evaluation of the dependency of the measured isotopic value on water vapor concentration by injecting different amounts of standard water into the vaporizer. Three tests have been done in field conditions, during 2013/09/01−2013/09/02 (Q = 15200±200 ppmv, δD = 183.1±1.1‰, Total number, n = 1516), 2014/09/16−2014/09/17 (Q = 6500±700 ppmv, δD = 184.3±3.3‰, n = 2109) and 2015/03/31−2015/04/01 (Q = 3700±100 ppmv, δD = 183.2±3.2‰, n = 1136).

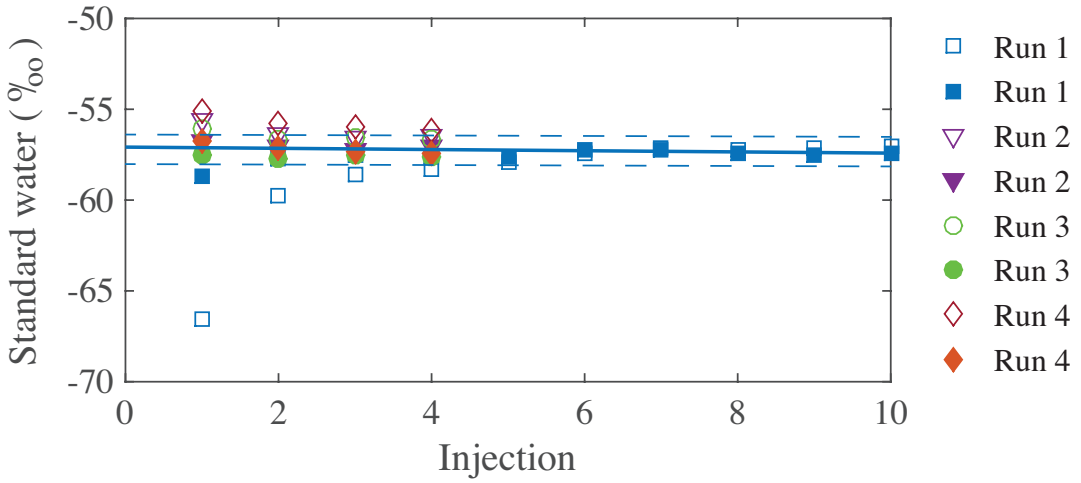

Figure 2.6: Comparison of dew temperature (T_d) and air temperature (T_a).

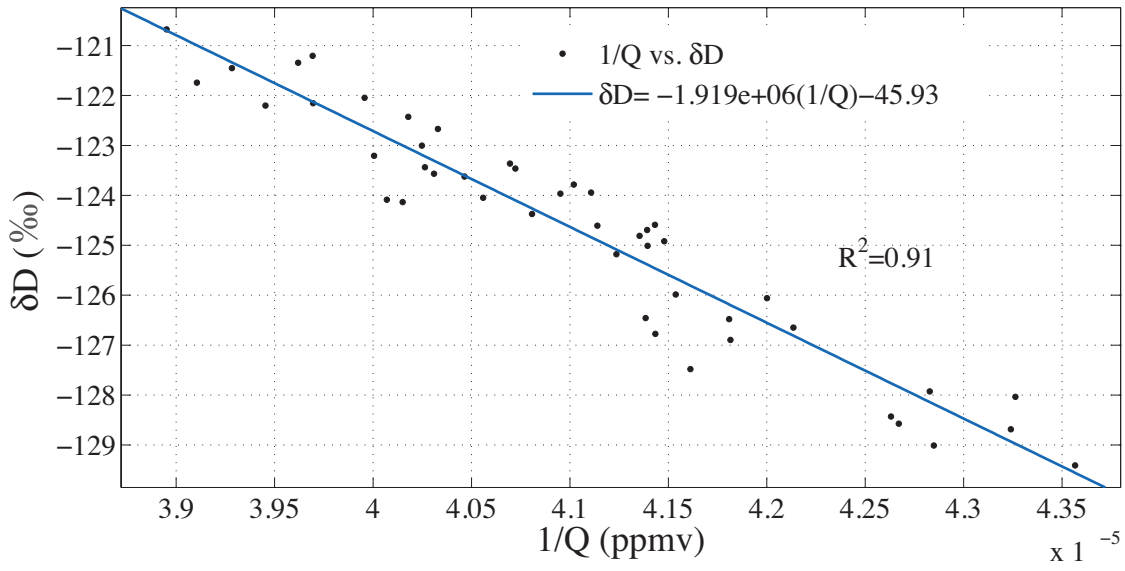

Figure 2.7: An example of δ_{ET} estimation using Keeling plot.

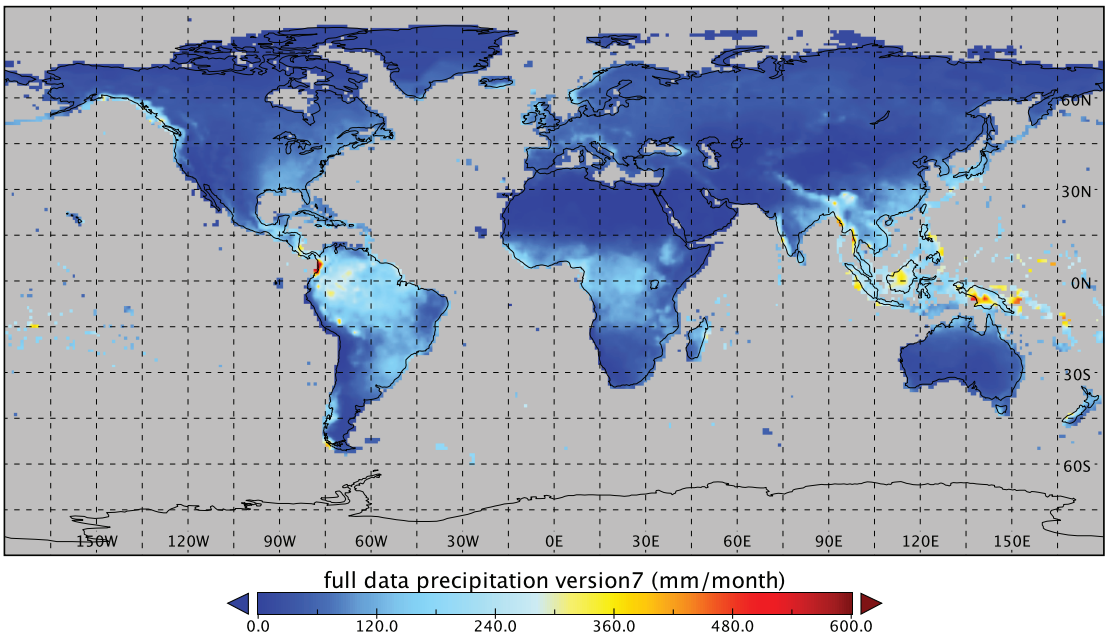

Figure 2.8: Mean precipitation in mm/month (2004−2010), 1.0 degree, obtained from *GPCC* full data product version 7.

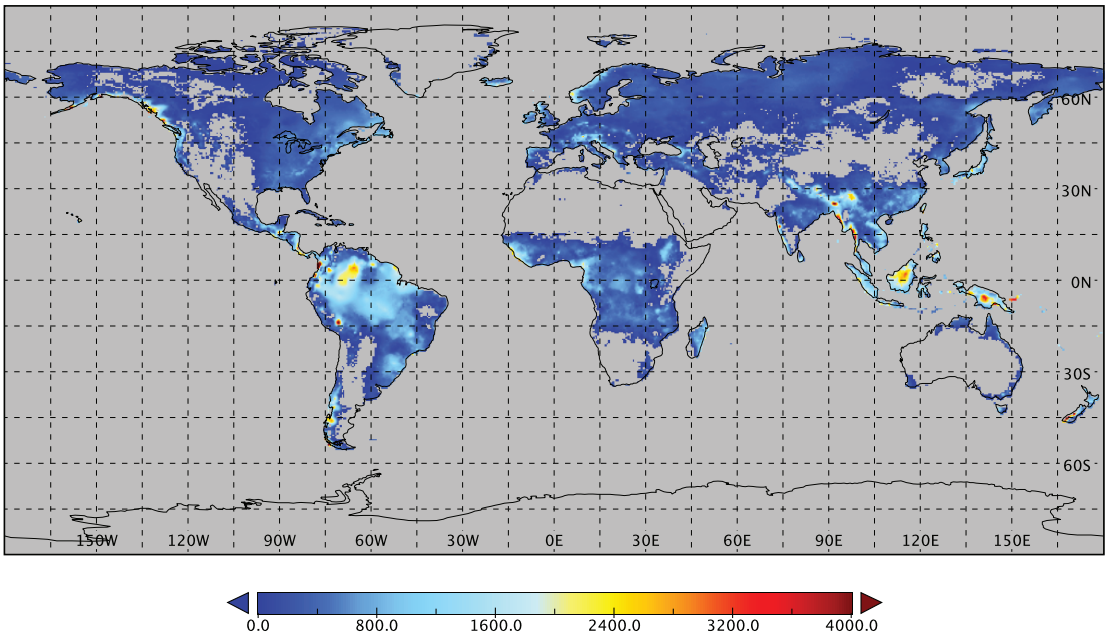

Figure 2.9: *GRDC* composite annual runoff (mm/year).

Table 2.1: The dataset used in global T/ET estimation.

Variables	Datasets	Spatial extent	Spatial Resolution	Temporal Resolution	Time Span	References
ET	CLM	Global	1°	Monthly	1850−2010	*Lawrence et al.* [2011]
	$GLEAM$	Global	0.25°	Daily	2000−2011	*Miralles et al.* [2011a]; *Miralles et al.* [2011b]
	$GRACE$ derived	Global	1°	Monthly	2002−2015	See Table 2.2
LAI	Improved $MODIS$ data	Global	1 km	8 days	2000−2013	*Yuan et al.* [2011]
Land cover	$ISLSCP$ II $MODIS$ $IGPB$ land cover	Global	1°	annual	2000−2001	*Friedl et al.* [2010]
Site measurements	Previous studies	site	-	-	-	See Appendix A

Table 2.2: Data used in estimation of $GRACE$-inferred ET.

Variable	Spatial Resolution	Temporal Resolution	Time Span	Reference
P	1°C	Monthly	1901−2013	*Schneider et al.* [2014]
R	0.5°C	Monthly	−	*Fekete et al.* [2002]
$TWSC$	1°C	Monthly	2002−2015	*Watkins et al.* [2015]

Table 2.3: Land cover type codes and definitions and *IGBP* and this study.

Codes In IGBP	Definitions	New classification
1	Evergreen Needleleaf Forests	Needleleaf Forests
3	Deciduous Needleleaf Forests	
2	Evergreen Broadleaf Forests	Broadleaf Forests
4	Deciduous Broadleaf Forests	
5	Mixed Forests	Mixed Forests
6	Closed Shrublands	Scrublands and Grasslands
7	Open Shrublands	
8	Woody Savannas	
9	Savannas	
10	Grasslands	
11	Permanent Wetlands	Wetlands
12	Croplands	Croplands
14	Cropland/Natural Vegetation Mosaic	
13	Urban and Built-Up	Others
15	Permanent Snow and Ice	
16	Barren or Sparsely Vegetated	
17	Unclassified	
0	Water surface	

Chapter 3

Understanding the variability of δ_v

3.1 Characteristics of observation and simulation

Figure 3.1 shows the daily precipitation (P), daily averaged water mixture ratio (Q), $\delta^{18}O$, δD and $d-excess$ of water vapor (with subscript v), and the weighted precipitation amount of $\delta^{18}O$, δD and $d-excess$ (with subscript p). Q varied from 3000 to 35000 ppmv. $\delta^{18}O_v$ fluctuated from -28.4‰ to -11.0‰, δD_v fluctuated from -206.8‰ to -78.6‰, and $d_v-excess$ fluctuated from -1.8‰ to 31.9‰. There was considerably less day-to-day variation in $\delta^{18}O_v$, δD_v, and $d_v-excess$ in the warm season than the cold season. Similar results were observed in Beijing (40° 00' N, 116° 23' E [*Lee et al.*, 2006]). The monthly isotopic variation can be explained by strong summer monsoon activity in East Asia, including Japan and southeastern China [*Wen et al.*, 2010; *Laskar et al.*, 2014]. The observed δ_p varied widely, ranging from -15.7‰ to 2.9‰ for $\delta^{18}O_p$, from -114.9‰ to 34.5‰ for δD_p, and from -21.6‰ to 27.7‰ for $d_p-excess$. Positive $\delta^{18}O_p$ and δD_p values tended to come up in light rain, which were subject to sub-cloud evaporation [*Wen et al.*, 2010; *Huang and Wen*, 2014]. Water vapor appeared to be isotopically in equilibrium with surrounding raindrops during a precipitation event. Because the water vapor mixing ratio increased with precipitation, the vapor isotope ratios became progressively lower during rainy periods. $\delta^{18}O_v$ and δD_v were consistently lower than but varied together

with precipitation isotopes. Similarly, $d_v - excess$ consistently varied with $d_p - excess$. As noted in previous studies [e.g., *Lee et al.*, 2006; *Welp et al.*, 2008; *Wen et al.*, 2010], near surface vapor isotope ratios approached the equilibrium state with the ratios in precipitation. These interactions between raindrops and the surrounding water vapor during precipitation events have been quantitatively estimated by *Lee and Fung* [2008].

Monthly isotope and weather variables are shown in Table 3.2. Seasonal changes of relative humidity (RH), δD, $d - excess$ and air temperature (T_a) are plotted in Figure 3.2. RH and T_a displayed a clear seasonal signal. There was no clear seasonal cycle in δ_v or δ_p, although slightly lower values were apparent in winter. In contrast, $d_v - excess$ and Q displayed a clear seasonal cycle, which was different from that observed in those areas influenced by the typical arid continental climate at similar latitudes (e.g., Zhangye, China (38° 51' N, 100° 22' E) [*Huang and Wen*, 2014]). The highest and lowest monthly mean values of $d_v - excess$ were found in January (27.3‰) and July (11.4‰), respectively. $d_p - excess$ was more variable with the highest value found in January (16.3‰) and the lowest in November (1.5‰). Different from those ocean surface studies [e.g., *Benetti et al.*, 2014, 2015; *Uemura et al.*, 2008, 2012; *Steen-Larsen et al.*, 2014b, 2015], the overall relationships between isotopes and weather variables were found weak and controversial (Table 3.1). Seasonal changes of diurnal averaged Q, isotope ratio $\delta^{18}O$, δD, $d - excess$ of water vapor were shown in Figure 3.3. $\delta^{18}O$ and δD diurnal variations was likely in phase with the variations in Q. The diurnal variability of $d - excess$ was in opposite phase with those of the vapor $\delta^{18}O$, δD. The vertical mixing of air between CBL and ET may have played a role in d-excess diurnal variations [*Wen et al.*, 2010].

Figure 3.1 compares an $IsoGSM$ isotopic simulation at 2 m with surface observations. $IsoGSM$ reproduced the variability of Q very well ($R^2 = 0.95$, RMSE = 832 ppmv). This implies that our site can reasonably capture δ_v variation under the influence of regional-scale advection of atmospheric moisture ($R^2 = 0.64$, RMSE = 10.8‰ for δD_v, $R^2 = 0.70$, RMSE = 1.2‰ for $\delta^{18}O_v$). Variability in $d - excess$ was difficult to simulate [e.g., *Bonne et al.*, 2014]. IsoGSM predicted a relatively constant $d_v - excess$ value of 10‰ and

generally underestimated observed $d_v - excess$ values throughout the observation period ($R^2 = 0.20$, RMSE = 5.5‰). Model discrepancies indicated that water vapor isotopes were an additional constraint that highlighted the misrepresentation of hydrological processes in the simulation. We did not further explore the possible causes of model bias. Rather, we focused on identifying the controls of near surface δ_v. Despite the discrepancy in modeled isotopic variability, $IsoGSM$ provided important information regarding how large-scale moisture transfer influenced δD_v. The strong fit at our site suggested that the variability of δ_v is primarily influenced by large-scale advection, whereas local evapotranspiration likely played an insignificant role (because $IsoGSM$ reproduces large-scale advection rather than local evapotranspiration). However, more evidence is required to determine the driving forces behind the variability of δD_v. Hereafter, we only present results based on δD and $d - excess$. Similar results obtained from $\delta^{18}O$ are not shown here.

3.2 Effect of precipitation on the δD_v variability

The observed and simulated isotopic ratios (Figure 3.1) indicated that during non-rainy days, there was no significant isotopic variation of water vapor. On rainy days, δD_v changed suddenly and considerably in relation to the isotopic composition of rain (Figure 3.1). For example, in association with a precipitation event that occurred on October 15 (19 mm), Q increased from 14520 ppmv to 18180 ppm, whereas $\delta^{18}O_v$ decreased from -99.2‰ to -180‰. This variation indicated a significant isotopic impact of raindrops on near surface water vapor. To verify this quantitatively, we calculated $\delta D_{v,e}$ based on Equation 2.3 and compared it with δD_v in Figure 3.4. δD_v agreed reasonably well with $\delta D_{v,e}$ (R = 0.74) at the daily time scale. This robust relationship indicated that atmospheric vapor approached an isotopic equilibrium with precipitation at daily time scale. At a monthly time scale, our equilibrium predictions differed greatly from the monthly δD_v (Figure 3.2, R = 0.22). These results contradicted previous findings, which demonstrated a reasonable agreement between δD_v and $\delta D_{v,e}$ on a monthly time scale[*Jacob and*

Sonntag, 1991; *Lee et al.*, 2006; *Wen et al.*, 2010; *Huang and Wen*, 2014]. Furthermore, we found no obvious relationship between monthly $d_v - excess$ and predicted equilibrium values. Predicted $d_{v,e} - excess$ was generally similar to that of precipitation. A possible reason for this is that condensation affected δ without changing $d - excess$ [*Dansgaard*, 1964; *Bonne et al.*, 2015].

3.3 Effect of local ET on the the δD_v variability

During non-rainy days, surface ET can significantly contribute to the temporal variation in δ_v. We investigated this effect using Equation 2.9 with three parameters, δ_{ET}, δD_v and δ_{bg} (the isotopic ratio of the background air). Hourly δ_{ET} values were calculated using the Keeling plot approach [*Keeling*, 1958], whenever data points were available (N > 40) in a given hour and with a high coefficient of determination ($R^2 > 0.8$) from each linear regression. *Wei et al.* [2015] demonstrated that at this site, the assumptions underlying the Keeling plot were rarely met and the uncertainty was quite large, especially under nighttime or weakly turbulent conditions. We assumed no evapotranspiration at night (19:00 p.m. - 7:00 a.m.) and used daily average δ_{ET} values (sensible heat weighted). δD_v at simulated CBL height (δ_{bg}) was derived from linear interpolation of water vapor isotopic ratio from 925 hpa (about 750 m), 850 hpa (about 1500 m) and 700 hpa level (about 3000 m) for three reasons: 1) $IsoGSM$ simulated the convective boundary layer extended with a height of 0.8 to 2 km during our observation periods (Figure 3.5); 2) $IsoGSM$ is nudged by United States National Centers for Environmental Prediction ($NCEP$) reanalysis data, and thus reproduces the day-to-day variability induced by large-scale convection; and 3) the model produces a satisfactory qualitative agreement for the isotopic composition of atmospheric moisture at 2-m level (Figure 3.1).

The daily variability of δ_{ET}, δ_{bg}, and δD_v is shown in Figure 3.6. δ_{ET} ranged from -112.2‰ to 37.1‰. A significant difference in δ_{ET} was found between the growing and after haverst seasons. During the summer season (June-July-August, JJA), δ_{ET} generally

depended on transpiration. δ_{ET} was closely coupled with irrigation water, indicating small isotopic fractionations during this period [*Wei et al.*, 2015]. In the non-growing season, δ_{ET} was considerably more variable than in JJA. Without irrigation and consequently with negligible transpiration, δ_{ET} was controlled by other meteorological parameters, such as precipitation and radiation. For example, a rapid decrease of δ_{ET} corresponded to evaporation after precipitation on 18 October (from -51.8‰ on 18 October to -97.81‰ on 20 October). Then δ_{ET} values gradually increased due to soil evaporation (-69.2‰ on 21 October). Compared to δ_{ET}, δD_v and δ_{bg} clearly displayed seasonal variation and were highly correlated with each other. These results suggest that δD_v was mainly controlled by the air from the free atmosphere. The largest difference between δD_v and δ_{bg} was found in JJA, whereas the smallest difference was found in winter (December-January-February, DJF). In JJA, relatively high δD_v values were likely due to enrichment by transpiration, whereas a low $d_v - excess$ is a result of the negligible kinetic effect associated with transpiration by short vegetation [*Lai et al.*, 2008]. Our results showed a large ET impact during the rice growing season (JJA). The monthly averaged δD_v, δ_{ET} and δ_{bg} used to estimate monthly F_{ET} are listed in Table 3.3. On average, F_{ET} was estimated as 16.0±12.3%, with the highest value in JJA (20.5±12.9%) and lowest in DJF (7.1±13.2%). These estimates are consistent with simulated seasonal averaged latent heat fluxes (Figure 3.7). Thus, we suggest that the primary control on the variability of near surface δ_v and humidity during non-rainy days is large scale moisture transfer, while local ET plays only the secondary role, especially in DJF.

Nevertheless, large uncertainties were still present in these estimates. The ability of $IsoGSM$ to reproduce water vapor and its isotopic variability observed at a single location was unexpected because the $IsoGSM$ simulation was performed at a coarse resolution (200 km × 200 km), which is far greater than the footprint of ground-based measurements [*Farlin et al.*, 2013]. Furthermore, feedback from the local land contribution was not carefully addressed. $IsoGSM$ neglects possible fractionation during transpiration, which is a common problem in most isotope-enabled GCMs. Bias also arises from neglecting

horizontal advection, which is likely to alter the near surface δD_v. Very few measurements of δ_{bg} are currently available [*Tsujimura et al.*, 2007]. Here, we used isotopic ratio of water vapor linear interpolated from water vapor isotopic ratio at different levels as background. However, $IsoGSM$ simulated CBL height is rough, and the vertical profile of water vapor isotopes is general non-linear. To reduce the uncertainty in evaluating F_{ET}, a further study based on measured middle and low troposphere isotopes of water vapor isotopes (such as satellite measurement) should be conducted. Nevertheless, our results suggested that near surface water vapor isotope ratio is not significantly affected by ET. As explained previously, the high correlation between measured δD_v at 2-m and simulated δ_{bg} at CBL height (R = 0.74) with the insignificant correlation between measured δD_v at 2-m and Keeling plot estimated δ_{ET} (R = 0.18) also suggested the dominant role of air from the free atmosphere.

3.4 Remote controls on the δD_v variability

To understand the remote controls on water vapor isotopic variation, we conducted a water tagging experiment to identify the origin of the water vapor. As an example, the model simulation indicated different sources of water vapor in JJA (Figure 3.8, Results of SON, DJF and MAM were shown in Appendix B). There was a significant contribution from the surrounding ocean (both the Japan Sea and Pacific Ocean; Areas c, d, e, and f). Assuming all water vapor originated from the tagged boxes, we were able to calculate the fractional relative contribution for each box. As Figure 3.9 shows, Area e had the most significant impact on moisture sources in JJA, corresponding to about 32% of the total contribution. In SON, flow from either the Japan Sea (Area d, 24%) or the high-latitude Pacific Ocean (Area f, 34%) had the dominant role in controlling the observed isotopic variability at our site. Water vapor generally originated from the Japan Sea in DJF (Area d, 40%). Likewise, variable sources of water vapor were found in MAM (March-April-May), with the largest contribution from Area d (29%). We documented

the 850 hpa isotope ratios based on the wind direction (0° to 90°, Area f; 90° to 180°, Area e; 180° to 270°, Area a+c; 270° to 360°, Area b+d). The results showed that the original source had a significant impact on water vapor isotopes (Figure 3.10). Seasonal and regional differences of δD_v at the 850 hpa level were related to RH relative sea surface temperature (SST) (RH_s) differences (not shown). More water vapor evaporated from areas with a low RH_s and a higher isotopic composition than from relatively high RH_s water bodies region. Through vertical mixing, surface water vapor isotopes can be significantly affected by different oceanic sources. Based on the tagging experiments, the observed seasonal cycle of $d_v - excess$ (Table 3.2) can also be explained by the seasonal change in the primary marine moisture sources. As shown in Figure 3.1, the highest $d_v - excess$ occurred in winter, while the lowest occurred in summer. Because moisture was generated under conditions with a high relative humidity in summer (not shown), evaporated water tended to have a lower $d_v - excess$. On the other hand, the high $d_v - excess$ resulting from strong kinetic effects corresponded to low relative humidity and strong evaporation (Figure 3.7) above the ocean in DJF. These results were consistent with the negative correlation between $d_v - excess$ and relative humidity observed above the ocean [*Uemura et al.*, 2008; *Dansgaard*, 1964; *Benetti et al.*, 2015, 2014].

The $IsoGSM$ simulation suggested that the mixing of air from multiple sources was likely a major factor controlling the water vapor isotopic variation at our study site on non-rainy days. To identify the source of atmospheric moisture and its transport pattern, we briefly describe the theoretical framework for interpreting paired isotope ratios and specific humidity established by *Noone* [2012]. The framework, composed of a set of simple processes, enables the use of isotopic data to identify the hydrological process under idealized atmospheric conditions. We used two processes in the framework: 1) Rayleigh distillation curves (case b in *Noone* [2012], hereafter RC), representing a pseudoadiabatic process based on oceanic temperatures, with an initial δD value of -80‰ (approximating the δD_v value in equilibrium with that evaporated from the ocean) in an open system, and 2) a mixing line (hereafter ML), which represents a special case when the source water

is the infinite reservoir of vapor in thermodynamic equilibrium (i.e., saturated) with the ocean surface (case e in [*Noone*, 2012]). We plotted daily mean of δD_v as a function of specific humidity (q) for each season. As shown in Figure 3.11, the moistening process (increasing q) acted to enrich water vapor isotope ratios. During the winter season (DJF), q generally varied from 2 to 10 g/kg. δD_v was clustered tightly around the mixing line, suggesting a mixing of marine moist air and a dry air mass. This supports the idea that in general, cold northerly winds transport water vapor that originates from the Japan Sea to our site (Figure 3.9). Outside of the winter season, q varied over a wide range ($2 < q < 25$ g/kg), while δD_v fell in the range between the RC and ML. ET might be one of the factors pulling data points away from the evaporation line. However, most data points were more depleted than -80‰, suggesting a negligible impact of ET on δD_v variation (most of the time, ET tends to increase δD_v [*Risi et al.*, 2010]). Local moisture at our site was likely a result of combined marine sources in these seasons. The large variability of q and δD_v was related to the mixing of different oceanic sources (Figure 3.9) of distinct isotopic ratios (Figure 3.10). Mixing can occur between several different air masses that deviate from a single curve. Hence, the entire area between RC and ML can be considered a result of mixing [*Galewsky and Samuels-Crow*, 2014a]. The tagging experiment and q-δD_v framework provide consistent evidence that the mixing of multiple moisture sources plays an important role in controlling δD_v variability of this region. In contrast to previous studies those conducted in inland regions [e.g., *Lee et al.*, 2006; *Huang and Wen*, 2014; *Welp et al.*, 2008; *Wen et al.*, 2010], our measurements showed that q was a poor predictor of δD_v because of the mixing processes. These results suggest that the common assumption in a Rayleigh distillation model which assmed that water vapor is contributed from a single source, is unable to reproduce the water vapor isotopic variability over a subtropical area. The isotopic variability of water vapor also depends on its air trajectory. In DJF, a lot of vapor is supplied from the Japan Sea, which creates large amounts of snow along the coast of the Japan Sea, resulting in isotopic depleted water vapor and a high $d - excess$. By contrast, in JJA, water vapor was derived from

several adjacent oceans, with high humidity and a low evaporation rate, which resulted in an enriched isotopic signature and low $d_v - excess$. Being different from those inland area, water vapor source area is very close to our site, the removal of heavy isotopes from water vapor by Rayleigh distillation processes (moisture recycling) is insignificant. On the other hand, large differences of δD_v at 850 hpa level from different areas were clearly observed in each season (Figure 3.12). Thus, we believe source origin of water vapor, rather than physical processes along an air mass moving trajectory, is the primary control of water vapor isotopic variation. We also noted that some of the δD_v values in the wet season were lower than those predicted by RC. These data can be explained by shallow dry convection. Strong shallow dry convective activity generates water vapor δD_v below the Rayleigh curve, in a process known as the isotope amount effect [*Galewsky and Samuels-Crow*, 2014a,b; *Bony et al.*, 2008]. However, more evidence is required to confirm this. Moreover, daily measured $d - excess$ vs. $IsoGSM$ estimated RH_s from the source regions (10×10 degree averaged) was plotted (Figure 3.13). A negative correlation similar with *Steen-Larsen et al.* [2015] was observed but with an insignificant correlation. The insignificant correlation may be resulted from 1): very rough resolution RH_s (10×10 degree averaged); 2) in this $d - excess$ v.s. RH_s analysis, we assumed only one source in each day. It would raise significant error if the mixing of multiple moisture sources within a day and 3) We also assume that no time delay during water vapor transport (the evaporated oceanic water was transported to our site immediately) because we used RH_s at same day as measured $d - excess$. The slope (-22.77) and intercept (36.0) are also different from *Steen-Larsen et al.* [2015]. Nevertheless, further study should be conducted to understand the relationship between $d - excess$ and water vapor source.

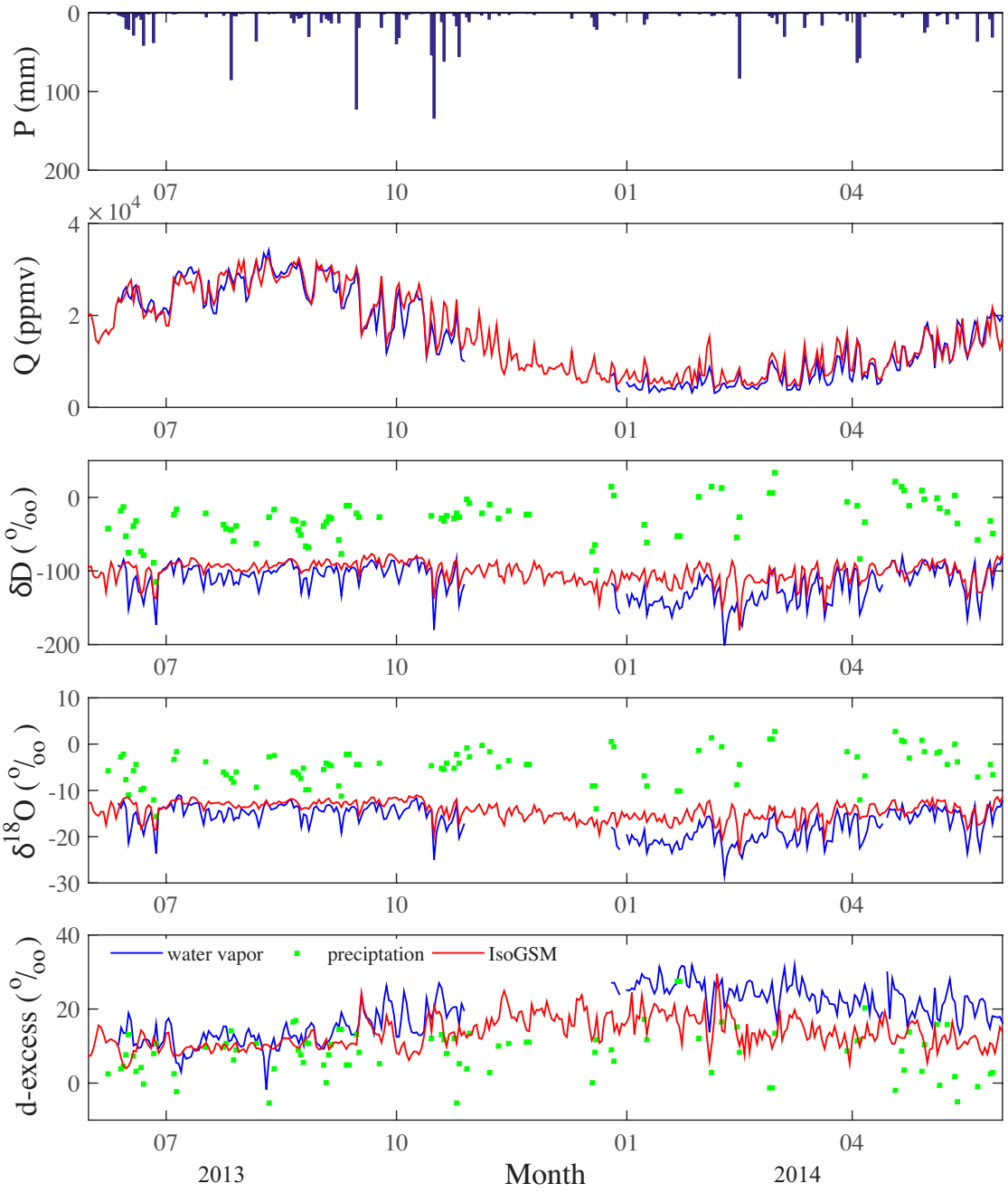

Figure 3.1: Time series of daily observation in precipitation amount (P), vapor mixing ratios (Q), water vapor and precipitation $\delta^{18}O$, δD and $d-excess$ (blue line for water vapor, green square for precipitation). The red lines represent the simulated Q and δ by $IsoGSM$.

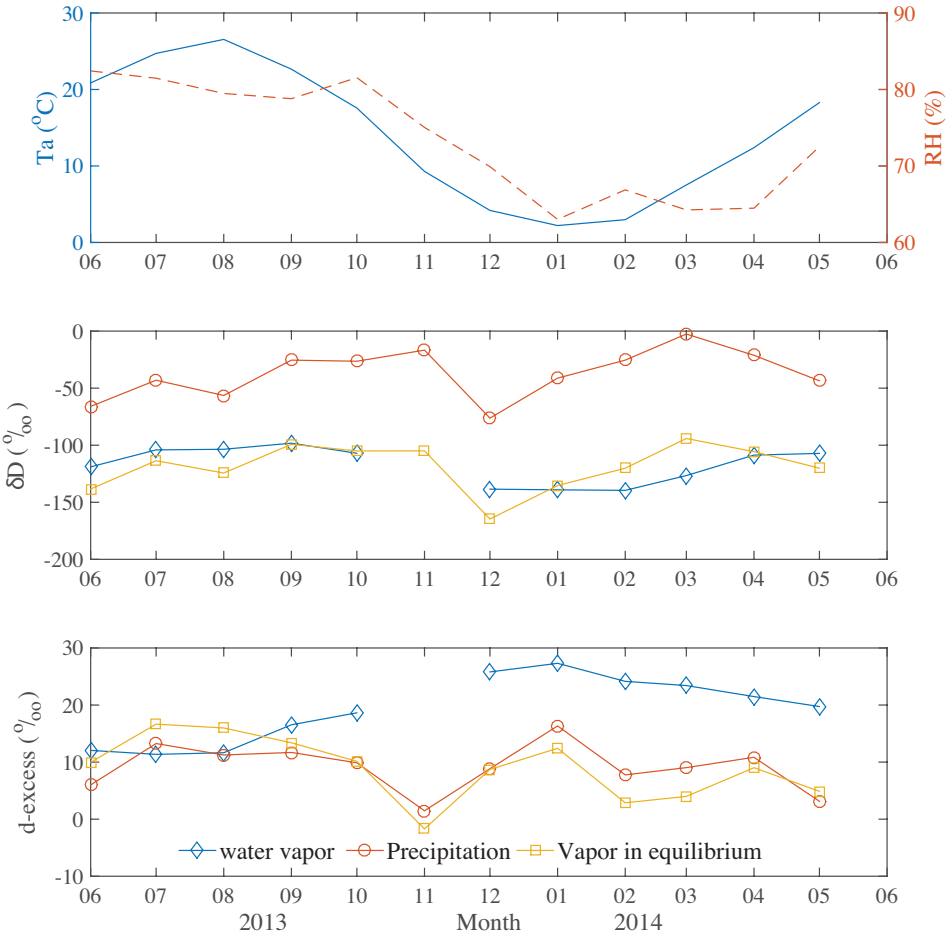

Figure 3.2: Monthly averaged relative humidity (RH, dash), Temperature (T_a, solid), isotope ratio δD, $d-excess$ of water vapor (diamond)and precipitation (circle). Water vapor isotope $\delta D_{v,e}$ and $d_{v,e}-excess$ predicted from precipitation (square) are also plotted.

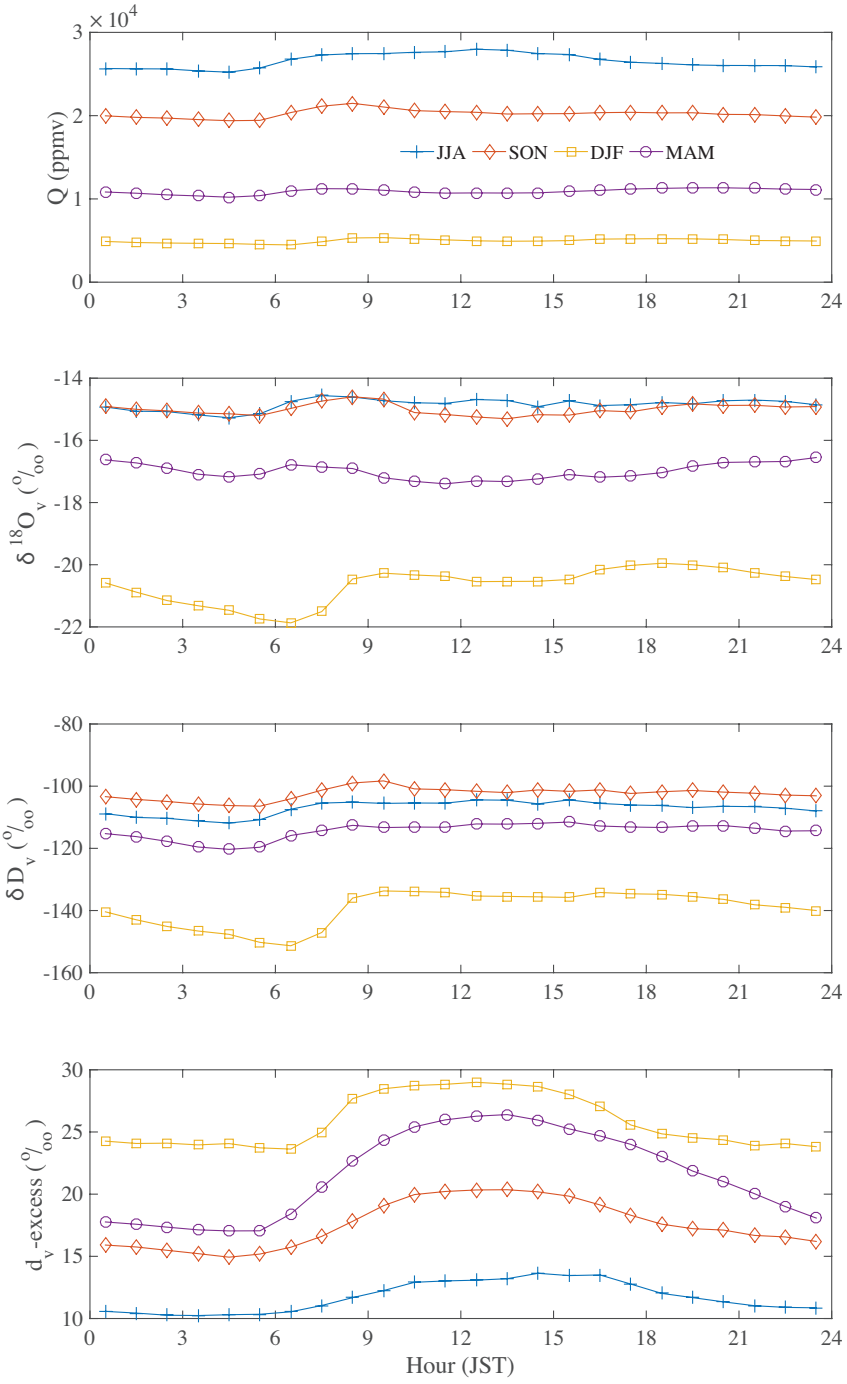

Figure 3.3: Diurnal averaged water vapor mixing ratio, isotope ratio $\delta^{18}O$, δD, $d-excess$ of water vapor.

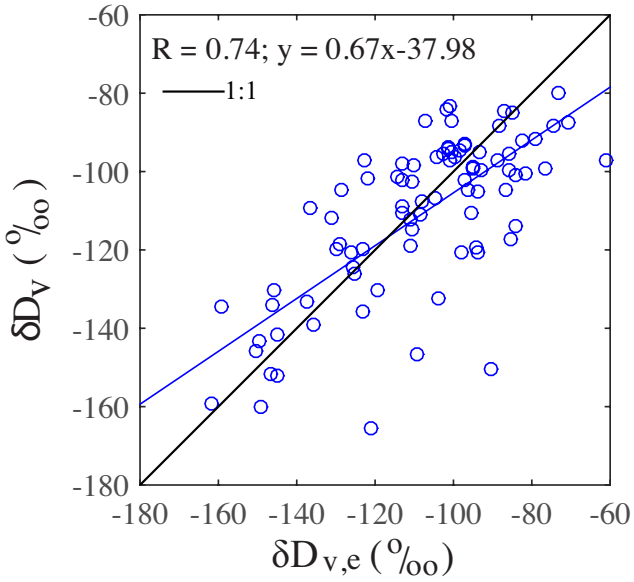

Figure 3.4: Comparison between the observed water vapor δD_v and precipitation predicted $\delta D_{v,e}$. Each point represents a rainy day.

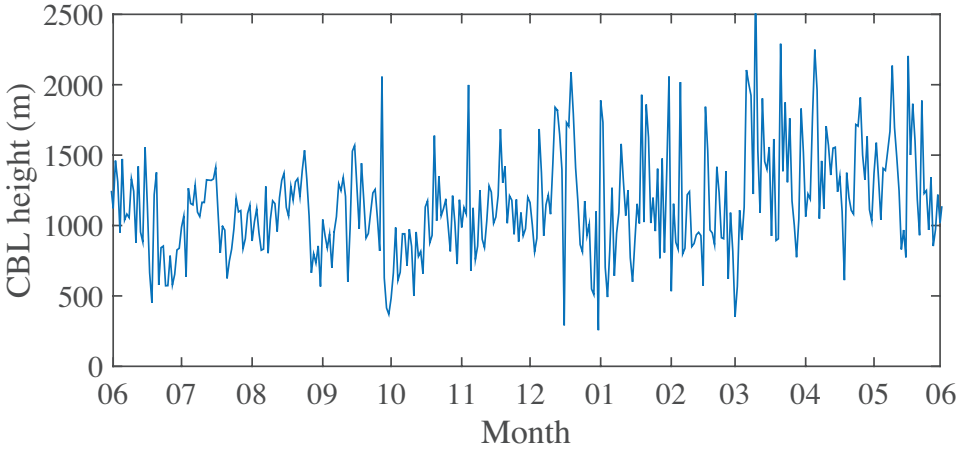

Figure 3.5: Day time CBL height simulated using $IsoGSM$.

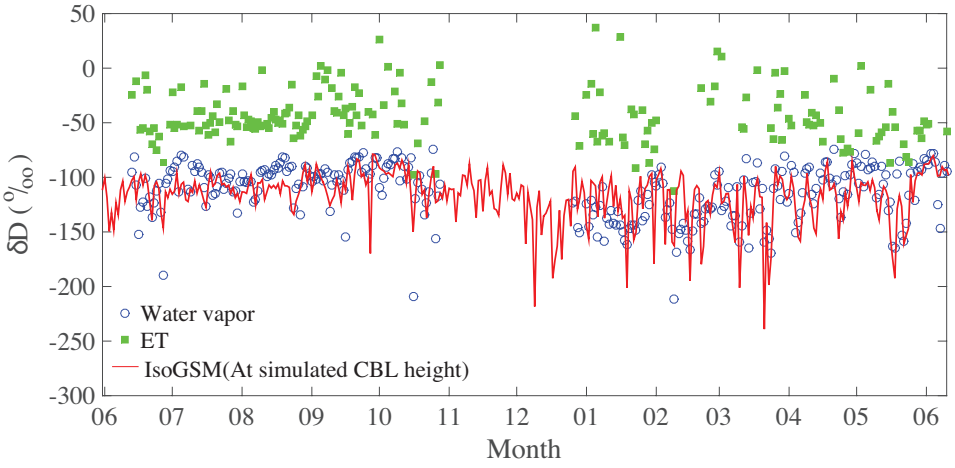

Figure 3.6: Daily variation of isotope ratios of evapotranspiration (green filled square, excluded rainy days), water vapor (blue unfilled circle, excluded rainy days) and background derived from $IsoGSM$ simulation.

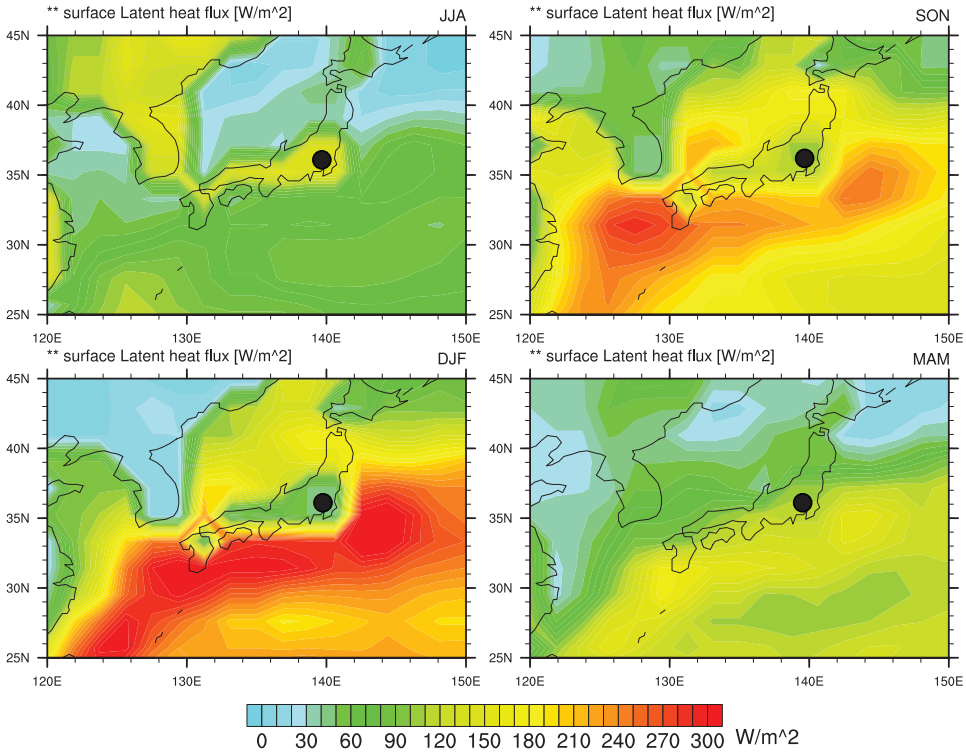

Figure 3.7: *IsoGSM* simulated seasonal mean latent heat fluxes. Black dot shows the study site.

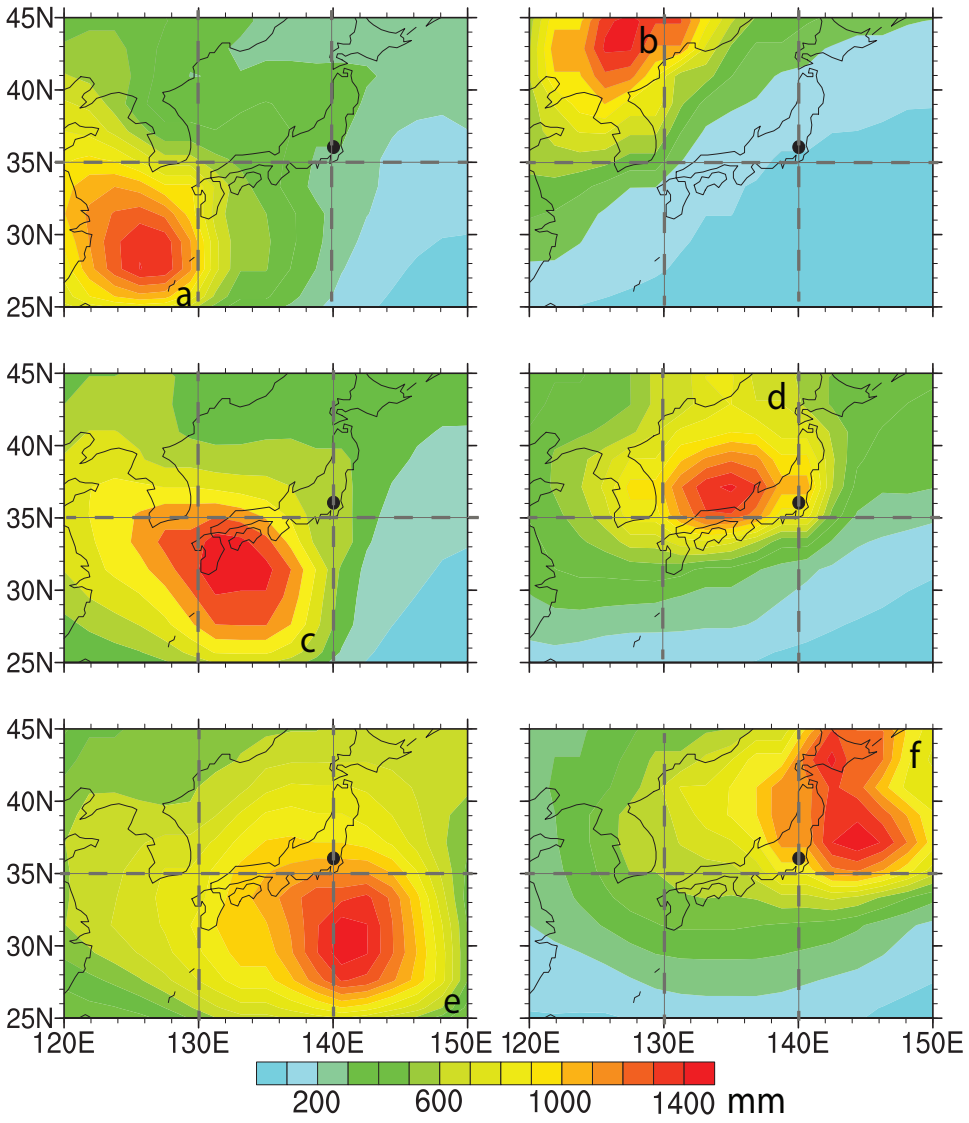

Figure 3.8: The atmospheric column precipitable water contributed from tagged boxes in JJA. Source regions for tagging experiments of water vapor tagged within 10×10 degree boxes (contour): a, 25°N−35°N, 120°E−130°E; b,35°N−45°N, 120°E−130°E; c, 25°N−35°N, 130°E−140°E; d, 35°N−45°N, 130°E−140°E; e, 25°N−35°N, 140°E−150°E; f, 35°N−45°N, 140°E−150°E.

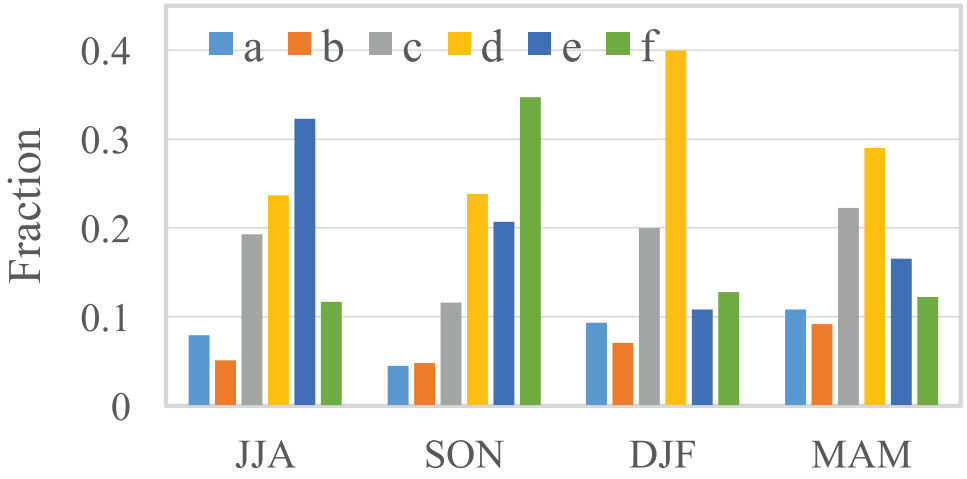

Figure 3.9: The contribution fraction from tagged boxes in JJA, SON, DJF and MAM.

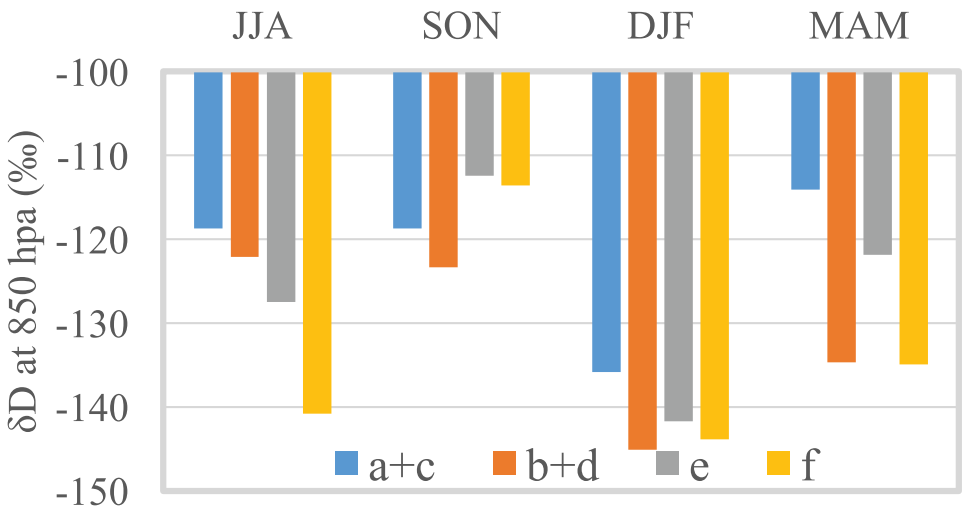

Figure 3.10: 850 hpa isotope ratios documented based on the wind direction (0° to 90°, Area f; 90° to 180°, Area e; 180° to 270°, Area a+c; 270° to 360°, Area b+d).

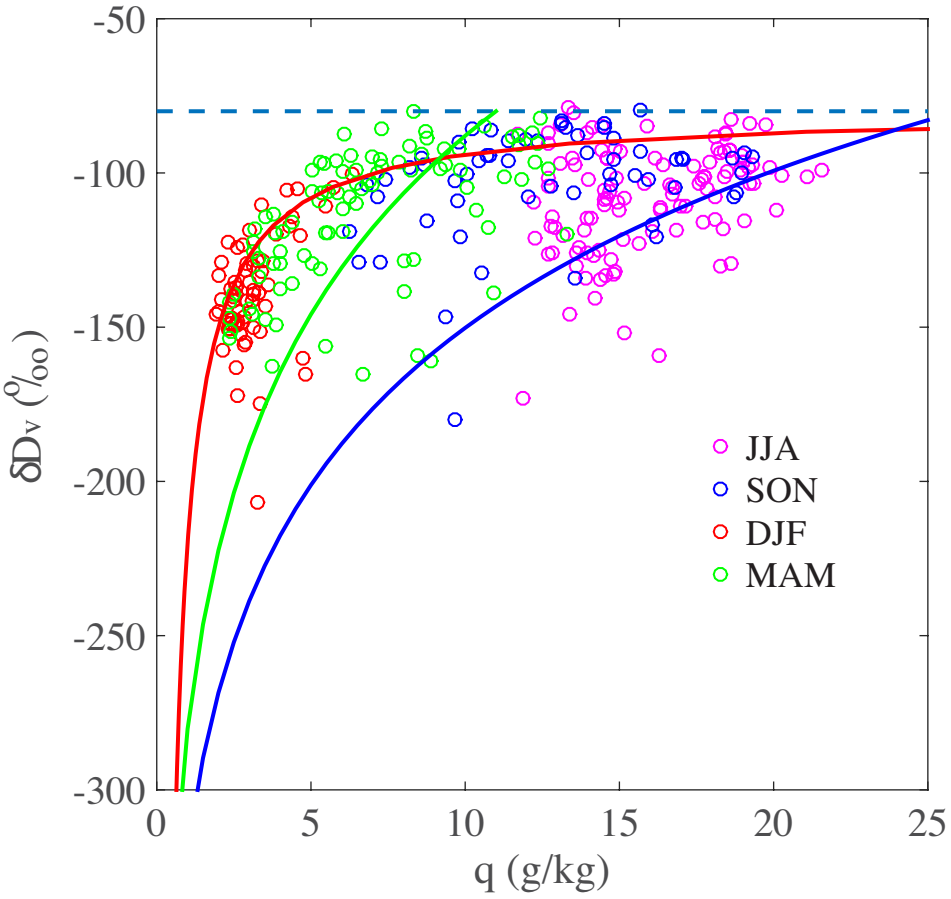

Figure 3.11: The variation of hourly water vapor δD as a function of q for JJA, SON, DJF and MAM. Rayleigh distillation curves representing a pseudoadiabatic process based on oceanic temperatures with an initial δD values of -80‰ (approximate value of vapor in equilibrium with ocean, shown as blue dash line) are shown as green solid line (15 °C) and blue solid line (25 °C). The red line called Evaporation line represents a special case where the source water is the infinite reservoir of vapor that is in thermodynamic equilibrium (i.e., saturated) with the ocean surface.

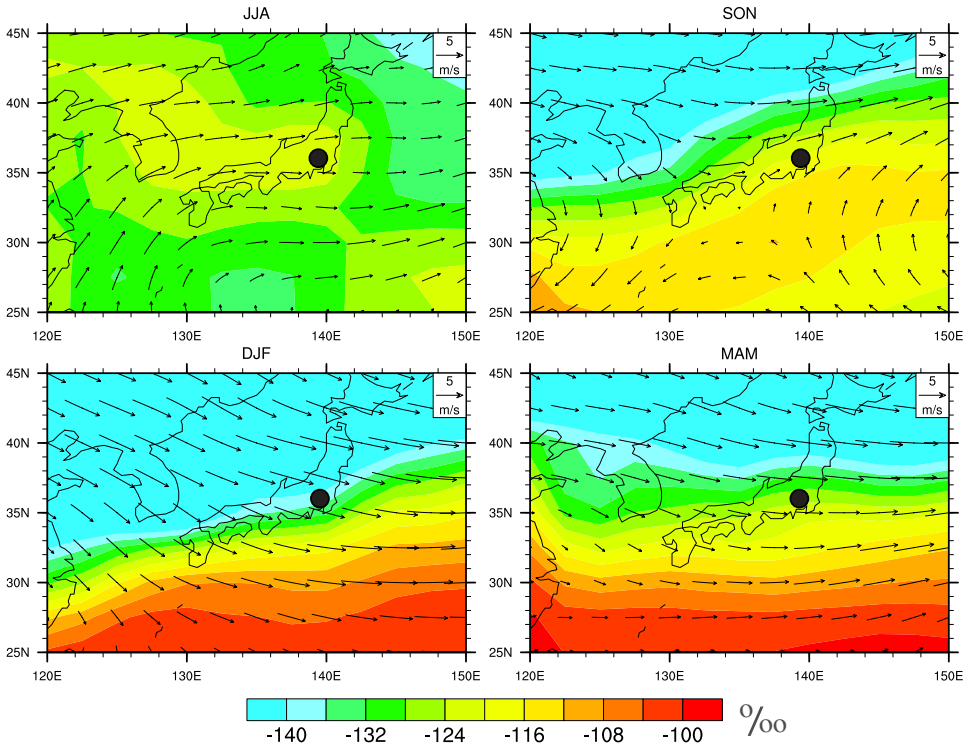

Figure 3.12: *IsoGSM* simulated the wind field and water vapor δD at 850 hpa.

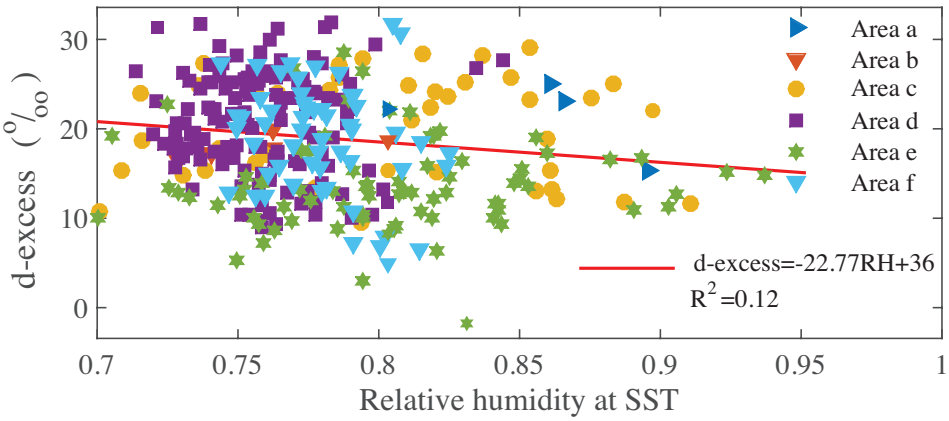

Figure 3.13: Relationship between daily $d-excess$ and RH at SST from the source regions (10×10 degree). Different symbols present water vapor from different source shown in Figure 3.8.

Table 3.1: The linear correlation coefficient R and p-value (a: p-value < 0.001; b: $0.001 <$ p-value < 0.05 and none: p-value>0.05) of hourly isotope ratios (δD, $\delta^{18}O$, and $d-excess$) with observed weather variables (water vapor mixing ratio Q, Relative humidity RH, surface air temperature T_a) for all observed data in each month from June 2013 to May 2014.

		$ln(Q)$			RH			T_a		
Year	Month	δD	$\delta^{18}O$	d-excess	δD	$\delta^{18}O$	d-excess	δD	$\delta^{18}O$	$d-excess$
2013	6	0.36^a	0.33^a	0.05	-0.03	0.01	-0.27^a	0.28^a	0.23^a	0.25^a
2013	7	0.33^a	0.42^a	-0.47^a	-0.14^a	-0.03	-0.36^a	0.35^a	0.34^a	-0.12^b
2013	8	0.41^a	0.48^a	-0.38^a	-0.29^a	-0.19^a	-0.27^a	0.46^a	0.45^a	-0.08^b
2013	9	0.02	0.24^a	-0.72^a	-0.15^a	0.08^b	-0.70^a	0.10^b	0.17^a	-0.25^a
2013	10	0.44^a	0.55^a	-0.59^a	0.06	0.15^a	-0.46^a	0.40^a	0.45^a	-0.29^a
2013	12	0.89^a	0.86 a	0.38^a	0.70^a	0.68^a	0.32^b	0.52^a	0.51^a	0.19
2014	1	0.49^a	0.50^a	0.01	-0.04	0.06	-0.42^a	0.36^a	0.28^a	0.36^a
2014	2	0.43^a	0.47^a	-0.19^a	0.02	0.08^b	-0.37^a	0.40^a	0.40^a	0.05
2014	3	0.65^a	0.68^a	-0.07	0.27^a	0.32^a	-0.20^a	0.41^a	0.41^a	0.04
2014	4	0.59^a	0.59^a	0.06	0.33^a	0.43^a	-0.32^a	0.28^a	0.17^a	0.43^a
2014	5	0.39^a	0.46^a	-0.44^a	0.21^a	0.38^a	-0.79^a	0.13^a	0.02	0.41^a

Table 3.2: Monthly mean values of observed δD, $\delta^{18}O$, and $d-excess$ for atmospheric water vapor, precipitation, and the vapor in Equilibrium with precipitation in Mase, Japan. Meteorological variables (Temperature T_a, Humidity RH, Precipitation amount P and water mixing ratio Q) are also listed. All isotope parameters were presented in ‰.

Date		Vapor			Precipitation			Vapor in equilibrium					
		δD	$\delta^{18}O$	d-excess	δD	$\delta^{18}O$	d-excess	δD	$\delta^{18}O$	d-excess	RH (%)	T_a (°C)	P (mm)
2013	6	-119.0	-16.4	12.1	-66.0	-9.0	6.0	-138.4	-18.5	10.0	82.4	20.9	176.5
2013	7	-104.1	-14.4	11.4	-43.0	-7.0	13.3	-113.6	-16.3	16.7	81.5	24.7	101.9
2013	8	-103.6	-14.4	11.6	-56.4	-8.5	11.3	-124.4	-17.5	16.0	79.5	26.6	102.0
2013	9	-98.2	-14.3	16.5	-25.5	-4.6	11.7	-99.2	-14.1	13.4	78.8	22.7	214.9
2013	10	-107.1	-15.7	18.6	-26.4	-4.5	9.9	-105.0	-14.4	10.1	81.5	17.6	432.9
2013	11	-	-	-	-16.69	-2.27	1.47	-104.92	-12.90	-1.70	75.0	9.3	18.6
2013	12	-138.5	-20.5	25.8	-76.3	-10.6	8.9	-164.7	-21.7	8.7	69.9	4.2	53.0
2014	1	-139.1	-20.8	27.3	-41.2	-7.2	16.3	-135.3	-18.5	12.4	63.0	2.2	26.6
2014	2	-139.6	-20.5	24.2	-25.4	-4.2	7.8	-120.2	-15.4	2.9	66.9	3.0	103.7
2014	3	-126.6	-18.8	23.4	-2.6	-1.5	9.0	-94.1	-12.3	4.0	64.3	7.5	93.0
2014	4	-108.7	-16.3	21.5	-21.2	-4.0	10.9	-105.6	-14.3	9.0	64.5	12.4	157.3
2014	5	-107.2	-15.9	19.7	-43.6	-5.8	3.1	-120.1	-15.6	4.9	72.5	18.3	118.3

Table 3.3: The contribution of evapotranspiration (F_{ET}) to that of the ABL water vapor estimated from monthly water vapor δD, background isotope ratio δ_{bg} and evapotranspiration isotope ratio δ_{ET}. Data from rainy days, data of latent heat $LE < 50$ W/m^2 and daily $F_{ET} < 0$ data were excluded. All isotope parameters presented in ‰.

Year	Month	δD_v	δ_{bg}	δ_{ET}	F_{ET}
2013	6	-99.6	-109.7	-56.9	19.2±14.0%
2013	7	-96.3	-111.1	-45.7	22.7±13.6%
2013	8	-97.8	-110.3	-46.8	19.7±11.1%
2013	9	-92.8	-107.4	-31.0	19.1±12.5%
2013	10	-89.7	-94.6	-36.3	8.4±10.6%
2013	11	-	-	-	-
2013	12	-	-	-	-
2014	1	-148.7	-149.7	-91.7	0.2±13.1%
2014	2	-124.3	-143.6	9.7	12.6±13.4%
2014	3	-115.2	-123.8	-49.5	11.6±8.3%
2014	4	-106.4	-124.5	-51.8	24.9±12.7%
2014	5	-117.2	-131.1	-62.5	20.2±14.2%

Chapter 4

ET partitioning over a paddy field

4.1 Estimation of δ_{ET}, δ_T, and δ_E

Hourly variations in δ_{ET} were estimated using the Keeling plot method. We selected hourly data whenever there were sufficient data points ($N > 40$) with a high coefficient of determination ($R^2 > 0.8$) for each linear regression, as shown in Figure 4.1. Several difficulties with the Keeling plot approach were found. Some of the calculation results did not satisfy the threshold of $R^2 > 0.8$. As a result, only 24% of the observed period could be used in our study. The results were divided into daytime (8:00−17:00) and nighttime (18:00−7:00). Daytime observations in the whole growing season were further divided into two periods, namely early (May to June) and late growing seasons (July to August). In the early growing season, δ_{ET} gradually increased with time because the dominance of evaporation resulted in significant heavy isotope enrichment of residual waters. In the late growing season, δ_{ET} mainly consisted of transpiration and was closely coupled with surface water. A possible reason was that isotopic fractionation through transpiration was much smaller than evaporation. It can be seen from Figure 4.1 that ambiguous changes in δ_{ET} during nighttime were frequently observed. Due to the weak nighttime turbulence conditions, the intercept parameter of the Keeling plot (even $R^2 > 0.8$) was generally an ambiguous quantity when the change in specific humidity was insufficient [*Lee et al.*, 2006].

This suggests that improving the estimation of δ_{ET} is an important objective in future studies, especially under low-evapotranspiration conditions, such as those experienced in semi-arid and arid areas. Due to the unreliable δ_{ET} at nighttime, we only considered daytime data in this study.

The water used for irrigation in the field was derived primarily from large storage reservoirs. The irrigation water used in the field had a stable isotope composition (δD) of approximately -47.46±6.50‰ and was relatively constant throughout the whole growing season. We used an average value for all sampling points due to the uncertainties induced by the uneven distribution of surface water isotope ratios. Figure 4.2 demonstrates that the spatially averaged pond water δD showed a general decreasing trend from May to June with considerable variability and then remained constant after June. The surface water was evaporating constantly in May and June, but then, there was a gradual shift to a transpiration loss. The δD of surface water decreased from -21.75‰ (May) to -33.22‰ (June) due to a change in the source of the water loss (shift from E to T) with large variability during this period. As the rice crop emerged and dense stands of plants were established after June, water in the ponded fields became less enriched in δD (-45.30‰). Large standard deviation in each measurement day in the early growing season indicated a significantly uneven spatial distribution of surface water isotope ratios (more enriched in outflow site because water evaporated for a longer time period during its flow from the inflow to outflow sites). In the late growing season, however, the dominance of transpiration might result in isotope ratios that were similar to those in the irrigation water (small deviation).

It was assumed that the δD value of transpiration was the same as that of collected surface water in this study. However, the NSS might increase the uncertainty in our estimation. We therefore selected data of mid-day (11:00−15:00) to guarantee the SSA satisfied. We assumed the rice plant can reach a SSA state in this time period because 1) We compared diurnal variations in δ_{ET} in the late growing season (July and August in 2013) and the non-growing season (September and October in 2013) that were shown

in Figure 4.3. During the late growing season, daytime δ_{ET} (8:00−17:00) did not vary significantly and was similar to that of the surface water (-43.15‰ for δ_{ET} and -45.30‰ for surface water on average), implying little isotopic fractionation during the water-exchange process, which supported the SSA. Compared with that in the late growing season, the variations in the diurnal δ_{ET} had larger amplitude due to the lack of transpiration after harvest. This demonstrated that the assumption of an isotopic steady state might be satisfied in the daytime. 2) Many studies found the SSA is satisfied in midday time [*Lai et al.*, 2006, 2008] because the magnitude of transpiration related to the volume of leaf water is large during mid-day. 3) The SSA is satisfied when the ratio of transpiration to leaf water volume is small (short turnover time of leaf water), which has been shown in shorter canopies [*Yakir and Wang*, 1996; *Lai et al.*, 2006, 2008]. Furthermore, *Lai et al.* [2008] showed that turnover time of leaf water is shorter under wet condition. On the other hand, based on the measured surface water and water vapor isotopes, the hourly δ_E could be estimated using the Craig and Gordon Equation (see sect. 2.2.3).

4.2 ET partitioning and its environmental control

We partitioned evapotranspiration on a daily averaged basis for a full growing season because the surface water measurements were temporally too coarse to provide a realistic description at a smaller scale, i.e., a diurnal time scale. Those sub-data sets that did not satisfy the criteria were removed from the near-continuous data set for a full growing season. To provide an accurate and representative result, the criteria for the data removal was (i) data measured on a rainy day were rejected, (ii) data measured outside the mid-day (11:00−15:00) period were rejected to avoid possible uncertainty due to NSS, and (iii) data acquired with a low coefficient of determination for each linear regression in the Keeling plot method ($R^2 < 0.8$) were excluded to maintain a high-quality δ_{ET} estimation. Since 72% water evapotranspired during the selected time period, it would not make significant bias in long-duration ET partitioning. The selected data was averaged on

a daily timescale, and was plotted in Figure 4.4. Isotopic ratios varied from -83.48 to -14.64‰ for δ_{ET}, -48.58 to -4.63‰ for δ_T, and -422.81 to -49.33‰ for δ_E. δ_E, δ_T, and δ_{ET} were similar during the early growing season; δ_{ET} and δ_T were less negative than δ_E and very similar during the late growing season; and δ_E displayed a decreasing trend during the full growing season. The mean contribution of transpiration to evapotranspiration estimated by Equation 2.5 was shown in Figure 4.5 as a function of time. The T/ET ranged from 0.2 to 1 and increased almost continuously in May and June, but then became relatively constant, with a value close to 1. The total uncertainty estimated by Equation 6 (also see sect. 4.1) and shown as a vertical bar in Figure 4.5, ranged from 0 to 0.8. Unexpectedly, T/ET on some days was over 1 or less than 0. This can be explained by the coarse resolution of surface water sampling, neglect of the leaf interception evaporation, and the measurement errors in δ_{ET} (see sect. 4.1). We excluded unreliable data (T/ET > 1.2 and $T/ET <$ -0.2; about 7% of the data used in Figure 4.5 were excluded) because they were clearly inaccurate and differed from the surrounding T/ET results. Because both underestimation and overestimation occurred, some of the errors tended to cancel out through averaging, and we therefore did not exclude data with an acceptable error ($1 < T/ET < 1.2$ or -0.2 $< T/ET < 0$). The monthly T/ET values during the growing season were 0.47, 0.78, 0.98 and 0.94 from May to August (Figure 4.5), respectively. The monthly T/ET variation can be seen in Figure 4.5 to be in the same phase as the variation of LAI in Figure 2.2. The averaged daily change in T/ET was represented quite well as a function of a 0.5-bin averaged LAI ($FT = 0.67LAI^{0.25}$, $R^2 = 0.80$), implying that vegetation plays a major role in driving the contribution of E and T. E played a large role in the early growing season while T dominated the later stage (Figure 4.7). Furthermore, it is suggested that a crop parameter such as LAI can be an effective alternative for the estimation of T/ET over a paddy field.

4.3 The error analysis

The results demonstrated the robustness of using isotope measurements for partitioning evapotranspiration. However, there were some uncertainties in our estimation. Potential uncertainty derived from neglecting the leaf interception evaporation in Equation 2.7 should have been taken into account, because the rainfall events occurred frequently during the observation period (Figure 4.2). The neglect of interception could be the cause that T/ET is higher than 1 during the late growing season if the interception evaporation isotope ratio is lighter than δ_E. Unfortunately, the interception losses are difficult to estimate in general. As shown in Figure 4.5, the T/ET uncertainty is large in some data used in our estimation. This uncertainty in the results of this single-isotope two-source mixing model is directly related to the uncertainty in all three of the terms: δ_{ET}, δ_T, and δ_E. The uncertainty therefore was estimated by Equation 2.8. It was assumed that the values of $\sigma_{\delta_{ET}}$ and σ_{δ_E} are the standard deviations of δ_{ET} and δ_E for each day, and the value of σ_{δ_T} is the standard deviation of δ_T of the spatial distribution on each measurement day. In addition to excluding the days where T/ET was higher than 1.2 or less than -0.2, we further excluded days where only one measurement of δ_T and less than 3 hours' highly accurate δ_{ET} estimation were available for each day. The average uncertainty in δ_{ET} was about 9.06‰. This uncertainty was smaller than the average uncertainty in δ_E (14.27‰), but larger than δ_T (5.79‰). The average uncertainty in T/ET was estimated as 14±10%. As shown in Figure 4.6, the uncertainty of δ_E was less important than that of the other two parameters throughout the study period, although a high average uncertainty value was obtained. The ET partitioning uncertainty was derived from the uneven spatial distribution of surface water isotopes (δ_T), with levels generally decreasing with increased T/ET. As T/ET increased, the impacts of the Keeling plot δ_{ET} uncertainty become much larger than that of δ_T and δ_E. This result is consistent with δ_T measurements. During the early growing season, δ_T was quite variable, whereas δ_{ET} was more poorly quantified than δ_T during the late growing season (Figure 4.4). This suggests that further improvement in the estimation of δ_T and δ_{ET} is necessary for partitioning evapotranspiration using the

isotopic method. It is noted that about 80% of the data have T/ET values above 0.75 because rice is a fast-growing plant (Figure 2.2). To partition evapotranspiration under low LAI conditions, more observations are necessary.

The uncertainty analysis mentioned above is a statistical analysis based on the assumption that source and end members are independently measured. The inherent errors in the estimation methods of δ_E, δ_T, and δ_{ET} should also be considered. In the estimation of δ_{ET}, the Keeling plot approach is robust when combined with high-temporal-resolution data [*Good et al.*, 2012]. However, that only 24% data ($R^2 > 0.8$) can be used in our study suggested the assumptions underlying the Keeling plot method are rarely met perfectly in nature. Even a high R^2 value can be obtained, the error in δ_{ET} estimation in some cases can still be quite large (e.g., under weak latent heat conditions). For example, *Lee et al.* [2006] reported that if the change in the range of the water mixing ratios was inconspicuous, the error would increase dramatically. To understand the uncertainty associated with the measured water vapor mixing ratio and isotopic composition, uncertainty assessments following *Good et al.* [2012] (Equation 16) were performed on 1-hr estimation of δ_{ET}. A significant uncertainty of δ_{ET} was found (22.05±12.14‰, excluding the data (41%) with uncertainty lager than 50‰). If we consider this uncertainty in $\sigma_{\delta_{ET}}$, the average uncertainty in T/ET would increase to 24±15% and 88% of this uncertainty is attributed from $\sigma_{\delta_{ET}}$. However, we believe the bias in δ_{ET} may be much smaller and may be cancelled out through averaging because we did not find a large variability of daily averaged δ_{ET} in the late growing season (Figure 4.4). We also found the uncertainty of δ_{ET} showed a similar variation with std$Q$ (Figure 4.8). The highest uncertainty can be found in mid-night and the lowest uncertainty of δ_{ET} can be found in mid-day. The result is that the turbulent is weakest at midnight and resulted a high uncertainty. We can found the standard deviation of water vapor mixing ratios in lower in nighttime. We confirmed that if a change in the range of the water mixing ratios were inconspicuous, the error would increase dramatically, which is suggested by *Lee et al.* [2006]. Therefore the reason of the lowest $\sigma_{\delta_{ET}}$ values during the 10-15 h window is that the uncertainty is

lowest during this time scale. On the other hand, we find when changes in the range of the water mixing ratios were inconspicuous, most of time $\sigma_{\delta_{ET}}$ tended to have a positive value. A similar trend has been observed by *Welp et al.* [2008]. The reason is still not clear. A further study thus should be conducted.

In addition to the uneven distribution of surface water isotopes mentioned in section 4.3, measurements of the time resolution of surface water isotopes should also be considered. Our measurements of the isotopic composition of transpiration were obtained through direct measurement of surface water and were assumed to be constant until the next measurement. Although the surface water isotope levels were consistent throughout the late growing season (since transpiration does not enrich the residual water), they changed significantly in the early growing season (Figure 4.2). For example, surface water δ_D in June 2 was much higher than that measured in May 29, 2014. During the early growing season, the residual water isotope was sensitive not only to plant cover but also to water amount (data is not available) and evaporation rate in the field. Assume the same T/ET in these two days, a higher daily averaged ET in June 2, 2014 (430 W/m^2) than in May 29, 2014 (298 W/m^2) might result in a more enrich surface water δD in June 2, 2014. To reduce the uncertainty, we therefore increased the surface water observation frequency in May and June 2014 (from 1.5 days per week in 2013 to 3 days per week in 2014). Furthermore, although the input water seemed to have a stable isotope ratio, the surface water sometimes received precipitation between two surface water measurements, resulting in a significant bias in the estimation of δ_T. For example, input from precipitation may play a significant role in determining surface water isotope during May and June 2013 (Figure 4.2). An additional observation has been done to understand the impact of precipitation, in which we observed the surface water δD in daily basis from August 11 to August 16, 2014. During the observation period, two precipitation events were observed (9.7 mm, 16:00−23:00 in August 12 and 3.9 mm, 16:00−17:00 in August 14). We did not find a significant change of surface water δD in the day after precipitation (-48.18±0.97‰ for the whole observation period). The possible reason was that

the pond water was refreshed by abundant input water and then showed a similar δD value with input water δD. Although this result suggests that rainfall does not have a significant influence on surface water isotope, it should be noted that this test was under a short period where only 2 small rainfall events occurred. The cause of changes in isotopic values in surface water may be confounded by the storm size, precipitation isotope value, surface water amount and so on. Nevertheless, frequent precise isotopic measurements of surface water are necessary especially during the early growing season. Further uncertainty derived from SSA assumption should also be considered. We did not measure the δ_T directly but assumed δ_T equal to surface water δD. The surface water might be enriched by evaporative enrichment compared to the root absorbed water from soil. However, we believe it would not induce a large error because of the well mixing of surface water and soil water under the flooded conditions. The soil water (Soil Water Sampler, DIK-8392, Japan) and surface water sampled on April 9, 2014 (the second day after a heavy rain, the field was flooded) showed a similar δD (-33.22‰ for soil water and -31.55‰ for surface water, without vegetation and irrigation). The NSS was neglectable in our long-duration T/ET estimation. Even given a high uncertainty raised by NSS ($\pm$10‰) in δ_T, it would not make a significant bias in our long-duration T/ET estimation (averaged T/ET uncertainty was estimated as 16$\pm$8.41%). For most of the time, T/ET was sensitive to δ_E rather than δ_T and δ_{ET} in Equation 2.7, because δ_E was significantly lower than δ_T and δ_{ET} (Figure 4.4). On the other hand, under low T/ET condition or on diurnal time scale, the NSS should be considered seriously. Nevertheless, a further study should be conducted on NSS impact on T/ET estimation. As shown in Equation 2.5, δ_E is controlled by several parameters. The uncertainty can either come from measurement errors or parameter selections. Measurement errors such as the uncertainty in surface water isotopes can significantly affect the accuracy of δ_E estimation. In addition to measurement errors, the choice of the kinetic fractionation factor ε_K is also important. In this study, D_i/D was taken as 0.9839 from *Cappa et al.* [2003], and $n = 0.67$ was taken from *Kim and Lee* [2011] in Equation 2.6. Furthermore, values of $D_i/D = 0.9755$, and n

= 1 are also widely used [*Gat*, 1996]. We tested the influence of these values on the T/ET, and the results were shown in Figure 4.9. Although there is no obvious difference in the high-T/ET period, the influence of this selection cannot be neglected in the low-T/ET period. Unfortunately, there is still no agreement on the selection of ε_K. Different values of ε_K are still in use for the purpose of δ_E estimation [e.g., *Braud et al.*, 2005, 2009a,b; *Dubbert et al.*, 2013, 2014b; *Mathieu and Bariac*, 1996; *Rothfuss et al.*, 2010], although this value may significantly affect ET partitioning from a vegetative surface with a low LAI. Generally, it was less important than δ_T and δ_{ET} in our study because the LAI was relatively high most of the time ($LAI > 1$).

In summary, to reduce the uncertainty in evaluating T/ET, it was necessary in our study to concentrate on the estimation of two parameters: δ_T and δ_{ET}. 1) With regard to δ_T, recent improvements have occurred in the temporal resolution at which surface/soil water samples can be collected and analyzed [*Pangle et al.*, 2013]. Incorporating these with a high frequency of water vapor isotope measurements will offer an extremely precise and quantitative insight into the partitioning of evapotranspiration. Moreover, the NSS should also be conducted in further study especially at the diurnal time scale. Recent studies showed that T/ET at diurnal time scale is significantly affected by non-steady state of transpiration [e.g., *Dubbert et al.*, 2013, 2014a,b]. 2) With respect to δ_{ET}, we suggest that dual-level measurements of isotopes should be made at the same time. Estimating δ_{ET} using the flux gradient relationship [e.g., *He and Smith*, 1999] has been found to decrease the uncertainty of this estimation [*Good et al.*, 2012].

4.4 Comparison with other studies

Several studies based on indirect methods such as the water isotope balance, or model simulations have been done because no direct measurements are available for partitioning evapotranspiration over a paddy field [e.g., *Kondo and Watanabe*, 1992; *Maruyama and Kuwagata*, 2010; *Simpson et al.*, 1992]. For example, *Simpson et al.* [1992] found that tran-

spiration accounted for about 60% of total losses to the atmosphere using a stable isotope mass balance based on a water budget (i.e. irrigation inflow + precipitation = evaporation + transpiration + infiltration). However, it was based on coarse measurements and without the consideration of the outflow and groundwater recharge in the water balance. This may result in a significant error in the water budget. By coupling land-surface and crop growth models, *Maruyama and Kuwagata* [2010] suggested that T/ET was about 45% during the rice growth period. The average T/ET from our results (80%) was higher than that reported in these studies. To compare with our ET partitioning result, a crop growth model [*Maruyama and Kuwagata*, 2010] coupled two-source model was developed (Detail can be found in Appendix.). The monthly averaged T/ET estimated from simulated T and measured ET during the growing season was similar to isotope-based estimation (0.24, 0.86, 0.93 and 0.84 from May to August (Figure 4.5), respectively). In daily time scale, high variability could be found in later growing season. This high variability might be attributable to the insufficient consideration and large uncertainty of parameters such as canopy resistance, which were not measured and validated. It highlights the simplicity and versatility of isotope-based method in long-duration T/ET partitioning. The parameters in this method can be easily determined by water vapor and soil isotope measurements. δ_E was estimated from the Craig and Gordon Equation and δ_{ET} can be determined by the Keeling plot. Over days to weeks timescales, δ_T can be assumed as soil water isotope ratios, because mass balance requires the isotope composition of the source water be equal to that transpired back to the atmosphere [*Griffis et al.*, 2011]. Compared to isotope-based methods, the simulation is difficult to apply to different vegetation cover since it is highly affected many factors such as radiation, air temperature, air humidity, wind, soil water content, crop characteristic, etc (also see Appendix). For cultivated land, the crop development stage, environment, irrigation practice, and crop management also strongly influence the transpiration rate [*Sutanto et al.*, 2014]. Compared to direct measurements of E and T, the problem of scaling up from leaf-level to canopy-scale in hydrometric methods diminishes when isotope-based is applied. On the

other hand, as mentioned above, it is still a great challenge in isotope-based study to determine the isotope ratios of ET, T and E.

In practice, it is difficult to partition ET at regional or global scale because of the lack of detailed data [*Hu et al.*, 2009]. However, we demonstrated that T/ET could be well described by a function of LAI. This suggests that LAI could be used to partition ET in spatial studies, as LAI can be easily obtained through both in situ observations and remote sensing techniques. Many previous studies identified a relationship between T/ET and LAI [e.g., *Hu et al.*, 2009; *Wang et al.*, 2010]. Recently, *Wang et al.* [2014] reviewed the published studies (48 individual publications) that measured at least two of the three components (E, T, and ET) and LAI simultaneously in an attempt to establish a quantitative relationship between ET partitioning and LAI for different systems (i.e., agricultural versus natural systems) and to explain the variations in observed T/ET at the global scale. Nonlinear relationships between T/ET and LAI were identified for both agricultural ($T/ET = 0.91LAI^{0.07}$) and natural ($T/ET = 0.77LAI^{0.10}$) data subsets, suggesting the feasibility of using LAI information to generate a global-scale T/ET data set. Our results generally agree with the global scale nonlinear relationships in *Wang et al.* [2014], but tend to have a slightly lower proportion of transpiration under low-LAI conditions (Figure 4.7). Estimations at both the global scale and local scale (this study) show that even under low-LAI conditions (e.g., $LAI = 0.5$), T/ET could have a very high value (0.72 and 0.90 for natural and agricultural systems in global estimations, respectively, and 0.58 in our study). *Wang et al.* [2014] suggested the possibility of a high proportion of water use by vegetation even under low-LAI conditions. However, as mentioned in section 3.1, the error under low-LAI conditions may also lead to a significant uncertainty with respect to T/ET. Nevertheless, LAI could be a useful tool to understand the contribution of transpiration water fluxes to continental evapotranspiration and to reduce the simulation uncertainty in water recycling circulation, which has been demonstrated in previous studies [e.g., *Hu et al.*, 2009; *Wang et al.*, 2010; *Wang and Yamanaka*, 2014].

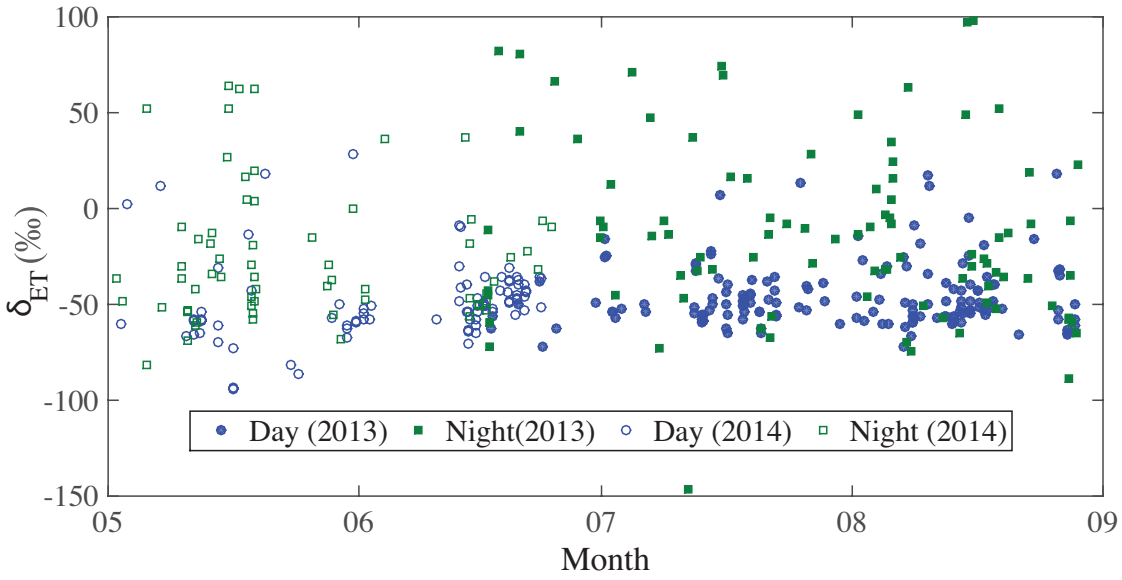

Figure 4.1: Hourly variation in the isotope ratios of *ET* from June to August 2013 and May to June 2014. Blue circles (filled, 2013; un-filled, 2014) indicate daytime data (8:00−17:00), and green squares (filled, 2013; un-filled, 2014). indicate nighttime data.

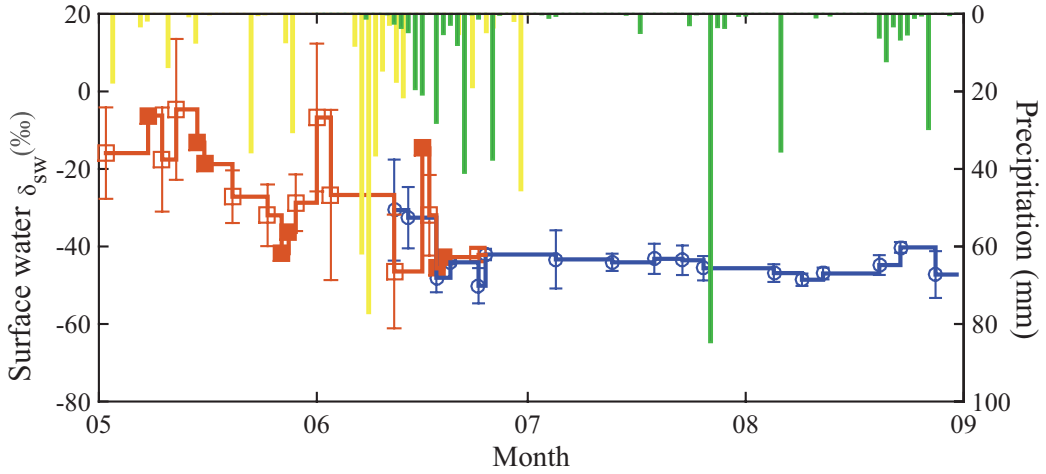

Figure 4.2: Observed δD in surface water from June to August 2013 (blue line) and May to June 2014 (red line). Filled squares with error bars indicate the spatial average values and their standard deviations. Unfilled squares represent the measurement of only one point in 2014. Vertical bars denote daily precipitation amount from June to August 2013 (green bar) and May to June 2014 (yellow bar).

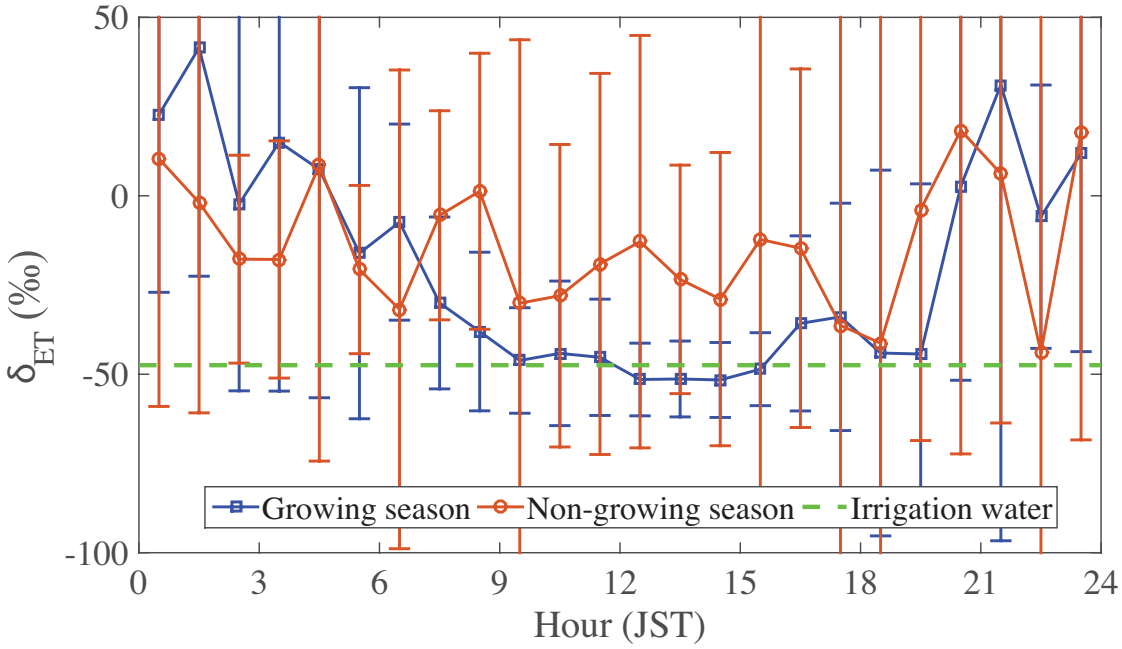

Figure 4.3: Comparison of the ensemble mean diurnal variation in the evapotranspiration δD signal during the growing season (July and August 2013, blue squares) and non-growing season (September and October 2013, red circles). Vertical bars denote the standard deviation for each hour. Green dash line indicates the mean irrigation water δD (-47.46‰).

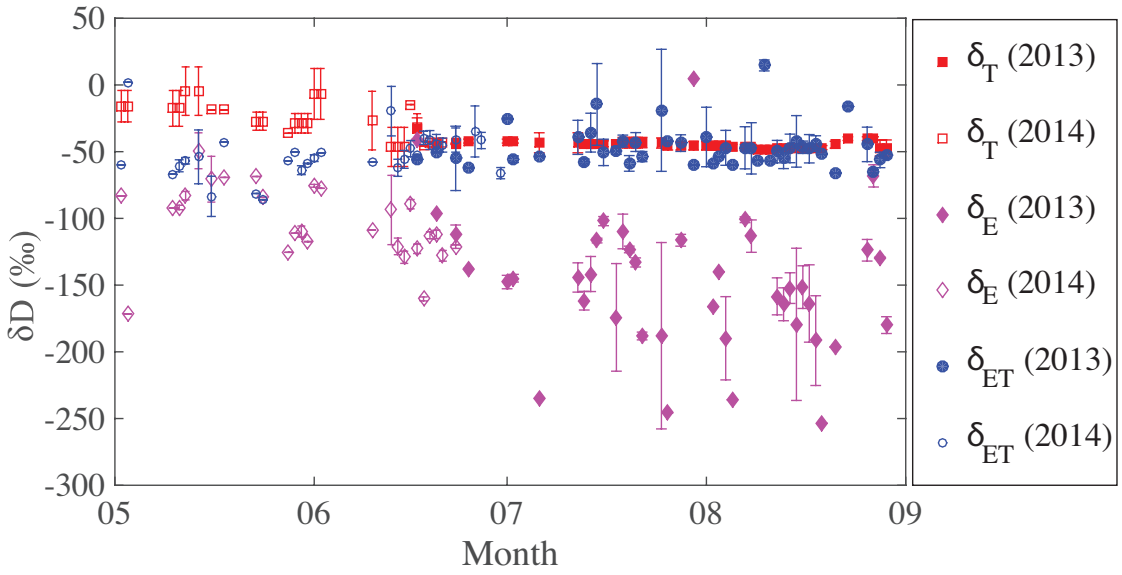

Figure 4.4: Daily averaged variation in isotope ratios of ET (blue circles), T (red squares), and E (pink diamonds). Two points of δ_E, which were less than -300‰, are not shown in this figure.

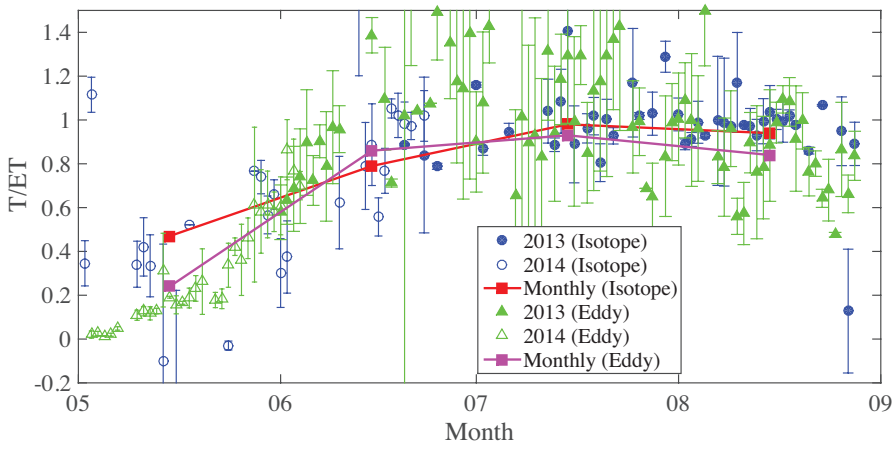

Figure 4.5: Transpiration faction determined by the isotope-based method and eddy correlation based method. Blue circles represent isotope-based daily averaged T/ET. Green triangles represent the simulated T and measured ET based daily averaged T/ET. Vertical bars denote the standard deviation for each day. The red line with filled squares represents the isotope based monthly average T/ET excluding unreliable values (T/ET $>$ 1.2 or T/ET $<$ -0.2). Pink line with filled squares represents the simulated T and measured ET based monthly averaged T/ET.

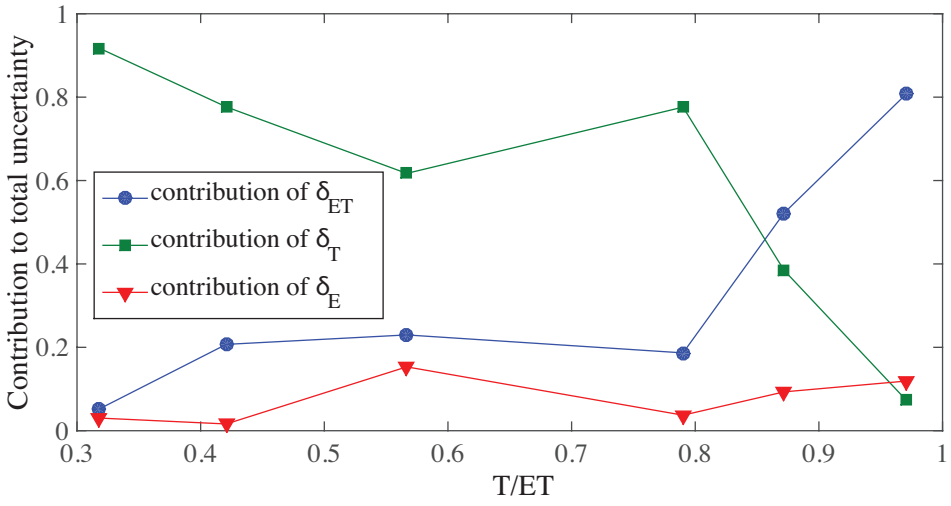

Figure 4.6: The fractional contribution to the partitioning uncertainty of uncertainty δ_{ET} (blue circle) and end-member uncertainty (δ_T (green square) and δ_E (red diamond)) as a function of the transpired fraction of evapotranspiration, T/ET. The fractional contribution was calculated from Equation 2.8. Data where $T/ET > 1.2$ or $T/ET <$ -0.2, with only one point measurement of δ_T and with less than 3 hours of highly accurate δ_{ET} estimation in each day excluded.

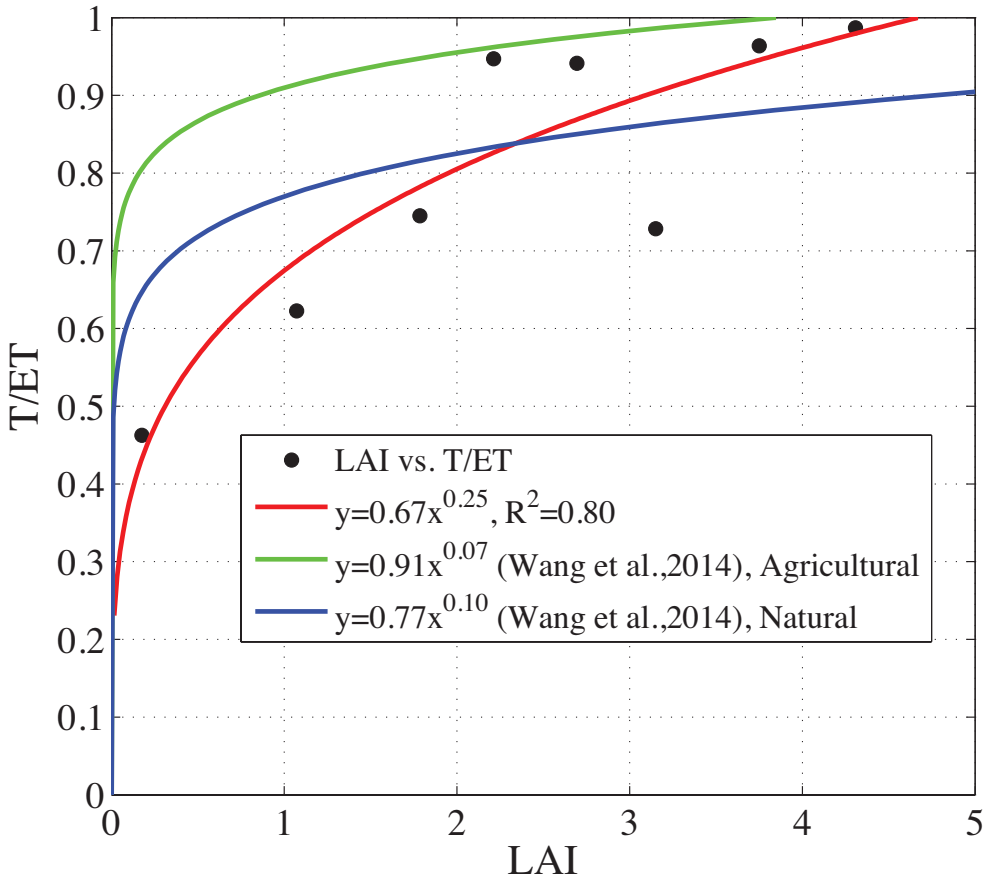

Figure 4.7: Relationship between the 0.5−bin averaged LAI and the daily averaged transpiration fraction (T/ET). $T/ET > 1.2$ or $T/ET <$ -0.2 data are excluded. Two regression lines (green, agricultural system; blue, natural system) derived from a global observation data set *Wang et al.* [2014] are also plotted.

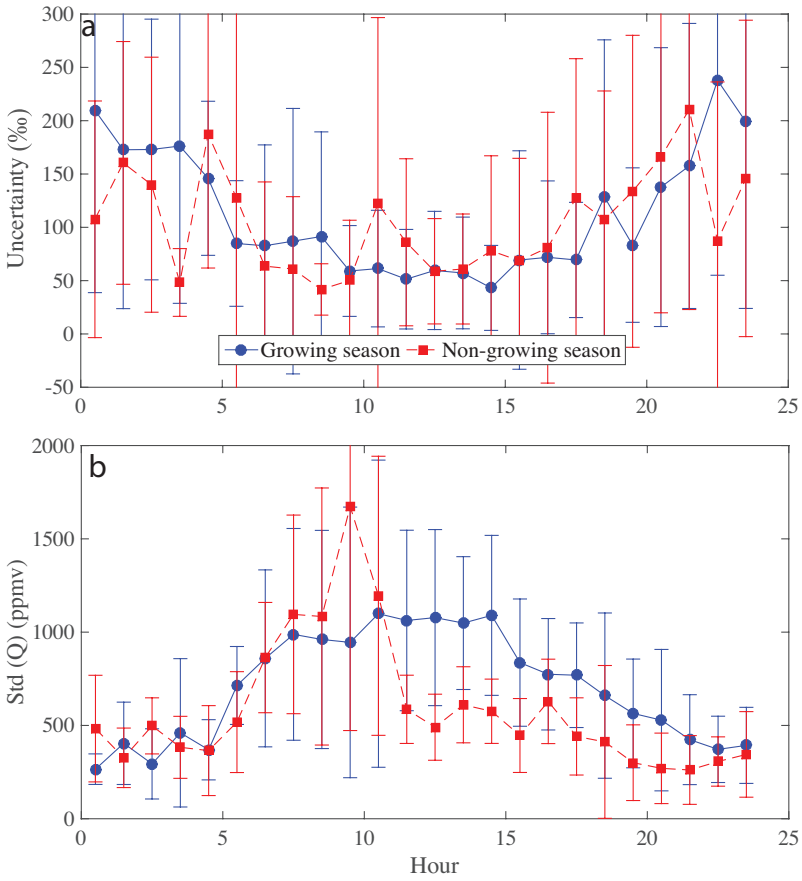

Figure 4.8: Comparison of the ensemble mean diurnal variation in uncertainty of δ_{ET} (a) and standard deviation of water vapor of mixing ratio (b) during the growing season (July and August 2013, blue circle) and non-growing season (September and October 2013, red square). Vertical bars denote the standard deviation for each hour.

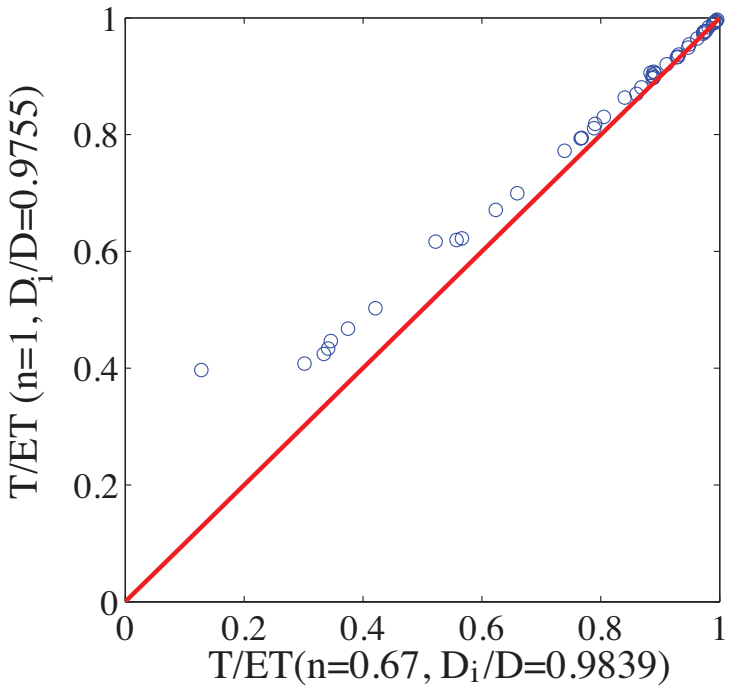

Figure 4.9: Impact of using different parameters for δ_E estimation in the T/ET estimation. Data with $T/ET > 1$ or $T/ET < 0$ are excluded.

Chapter 5

Global ET partitioning

5.1 Global synthesis of LAI control on dry canopy ET partitioning

T/ET ratio has been shown highly relative to LAI [e.g., *Raz-Yaseef et al.*, 2010; *Yepez et al.*, 2005; *Lawrence et al.*, 2007; *Mitchell et al.*, 2009], but varying among ecosystems [e.g., *Raz-Yaseef et al.*, 2012; *Cavanaugh et al.*, 2011]. Additional suggesting causes including (1) water stress, (2) ET amount related to T/ET partitioning and (3) climate condition, are not considered as the major factor of T/ET variations (see [*Wang et al.*, 2014]). A plant growing stage function was included in *Wang et al.* [2014] to explain the variations, with a correlation of $R^2 = 0.43$ for the global T/ET and LAI dataset. However, as *Wei et al.* [2015] suggested, the growing stages is generally related to LAI variation (growing stages is also a function of LAI). Here we classified the whole vegetation into six classes and document previous studies related to each class in Sec 2. The majority of prior ET partitioning studies focused on crops (30/64) and grasses (13/64), and most of which were conducted in South America. The global synthesis of LAI controls on ET partitioning for each class is shown in Figure 5.1. In gerenal, T/ET was represented quite well as a function of a $0.5-$bin averaged LAI for different vegetation types, implying that vegetation plays a major role in driving the contribution of T/ET.

However, different vegetation types showed different exponential relationships and correlations (Table 5.1). The best regression was $T/ET = 0.69\mathrm{LAI}^{0.31}$ for grasses (R^2=0.95) and the worst one was $T/ET = 0.52LAI^{0.25}$ for crops (R^2=0.51). The crops showed large variation in T/ET under different LAI conditions before bin-averaged process. Variable vegetations can be found in crops class, including corn [*Sauer et al.*, 2007], wheat [*Zhang et al.*, 2002; *Herbst et al.*, 1996], rice [*Wei et al.*, 2015], cowpeas [*Sepaskhah and Ilampour*, 1995], grapevines [*Yunusa et al.*, 2004] and so on. Although we futher divided crops class into C3 and C4 group, no improved correlation was found. A further sub-classification may be required for the large difference of stomatal characteristic among these crops, although a well correlation was found after 0.5-bin averaged of LAI.

The T/ET estimated from LAI regression is described in Table 5.1. Overall, the crops systems tended to have high T/ET, mainly because agricultural vegetations are typically less constrained by environmental stress [*Wang et al.*, 2014]. T/ET ranged from 0.43 to 0.69 under low LAI conditions (i.e. LAI=1), which is significant higher than we thought. Although *Wang et al.* [2014] suggested a possibility of high proportion of vegetation water use under low LAI conditions, measurement errors at the same time, should also be noted [*Wei et al.*, 2015]. Forests dataset tended to have a low T/ET at the same LAI value (T/ET=0.47, LAI=1), whereas a high T/ET value can be found in crops, shrubs and grasses datasets (T/ET=0.63, LAI=1). For all the classes T/ET were positively related to LAI. When LAI=3, ET of shrubs and grasses class increased dramatically (T/ET=0.97), which shows a dominate role of T. Due to canopy structure, no LAI>3 study was found in this class. For high LAI condition, a consistent value of T/ET can be found in forests class (about 0.79). The wetlands class (Only one study [*Wei et al.*, 2015] based on isotope method was used in this class.) showed the highest value (T/ET=0.88, LAI=3; T/ET=1.0, LAI=6), perhaps because of the consideration of only high T/ET timescale (mid-day) (see below). Nevertheless, well correlation between LAI and T/ET obtained from different datasets suggested that vegetation plays a major role in driving the contribution of T/ET.

5.2 ET and E_c estimation from CLM, $GLEAM$ and $GRACE$

Global patterns of ET estimated from $GLEAM$, CLM and $GRACE$ based water balance are displayed in Figure 5.2. The mean values of the three products reveal high congruence. For example, high ET can be found in equator area while low ET can be found in high latitude area. On the other hand, the uncertainties also increase with increasing ET. $GRACE$ derived ET appears to be the noisiest among these ET products. $GRACE$ ET overestimates ET gradients in warm area (e.g. Amazon, South Asia). Mean annual $GRACE$ inferred ET from 2004 to 2010 is 11% and 31% higher than CLM and $GLEAM$, respectively. $GLEAM$ estimated ET is very similar to CLM estimated but lower than that of LCM in most of cases, except in Amazon basin. These differences could be related to energy balance or water balance constraints [*Long et al.*, 2014]. $GRACE$-inferred ET is easy to calculate but highly sensitive to the input data ($TWSC$, R and P) and their related uncertainties. Non-closure errors ranging from 5% to 25% of P are primarily attributed to errors in satellite-derived $TWSC$ and P. *Long et al.* [2014] thus suggested uncertainties in $GRACE$ inferred ET is higher than that in land surface model and remote sensing ET products. Moreover, large uncertainty of runoff estimation is a remained issue in this approach. On the other hand, CLM is based on $SVAT$ schemes, in which actual ET is constrained directly by simulated soil moisture as well as meteorological forcing. In contrast, ET from $GLEAM$ is determined lagerly by radiation, without explicit soil moisture constraints based on water balance. Considering that each product has its own uncertainties, it is necessary to investigate T/ET based on different ET products. E_c is derived from $GLEAM$ and CLM. Though CLM and $GLEAM$ ET generally consist with each other, significantly lower E_c can be found in $GLEAM$ (about 14% of E_c/ET in global scale).

5.3 Global ET partitioning

Based on global synthesis of LAI control on ET partitioning, LAI dataset, land cover, different ET and E_c products, the T/ET ratio can be estimated by our developed algorithm (Equation 2.13). The $GRACE$ based results are shown in Figure 5.5 and the others were shown in Table 5.3. It is shown that T dominates in the densely vegetated areas of the tropic region. Moveover, T/ET is also very high over the grasses and crops areas. T/ET obtained from different E_c datasets show about 8% uncertainty (Figure 5.5). Interestingly, the Amazon area showed much lower T/ET (about 60% on average) than we thought, compare to grasses regions. There can be two reasons for this phenomenon: 1) A high canopy E_c can be found in Amazon region (Broadleaved, evergreen forest) because rainfall interception varies from 14 to 21% of annual rainfall [*Kelliher et al.*, 1993]. It means that much of the atmospheric demand for evaporation is satisfied by E_c, thereby limiting transpiration. 2) Compare to grasses, even with a high LAI (e.g. LAI=4), the dry leaf condition ET is not dominated by T (Figure 5.1). Because T/ET in each grid cell is spatiotemporally weighted by ET, our results are highly sensitive to those latitudes and regions that contribute most of the ET in global hydrologic cycle (i.e. tropical and mid-latitude region). As shown in Figure 5.6, we note that our global mean of T/ET (50%-60%) is smaller than those of the literature complication studies [*Wang et al.*, 2014; *Schlesinger and Jasechko*, 2014] but in good agreement with the value reported in GCMs (47%) (also see Table 1.1). On the other hand, it is significantly smaller than that reported in isotopic approaches [e.g., *Jasechko et al.*, 2013; *Good et al.*, 2015b].

5.4 The uncertainties in our partitioning

The results demonstrated the robustness of our algorithm for ET partitioning. However, there were some uncertainties in our estimation. Multi-monthly averaged LAI and vegetation types were used in Equation 2.13. The day to day variation of these parameters may bias our LAI regression results. Because the runoff data on which our analysis is

based is not valid at daily timescale, we cannot account for this possible effect in current analysis. However, because our global analysis is mostly sensitive to tropical and mid-latitude regions (LAI and vegetation type has not significantly changed through the years), the time scale induced bias in the majority of the globe hydrologic cycle is likely small. The uncertainties derived from LAI regression ($a\text{LAI}^b$ in Equation 2.13) should also be considered. Vegetation type, through its effect on the proportion of the shaded surface fraction, also influences T/ET, which generally increases from grasses to forests [*Raz-Yaseef et al.*, 2012]. T/ET also varies among ecosystems according to the depth of water uptake. Tree responds primarily to deep soil moisture availability while grasses responds to water in the uppermost soil layer [*Holdo and Nippert*, 2015]. Some previous studies suggested that T/ET is larger for deep-rooted trees than for grasses, as well as for soil with better infiltration regimes than more impermeable soils [e.g., *Raz-Yaseef et al.*, 2012; *Cavanaugh et al.*, 2011]. Different from these views, our results found under the same LAI condition, transpiration fraction shows a larger values for grasses. One possibility is grasses transpiration predominantly reduces shallow soil moisture content which is the dominant factor in E_s estimation. Another possible reason is that the maximum stomatal conductance difference for different vegetation (transpiration efficiency). Canopy stomatal control of gas exchange is quantified by the stomatal conductance, g_s, which is a function of maximum stomatal conductance (g_{smax}). Under similar meteorology, soil and LAI condition, a higher g_{smax} would give a higher T value. Generally, high g_{smax} can be found in crops and grasses, as concluded in *Kelliher et al.* [1995]: A highest g_{smax} can be found in crop (12.2 mm s^{-1}) while the lowest in forest (5.7 mm s^{-1}). Moreover, there is no significant different regression results among different forest classes, which was also confirmed in *Kelliher et al.* [1995] (no significant g_{smax} variation for different forest pieces). Furthermore, another uncertainty is T transpired by understory vegetation. Some studies suggested understory vegetation ranges from 10% to 50% of total ET and tends to increase with decreasing LAI [*Kelliher et al.*, 1997; *Wilson et al.*, 2000]. Nevertheless, the regression between T/ET and LAI suggested vegetation

generally controlled ET partitioning, but with some variability among vegetation types.

Another uncertainty is conducted from different measurement methods. Both isotopic and non-isotopic measurement have been included in our LAI regression estimation. Isotopic method provides an unprecedented opportunity for ET partitioning across a variety of spatial and temporal scale which is unattainable by conventional technique. However, most of isotope-based studies showed that T generally contributes more than 70% to the ET, while non-isotopic measurement generally leads to considerably smaller transpiration fractions. Thus some studies argued that the isotopic measurement may overestimate the contribution of T. However, *Wei et al.* [2015] and *Sutanto et al.* [2012] found that no systematic internal difference between isotope and non-isotope methods. Moreover, global simulation shows large discrepancy (Table 1.1). To understand the discrepancy among different methods, we divided the whole dataset into isotope and non-isotope groups. We further analyzed two satellite-based global ET datasets, ($GLEAM$ and $CLM4.5SP$), and compared them with in-situ measurements. Without considering interception ($ET = E_s + T$ here), relationships between the 0.5 bin averaged LAI and T/ET are shown in Figure 5.4. The T/ET is represented quite well as a function of a 0.5 bin averaged LAI. However, different datasets showed different nonlinear relationships. $GLEAM$ dataset tended to have the highest T/ET under the same LAI value. Even under low LAI conditions ($LAI < 1$), T/ET in $GLEAM$ data was about 80%. Isotopic measurement showed a similar result under high LAI condition. However, T/ET derived by isotopic method was much smaller than that derived from $GLEAM$ (60% at $LAI = 1$). CLM and non-isotope method showed similar results, tending to have lower T/ET under high LAI conditions ($< 80\%$ after $LAI > 2$). The discrepancy between isotope and non-isotope measurement may result from mismatch of measurement time scale. The limitation of isotope method is that it is only applicable under strong latent heat condition. Under weak turbulence condition such as in the morning or evening, the uncertainties of Keeling plot was quit large. As a result, the isotope method estimated T/ET is only for mid-day (strong T condition), whereas non-isotope may also account for other time scale

(night-time, weak T but E still occurs). For example, from our paddy field observation, we found about 20% of total ET occurred at night-time (Figure 5.8) because the surface water temperature was higher than air temperature. This night-time evaporation was not accounted into LAI regression estimation. Thus, those isotopic based studies included in LAI regression estimation might resulted a overestimation of T/ET at the same LAI condition. The different LAI regression between CLM and $GLEAM$ is resulted from significantly different interception fractions in evapotranspiration (also see below). E_c/ET in $GLEAM$ is low (8%), resulting in high transpiration ratios.

Clearly, the most egregious bias in ET partitioning is the excessively large contribution from E_c. Not only in our study, *Jasechko et al.* [2013] showed a high T/ET because of the low E_c/ET in their study. If we change the interception data, T/ET would reduces to about 60%. The same problem can also be found in *Good et al.* [2015b]. The two E_c datasets used in our study was not verified. A further study about interception is required because canopy interception loss at various regions of the globe was few reported in the literature. Here we compared these datasets with observations (Figure 5.7 and comparison of measured value and simulated result of each study was shown in Table 5.2). These data were based on the published studies we reviewed (14 individual long term ET partitioning measurement studies) that measured at least two of the three components in an attempt to compare them with global simulation. E_c is significantly underestimated for both datasets. If a higher E_c was confirmed, T/ET in our analysis would be smaller. Moreover, the omission of snow interception in global simulation clearly needs to be addressed. Until now, there has been very little research on snow and there is no obvious candidate model to employ [*Miralles et al.*, 2010]. In summary, to reduce the uncertainty in evaluating global T/ET, the improvement of interception evaporation is a prereguisite in our futher study. Although further validation is required, our measurements provided a new inspiration for partitioning global evapotranspiration and suggested vegetation plays a major role in driving the contribution of T/ET.

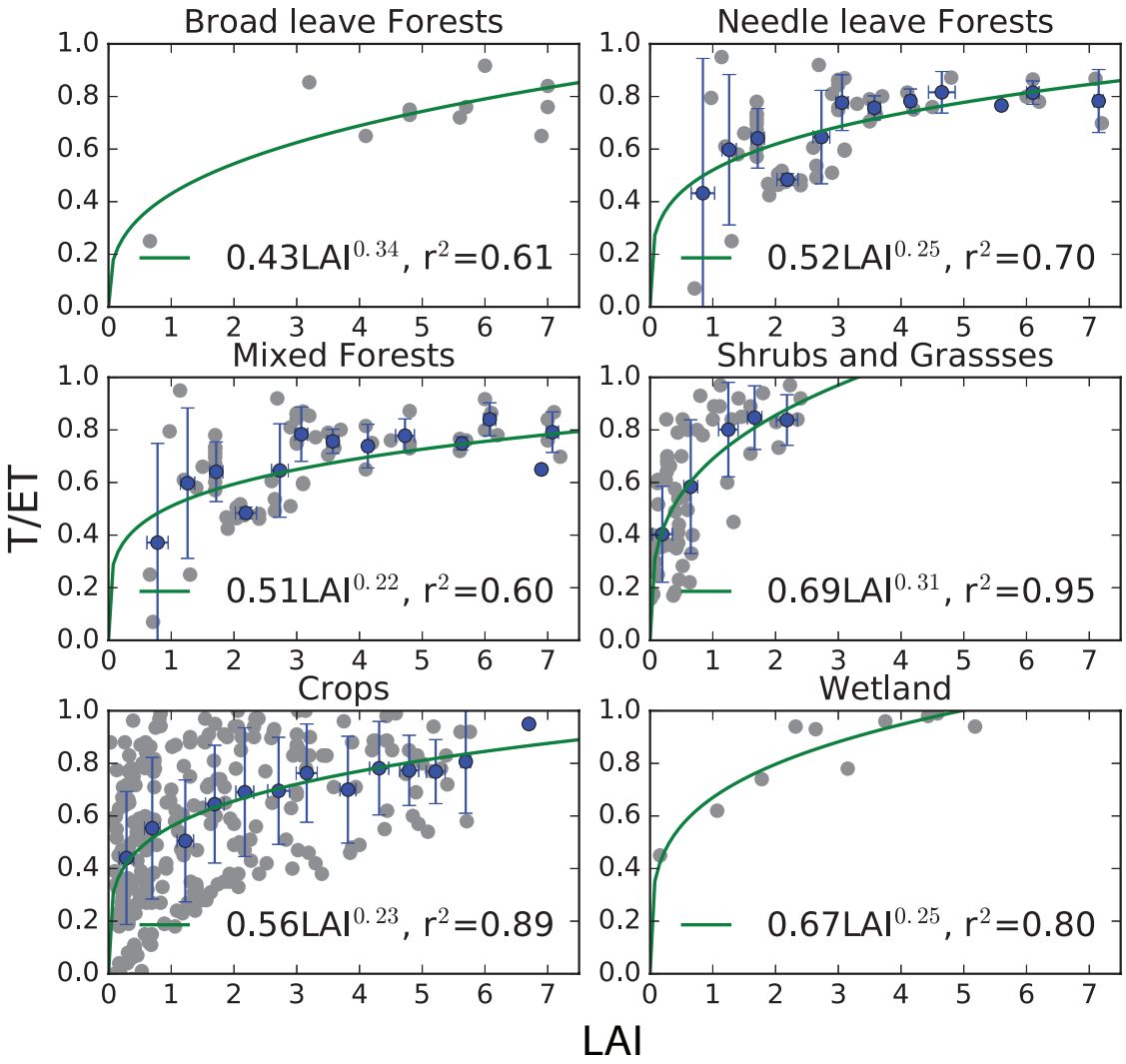

Figure 5.1: Global systhesis of LAI control on ET partitioning.

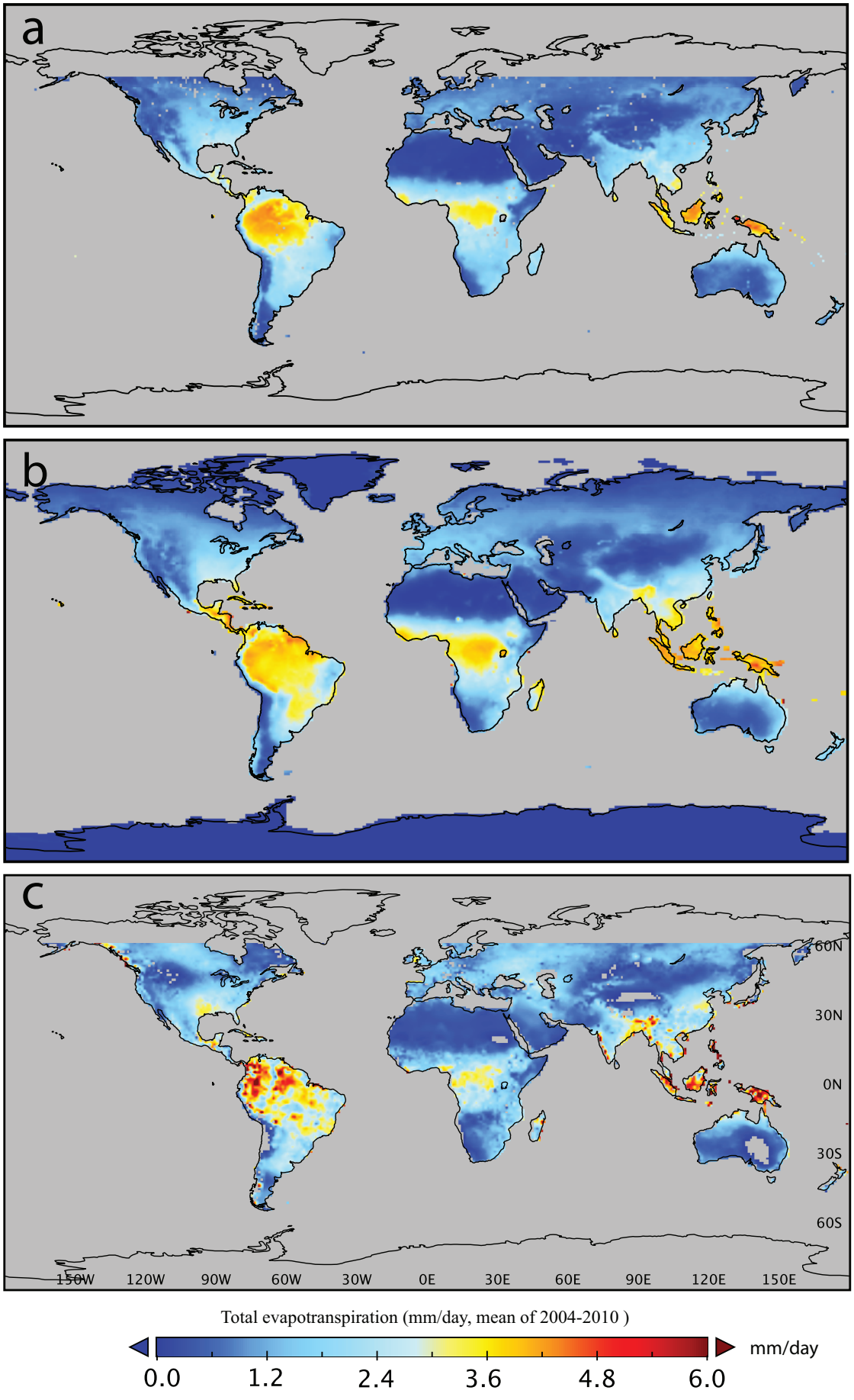

Figure 5.2: Comparison of *ET* derived from *GLEAM* (a), *CLM* (b) and *GRACE* (c).

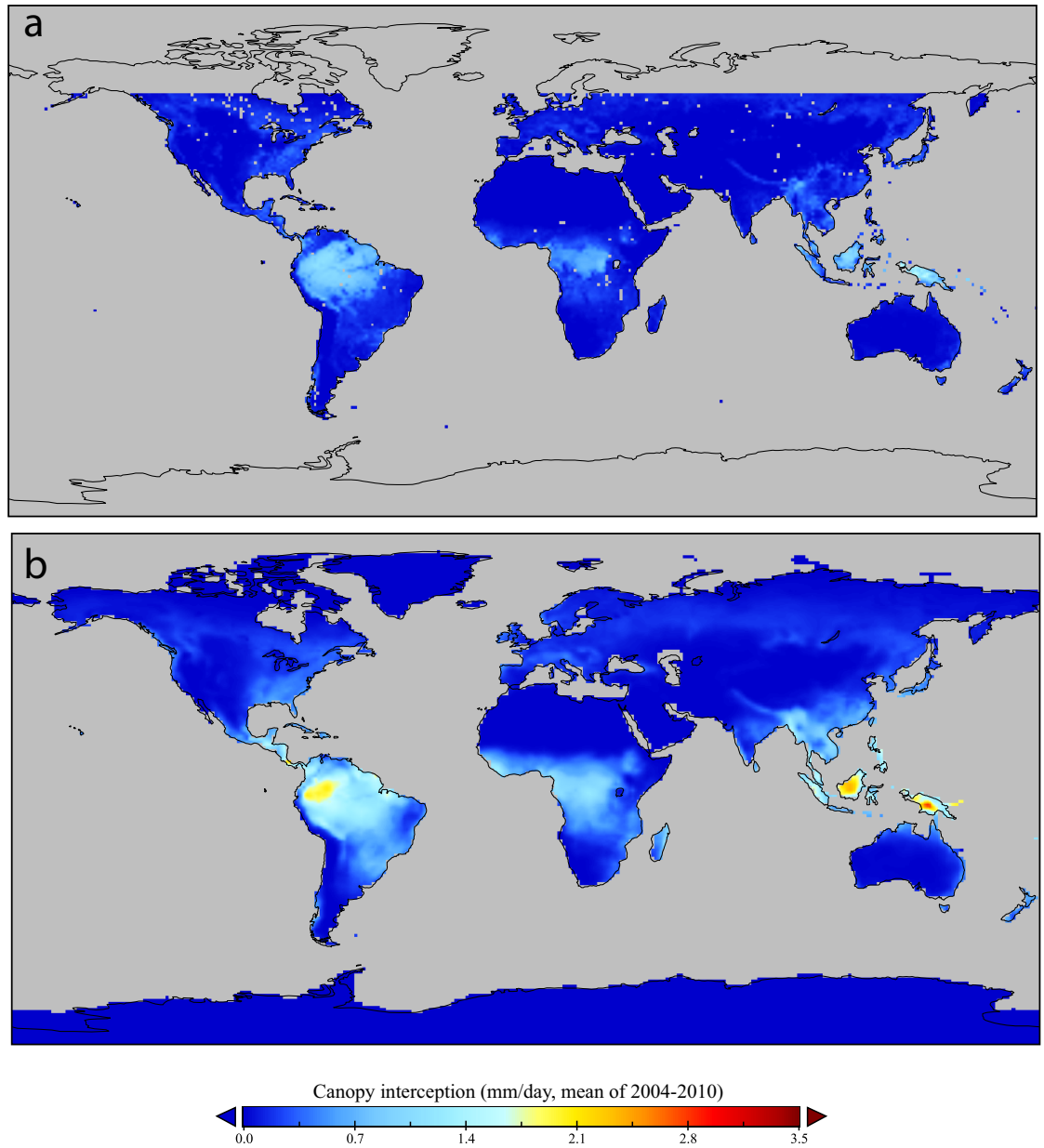

Figure 5.3: Comparison of canopy interception derived from *GLEAM* (a) and *CLM* (b).

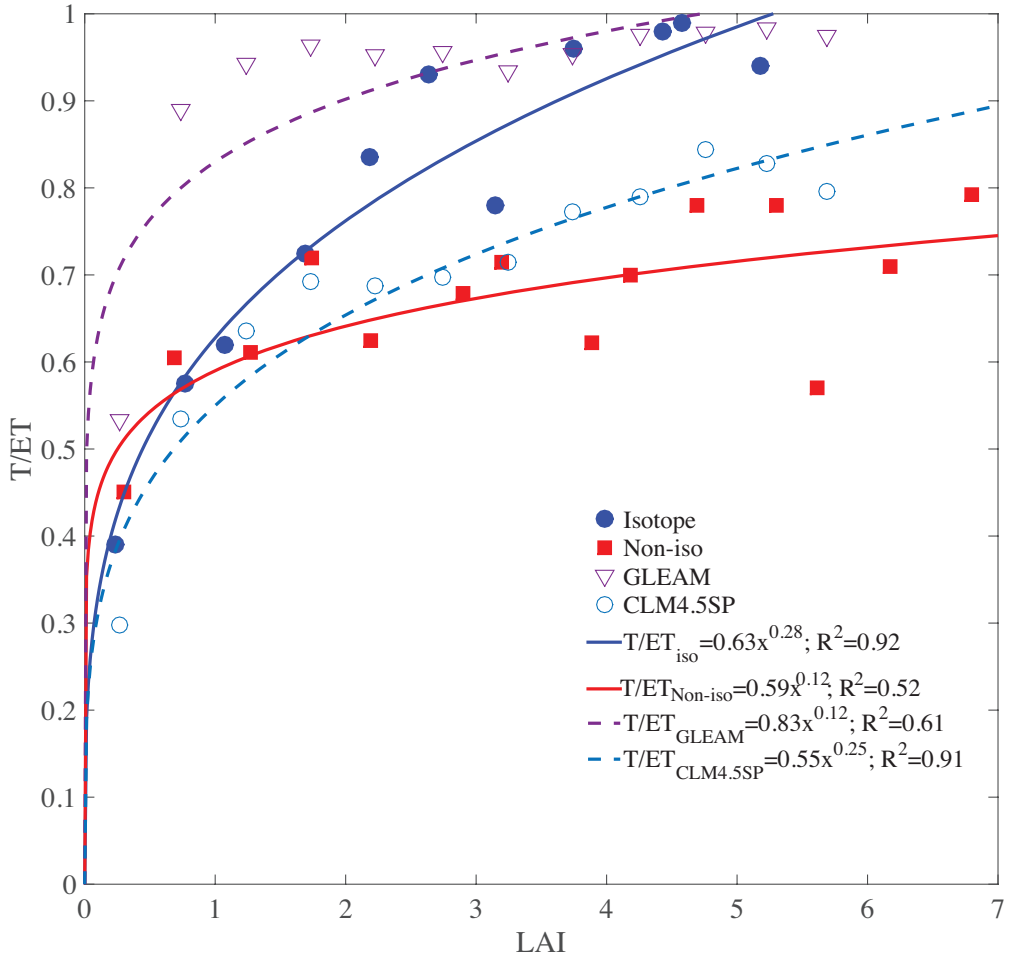

Figure 5.4: *LAI* control on *ET* partitioning based on different methods.

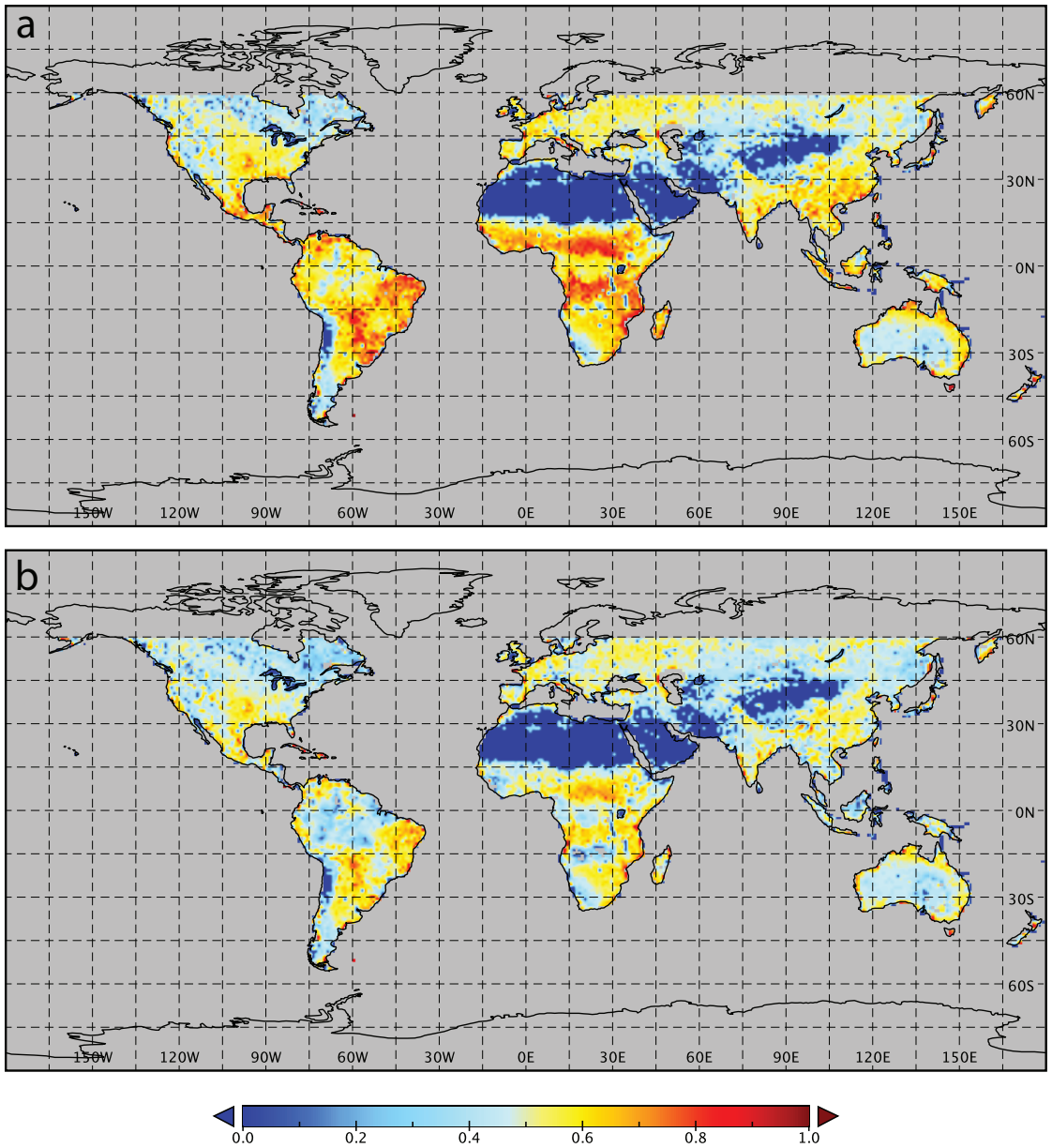

Figure 5.5: Global T/ET derived from LAI regression: (a) $GRACE$ derived ET with GLEAM E_c (b) $GRACE$ derived ET with CLM E_c).

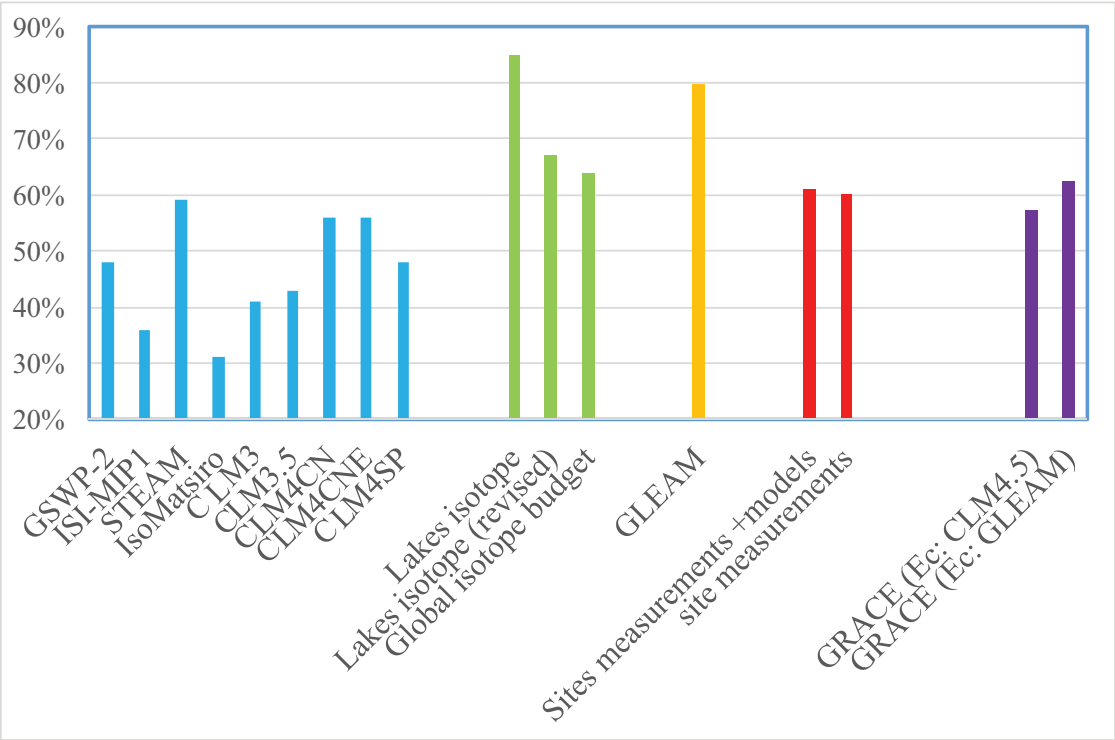

Figure 5.6: Global T/ET estimated from land surface models, isotopes, satellites, site measurements and LAI regression.

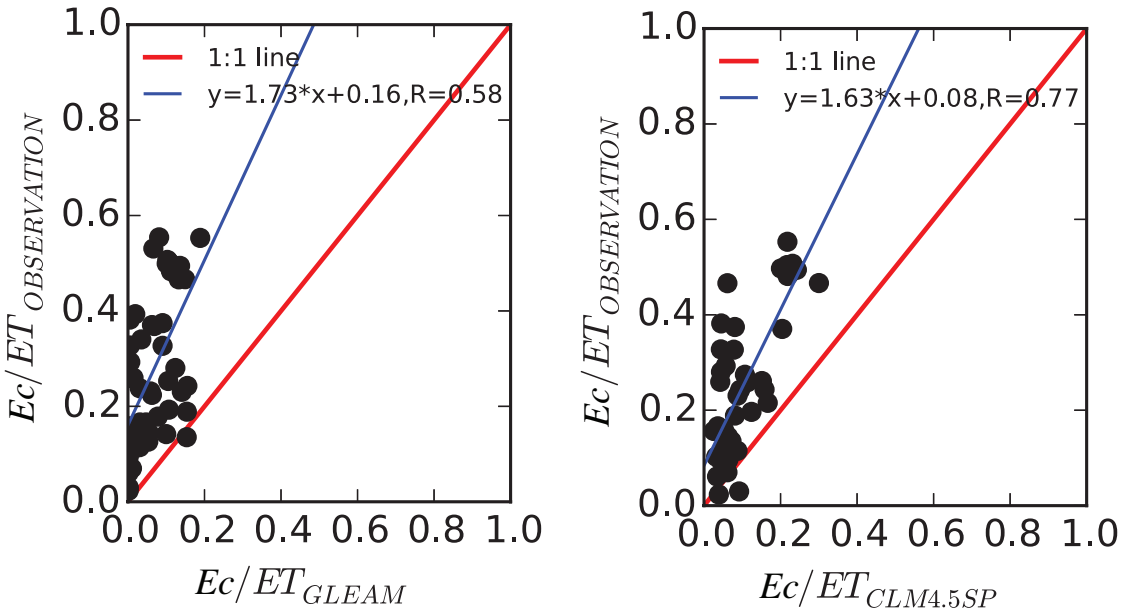

Figure 5.7: Comparison of simulated E_c/ET and measured E_c/ET. The measured data was obtained from *Mitchell et al.* [2009], *Mitchell et al.* [2012], *Lee et al.* [2010], *Oishi et al.* [2008] and *Jian et al.* [2015]

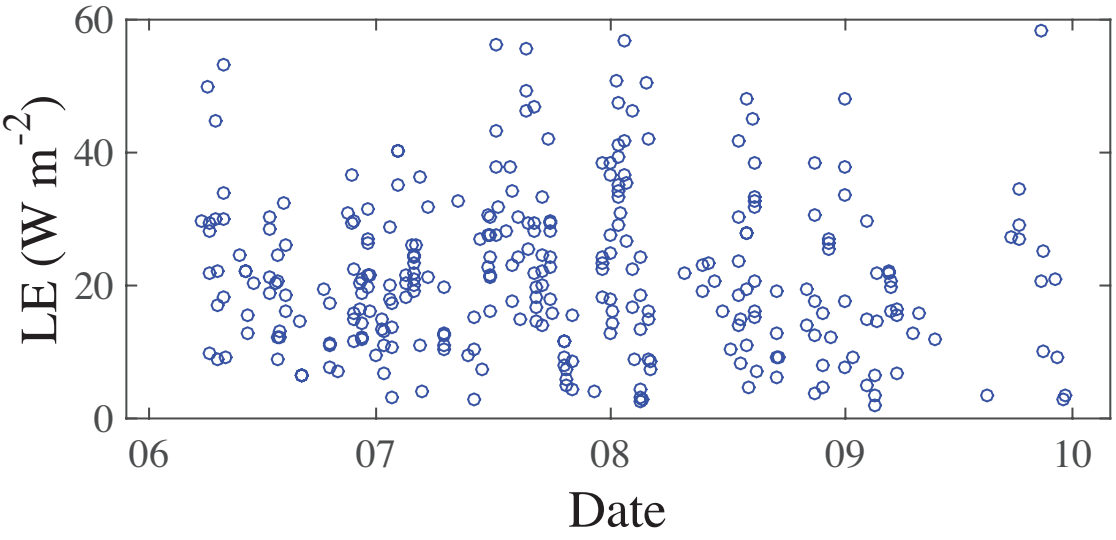

Figure 5.8: Hourly averaged latent heat observed at night time.

Table 5.1: Global systhesis of LAI control on ET partitioning.

Vegetation Class	T/ET Regression	Correlation (R^2)	T/ET (LAI=1)	T/ET (LAI=3)	T/ET (LAI=6)
Broad leave forests	$0.43LAI^{0.34}$	0.61	0.43	0.62	0.79
Needle leave forests	$0.52LAI^{0.25}$	0.70	0.52	0.68	0.81
Mixed Forests	$0.51LAI^{0.22}$	0.60	0.51	0.65	0.77
Shrubs and Grassses	$0.69LAI^{0.31}$	0.95	0.69	0.97	-
Crops	$0.56LAI^{0.23}$	0.89	0.56	0.72	0.84
Wetlands	$0.67LAI^{0.25}$	0.80	0.67	0.88	1

Table 5.2: Comparison of measured and simulated E_c/ET

Studies	VT	Lat	Lon	E_c/ET (obs)	E_c/ET (CLM)	E_c/ET $(GLEAM)$
Verstraeten et al. [2005]	Forest	51.3	4.5	0.24	0.11	0.06
Mitchell et al. [2009]	Forest	-32.3	117.9	0.15	0.08	0.15
Mitchell et al. [2012]	Forest	-36.7	146.7	0.06	0.01	0.01
Lee et al. [2010]	Forest and crop	37.7	127.1	0.49	0.22	0.11
Oishi et al. [2008]	Forest	37.0	-79.1	0.01	0.04	0.03
Jian et al. [2015]	Forest	35.6	104.7	0.09	0.05	0.09
Yimam et al. [2015]	Grass	36.2	-97.0	0.25	0.19	-
Ringgaard et al. [2014]	Forest	56.0	9.3	0.39	0.15	0.11
Kumagai et al. [2014]	Forest	33.1	130.7	0.46	0.69	0.15
Herbst et al. [2008]	Shurb	51.4	-1.3	0.20	0.30	0.30
Sun et al. [2013]	Forest	36.4	139.6	0.55	-	0.08
Raz-Yaseef et al. [2012]	Forest	32.35	35.0	0.11	0.09	0.02

Table 5.3: T/ET estimated based on Equation 2.13 with different ET and E_c.

ET	E_c	T/ET
$GRACE$	CLM	57%
$GRACE$	$GLEAM$	62%
CLM	CLM	52%
CLM	$GLEAM$	61%
$GLEAM$	CLM	53%
$GLEAM$	$GLEAM$	60%

Chapter 6

Conclusions and Future Plan

We collected long-term observations of stable isotopes for oxygen and hydrogen in precipitation and water vapor from June 2013 June to May 2014 in Tsukuba, Japan. We also investigated the isotopes of precipitation, water vapor, evapotranspiration, and large-scale moisture derived by IsoGSM to understand the variability of water isotopologues in near-surface atmospheric moisture. We conducted water tagging experiments, together with the observed $d_v - excess$ and $q - \delta D_v$ framework, to discuss how remote controls could affect the isotopic variability of water vapor. The following conclusions were drawn:

(1) $d_v - excess$ and Q displayed clear seasonal cycles, while the seasonal variations of δD_v and $\delta^{18}O_v$ were insignificant.

(2) We successfully combined the GCM simulation ($IsoGSM$) with high-frequency water vapor isotopic measurements to disentangle the water vapor source and its hydrological processes. The model successfully replicated observed isotopic variability, suggesting its ability to reproduce moisture transport.

(3) The isotopic measurements of near surface water vapor and precipitation suggested that water vapor appeared to be isotopically in equilibrium with surrounding raindrops during a precipitation event. However, the equilibrium predictions from monthly δD_v were heavily biased.

(4) The contribution of land evapotranspiration to local water vapor content (F_{ET}) was approximately 16.0±12.3% on average. This revealed a significant seasonal cycle, where F_{ET} was highest in JJA (20.5±12.9%) due to the increased transpiration while lowest in DJF (7.1±13.2%). Our results indicated that the primary control on near surface water vapor δD variability is atmospheric circulation, with local evapotranspiration playing a secondary role.

(5) The tagging experiments together with the $d_v - excess$ and $q - \delta D_v$ framework provided consistent evidence that the large temporal variation of δD_v could primarily be attributed to the advection of moisture from different source regions.

In this study, we adopted a recently developed partitioning technique using high-frequency in situ water vapor isotopic measurements and surface/soil water sampling over a paddy field near Tokyo, Japan, throughout a full growing season. We partitioned ET by estimating the isotopic signals of ET, T and E, i.e., δ_{ET}, δ_T, and δ_E, respectively. δ_{ET} was determined using the Keeling plot method. Estimates of δ_T were obtained directly from surface/soil isotopic measurements, assuming a steady state of transpiration. δ_E was estimated using the Craig-Gordon model in combination with surface and vapor water isotopic measurements. The fraction of transpiration in evapotranspiration (T/ET) ranged from approximately 0.2 to 1, with an almost continuous increase during the early growing season before finally reaching a relatively constant value close to 1, which was confirmed by a two source model simulated T and eddy correlation ET measurement. We also investigated the measurement uncertainties when estimating these three terms (δ_{ET}, δ_T, and δ_E) and their effect on ET partitioning. The average uncertainty of T/ET estimation was 14±10%, and the average uncertainty in δ_{ET}, δ_T, and δ_E were about 9.06, 5.79, and 14.27‰, respectively. It was apparent that the uncertainties in the estimation of δ_T and δ_{ET} significantly affected ET partitioning. The uncertainty in ET partitioning resulted from the uneven spatial distribution of decreases in the levels of surface water isotopes with an increase in T/ET, whereas as T/ET increased, the impact of uncertainty in δ_{ET} became much larger than that for the other parameters (δ_T and δ_E). FT was strongly

controlled by the leaf area index (LAI) on a daily time scale ($T/ET = 0.67LAI^{0.25}$, R^2 = 0.80), suggesting the possibility of using LAI data to partition evapotranspiration at the global scale. The results demonstrated the robustness of using isotope measurements for partitioning evapotranspiration.

In order to understand global synthesis of LAI control on ET partitioning, we collected relevant article from Google scholar and Web of Science and analyze the relationship between LAI and T/ET. Based on vegetation types, we classified all the studies into 6 species: Broad leave forests, Needle leave forests, Mixing forests (combination of broad and needle forests), Shrubs-Grasses, Crops and wetlands. The T/ET was represented quite well as a function of a 0.5-bin averaged LAI, implying that vegetation plays a major role in driving the contribution of T/ET. However, different vegetation showed different nonlinear relationships. Forest dataset tended to have a low transpiration proportion under the same LAI value, whereas a high T/ET value can be found in Crops and Shrubs-Grasses datasets. This discrepancy may result from vegetation differences in height and bulk density. The ET estimated from RS, LSM and $GRACE$ based water balance showed a similar large-scale pattern. Based on global synthesis of LAI control on ET partitioning and different ET products, the T/ET ratio was reported to be 50% at the global scale, supporting the results reported in GCM models (47%). However, it was significantly smaller than that reported in isotopic approaches [e.g., *Jasechko et al.*, 2013; *Good et al.*, 2015a]. Although further validation is required, our measurements provided a new inspiration for partitioning global evapotranspiration and suggested vegetation plays a major role in driving the contribution of T/ET. Moreover, a further study about interception is also required because canopy interception loss at various regions of the globe has been scarcely reported in the literature.

Appendix A

Previous studies used in LAI regerssion estimation.

Table A.1: Previous studies used in LAI regerssion estimation.

Study	Latitude	Longitude	Method
Broad leave forests			
Wilson et al. [2000]	36.0	-84.3	Non-iso
Wilson et al. [2001]	36.0	-84.3	Non-iso
Kelliher et al. [1992]	-42.1	172.2	Non-iso
Mitchell et al. [2009]	-32.3	117.9	Non-iso
Granier et al. [2000]	48.7	7.1	Non-iso
Unsworth et al. [2004]	45.8	-122.0	Non-iso
Nizinski et al. [2011]	-4.6	11.9	Non-iso
Oishi et al. [2008]	37.0	-79.1	Non-iso
Tang et al. [2006]	46.2	89.4	Non-iso
Raz-Yaseef et al. [2012]	31.4	35.0	Non-iso
Needle leave forests			
Diawara et al. [1991]	44.7	-0.8	Non-iso
Lee et al. [2010]	37.8	127.1	Non-iso
Jian et al. [2015]	35.6	104.7	Non-iso
Benyon and Doody [2015]	-37.8	140.8	Non-iso
Barbour et al. [2005]	-43.2	170.3	Non-iso
Oren et al. [1998]	32.9	80.0	Non-iso
Raz-Yaseef et al. [2012]	31.4	35.0	Non-iso
Simonin et al. [2007]	35.3	-111.6	Non-iso
Domec et al. [2012]	35.1	-76.11	Non-iso
Lin et al. [2012]	29.3	101.5	Non-iso
Sun et al. [2013]	36.4	139.6	Non-iso
Jansson et al. [1999]	60.5	17.3	Non-iso

Table A.2: Previous studies used in *LAI* regerssion estimation (continue).

Study	Latitude	Longitude	Method
Shrubs and grasses			
Allen and Grime [1995]	13.3	2.2	Non-iso
Gibbens et al. [1996]	32.6	-106.8	Non-iso
Dugas et al. [1996]	32.8	-106.8	Non-iso
Stannard and Weltz [2006]	29.8	52.8	Non-iso
Schlesinger et al. [1987]	33.6	-101.9	Non-iso
Cavanaugh et al. [2011]	31.9	-110.8	Non-iso
Li et al. [2015]	43.5	116.5	Non-Iso
Yepez et al. [2003]	31.7	-110.2	Iso
Xu et al. [2008]	30.9	103.0	Iso
Yepez et al. [2005]	31.8	-110.9	Iso
Good et al. [2014]	0.3	36.9	Iso
Wang et al. [2010]	-	-	Iso
Wang et al. [2015]	36.1	140.1	Iso
Crops			
Ashktorab H. and Paw U [1994]	38.5	-121.7	Non-iso
Soegaard and Boegh [1995]	13.5	2.5	Non-iso
Allen [1990]	35.9	37.1	Non-iso
Ham et al. [1990]	33.6	-101.8	Non-iso
Wallace et al. [1993]	13.2	2.3	Non-iso
Massman and Ham [1994]	33.6	-101.8	Non-iso
Gutiérrez and Meinzer [1994]	21.9	-154.5	Non-iso
Sepaskhah and Ilampour [1995]	29.8	52.8	Non-iso
Cooper et al. [1983]	35.9	37.1	Non-iso
Sadras et al. [1991]	-36.4	145.2	Non-iso
Yunusa et al. [2004]	-34.2	142.0	Non-iso
Sauer et al. [2007]	41.9	-93.6	Non-iso
Jara et al. [1998]	46.2	-119.7	Non-iso
Eastham et al. [1999]	-32.1	117.2	Non-iso
Sakuratani [1987]	36.0	140.1	Non-iso
Zhang et al. [2002]	37.9	114.7	Non-iso
Eberbach and Pala [2005]	35.6	37.1	Non-iso
Yunusa et al. [1997]	-34.2	142.03	Non-iso
Herbst et al. [1996]	54.1	10.25	Non-iso
Roupsard et al. [2006]	-15.4	167.2	Non-iso
Al-Khafaf et al. [1978]	32.3	-106.8	Non-iso
Harrold et al. [1959]	-	-	Non-iso
Lascano et al. [1987]	32.6	-106.8	Non-iso
Villegas et al. [2015]	-	-	Non-iso
Ding et al. [2015]	37.9	102.5	Non-iso
Wei et al. [2015]	36.0	140.1	Iso
Wen et al. [2016]	38.9	100.3	Iso
Wetland			
Wei et al. [2015]	36.0	140.1	Iso

Appendix B

Water tagging experiments for SON, DJF and MAM.

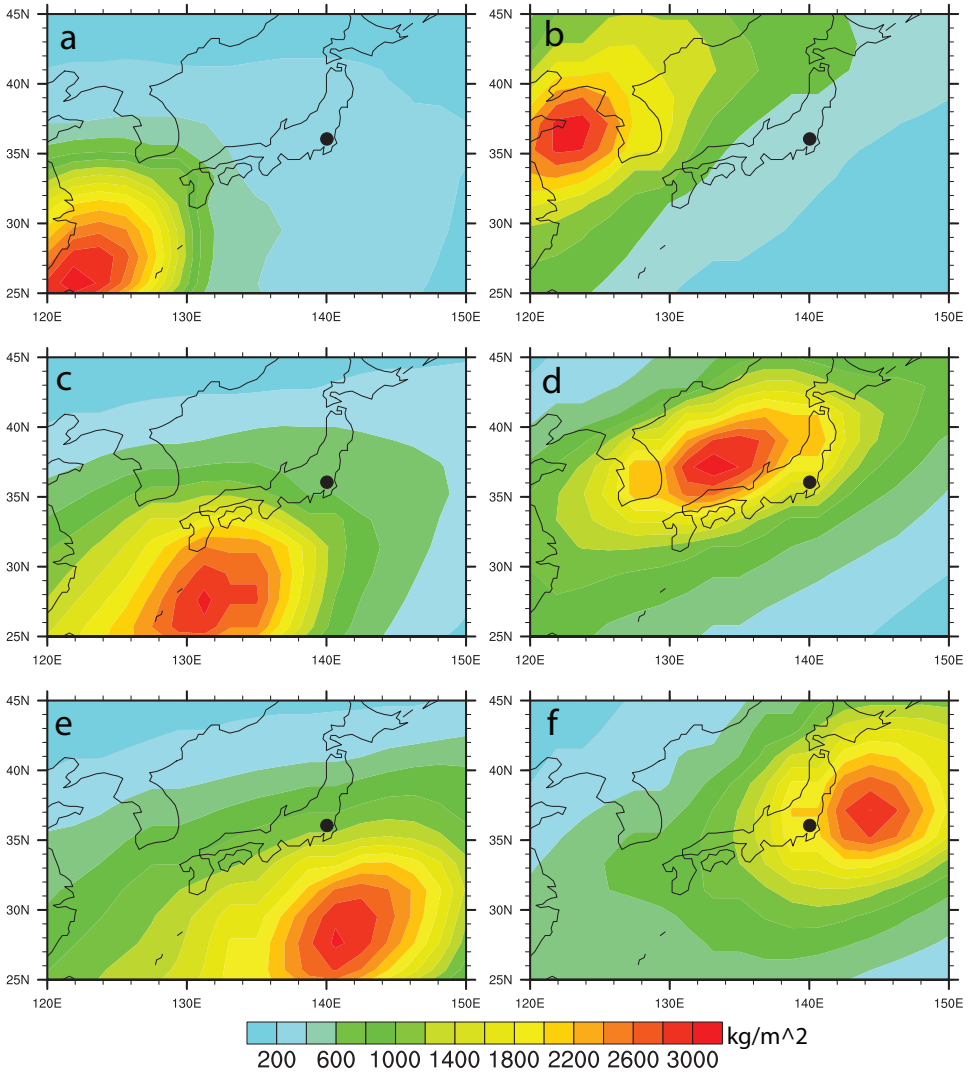

Figure B.1: The atmospheric column precipitable water contributed from tagged boxes in SON. Source regions for tagging experiments of water vapor tagged within 10×10 degree boxes (contour): a, 25°N−35°N, 120°E−130°E; b,35°N−45°N, 120°E−130°E; c, 25°N−35°N, 130°E−140°E; d, 35°N−45°N, 130°E−140°E; e, 25°N−35°N, 140°E−150°E; f, 35°N−45°N, 140°E−150°E.

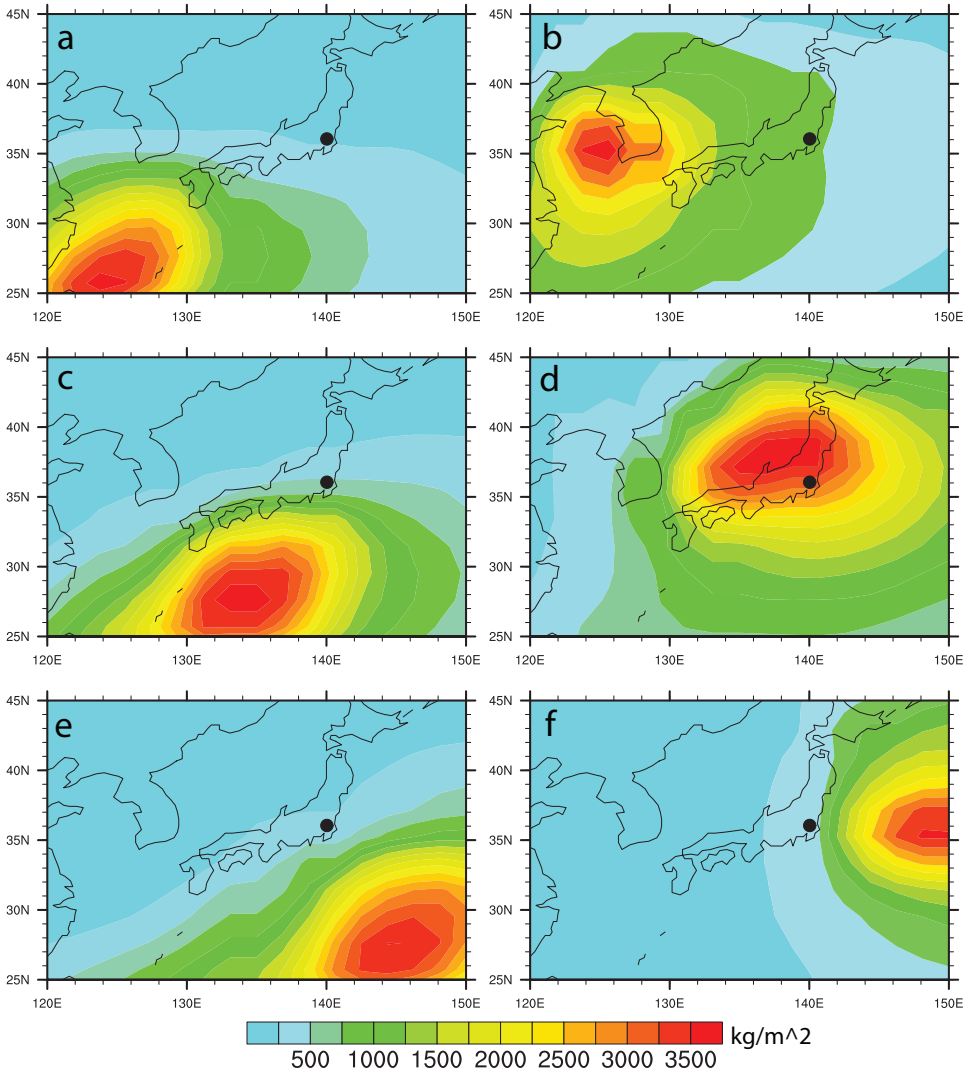

Figure B.2: The atmospheric column precipitable water contributed from tagged boxes in DJF. Source regions for tagging experiments of water vapor tagged within 10×10 degree boxes (contour): a, 25°N−35°N, 120°E−130°E; b,35°N−45°N, 120°E−130°E; c, 25°N−35°N, 130°E−140°E; d, 35°N−45°N, 130°E−140°E; e, 25°N−35°N, 140°E−150°E; f, 35°N−45°N, 140°E−150°E.

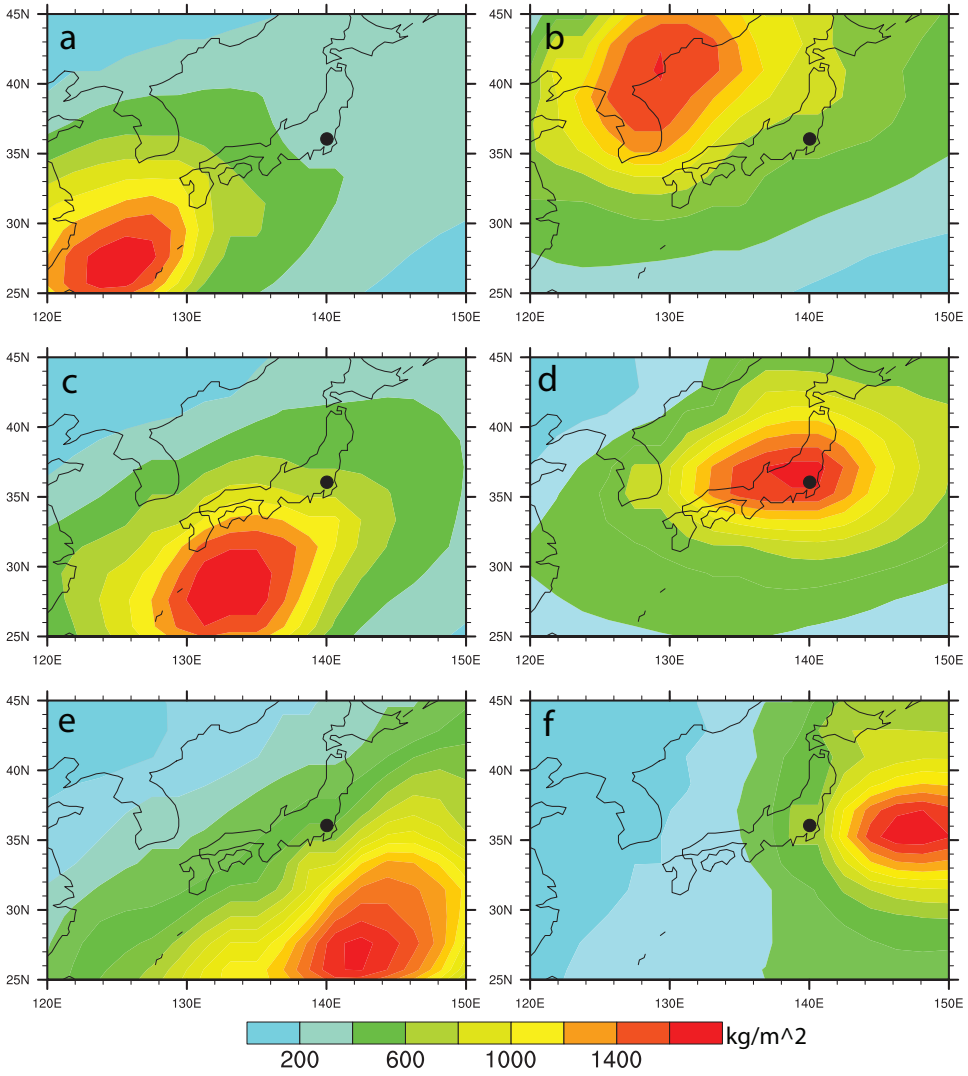

Figure B.3: The atmospheric column precipitable water contributed from tagged boxes in MAM. Source regions for tagging experiments of water vapor tagged within 10×10 degree boxes (contour): a, 25°N−35°N, 120°E−130°E; b,35°N−45°N, 120°E−130°E; c, 25°N−35°N, 130°E−140°E; d, 35°N−45°N, 130°E−140°E; e, 25°N−35°N, 140°E−150°E; f, 35°N−45°N, 140°E−150°E.

Appendix C

ET partitioning based on Two layer method.

The partitioning of water fluxes into canopy and soil components could also be performed on the basis of eddy correlation measured ET and simulated T. Based on two-source model, T can be given by the following bulk equation:

$$T = \frac{\rho_a \left[q_{sat}\left(T_c\right) - q_a\right]}{r_{av} + r_c} \tag{C.1}$$

where ρ_a is the density of air (kg m^{-3}), $q_{sat}(T_c)$ is saturated specific humidity for the canopy temperature (kg kg^{-1}), q_a is the air specific humidity (kg kg^{-1}), the canopy temperature T_c (°C) which can be estimated according to the aerodynamic principle [*Lee et al.*, 2007]:

$$T_c = Ta + \frac{\overline{w't'}u}{u_*^2} \tag{C.2}$$

where u_* is friction velocity and $\overline{w't'}$ is kinematic sensible heat. The aerodynamic resistance for water surface r_{av} (s m^{-1}) can be determined as follow [*Brutsaert*, 1982]:

$$r_{av} = \ln\left(\frac{z_m - d_0}{z_{0mv}}\right) \ln\left(\frac{z_h - d_0}{z_{0hv}}\right) \Big/ k^2 u \tag{C.3}$$

where z_m is the height of wind speed measurement (m), $d_0 = 0.666 z_v$ (z_v is vegetation height in m) is the zero-plane displacement height (m), z_{0mv} ($= 0.123 z_v$) is the roughness length governing momentum transfer above vegetation canopy (m), z_h is the height of temperature and humidity measurements (m), z_{0hv}($= 0.1 z_{0mv}$) is the roughness length governing latent heat transfer above vegetation canopy (m) [*Wang and Yamanaka*, 2014], $k = 0.40$ is the von Karman's constant and u is the wind speed at measurement height (m s^{-1}). The canopy resistance r_c (sm^{-1}) is estimated from:

$$r_c = r_{st}/LAI \tag{C.4}$$

the leaf stomatal resistance r_c is derived from rice crop growth model [*Maruyama and Kuwagata*, 2010]:

$$\begin{aligned} r_{st} &= (1 + S_{absH}/S_{abs})/g_{Smax} \\ S_{abs} &= [(1-r) - \tau_s(1-r_g)]Rs/L \end{aligned} \tag{C.5}$$

where S_{abs} is the mean absorbed solar radiation per unit leaf area (Wm^{-2}); τ_s is the transmissivities of the canopy for short-wave; g_{Smax} is the maximum bulk stomatal conductance (m s^{-1}) for saturated S_{abs}; and $S_{absH} = 66$ W m^{-2} is the absorbed solar radiation (Wm^{-2}) when g_s is equal to half of g_{Smax}. g_{Smax} for rice canopy decreases with rice growth due to change in plant phenology is expressed using following empirical function of developmental stage (P_s):

$$\begin{aligned} g_{Smax} = g_{Smax1} + (g_{Smax0} - g_{Smax1}\exp(-(\theta_1 P_s)^{\mu_1}) + \\ (g_{Smax2} - g_{S_{max1}})\exp[-(\theta_2(2-P_s))^{\mu_2}] \end{aligned} \tag{C.6}$$

where $g_{Smax0} = 0.060$, $g_{Smax1} = 0.023$ and g_{Smax2}=0.009 are the values of g_{Smax} at transplanting ($P_s = 0$), heading (P_s=1) and maturity ($P_s = 2$), respectively; $\theta_1 = 1.65$ and $\theta_2 = 1.08$ are parameters affecting the timing of the decline in g_{Smax} after transplanting and heading, respectively; and $\mu_1 = 8$ and $\mu_2 = 8$ are parameters affecting the gradient of the

decline in g_{Smax} after transplanting and heading, respectively [*Maruyama and Kuwagata*, 2008, 2010]. The developmental stage P_s is determined by:

$$\begin{aligned} P_s &= N_{DAT}/N_{DTH} (0 < P_s \leq 1) \\ &= 1 + N_{DAH}/N_{DHM} (1 < p_s \leq 2) \end{aligned} \tag{C.7}$$

where N_{DAT} is days after transplanting, N_{DTH} is days from transplanting to heading, N_{DAH} is days after heading, and N_{DHM} is days from heading to maturation [*Maruyama and Kuwagata*, 2008]. Using these parameters and Equations C(1)-(7), the transpiration can be calculated at any given growth stage. As same as isotope-based method, data measured on a rainy day and outside the mid-day (11:00−15:00) period were rejected. Moreover, the weak turbulent cases ($u_* < 0.05$) were excluded to maintain a high-quality LE estimation.

References

Agam, N., S. R. Evett, J. A. Tolk, W. P. Kustas, P. D. Colaizzi, J. G. Alfieri, L. G. Mckee, K. S. Copeland, T. A. Howell, and J. L. Chavez (2012), Evaporative loss from irrigated interrows in a highly advective semi-arid agricultural area, *Advance water Resource*, *50*, 20–30, doi:10.1016/j.advwatres.2012.07.010.

Al-Khafaf, S., P. Wierenga, and B. Williams (1978), Evaporative flux from irrigated cotton as related to leaf area index, soil water, and evaporative demand, *Agronomy Journal*, *70*(6), 912–917.

Allen, S. (1990), Measurement and estimation of evaporation from soil under sparse barley crops in northern syria, *Agricultural and forest meteorology*, *49*(4), 291–309.

Allen, S., and V. Grime (1995), Measurements of transpiration from savannah shrubs using sap flow gauges, *Agricultural and Forest Meteorology*, *75*(1), 23–41.

Angert, A., J.-E. Lee, and dan Yakir (2008), Seasonal variations in the isotopic composition of near-surface water vapour in the eastern Mediterranean, *Tellus B*, *60*(4), 674–684, doi:10.1111/j.1600-0889.2008.00357.x.

Ashktorab H., P. W., and K. Paw U (1994), Partitioning of Evapotranspiration Using Lysimeter and Micro-Bowen-Ratio System, *Journal of Irrigation and Drainage Engineering*, *120*(2), 450–464, doi:10.1061/(ASCE)0733-9437(1994)120:2(450).

Barbour, M. M., J. E. Hunt, A. S. Walcroft, G. N. D. Rogers, T. M. McSeveny, and D. Whitehead (2005), Components of ecosystem evaporation in a temperate coniferous

rainforest, with canopy transpiration scaled using sapwood density, *New Phytologist*, *165*(2), 549–558, doi:10.1111/j.1469-8137.2004.01257.x.

Bastrikov, V., H. C. Steen-Larsen, V. Masson-Delmotte, K. Gribanov, O. Cattani, J. Jouzel, and V. Zakharov (2014), Continuous measurements of atmospheric water vapour isotopes in western Siberia (Kourovka), *Atmospheric Measurement Techniques*, *7*(6), 1763–1776, doi:10.5194/amt-7-1763-2014.

Benetti, M., G. Reverdin, C. Pierre, L. Merlivat, C. Risi, H. C. Steen-Larsen, and F. Vimeux (2014), Deuterium excess in marine water vapor: Dependency on relative humidity and surface wind speed during evaporation, *Journal of Geophysical Research: Atmospheres*, *119*(2), 584–593, doi:10.1002/2013JD020535.

Benetti, M., G. Aloisi, G. Reverdin, C. Risi, and G. S\graveeze (2015), Importance of boundary layer mixing for the isotopic composition of surface vapor over the subtropical North Atlantic Ocean, *Journal of Geophysical Research: Atmospheres*, *120*(6), 2190–2209, doi:10.1002/2014JD021947.

Benyon, R. G., and T. M. Doody (2015), Comparison of interception, forest floor evaporation and transpiration in Pinus radiata and Eucalyptus globulus plantations, *Hydrological Processes*, *29*(6), 1173–1187, doi:10.1002/hyp.10237.

Berkelhammer, M., J. Hu, A. Bailey, D. C. Noone, C. J. Still, H. Barnard, D. Gochis, G. S. Hsiao, T. Rahn, and A. Turnipseed (2013), The nocturnal water cycle in an open-canopy forest, *Journal of Geophysical Research: Atmospheres*, *118*(17), 10,210–225,242, doi:10.1002/jgrd.50701.

Bonne, J.-L., V. Masson-Delmotte, O. Cattani, M. Delmotte, C. Risi, H. Sodemann, and H. C. Steen-Larsen (2014), The isotopic composition of water vapour and precipitation in Ivittuut, southern Greenland, *Atmospheric Chemistry and Physics*, *14*(9), 4419–4439, doi:10.5194/acpd-13-30521-2013.

Bonne, J.-L., H. C. Steen-Larsen, C. Risi, M. Werner, H. Sodemann, J.-L. Lacour, X. Fettweis, G. Cesana, M. Delmotte, O. Cattani, P. Vallelonga, H. A. Kjær, C. Clerbaux, Á. E. Sveinbjörnsdóttir, and V. Masson-Delmotte (2015), The summer 2012 greenland heat wave: In situ and remote sensing observations of water vapor isotopic composition during an atmospheric river event, *Journal of Geophysical Research: Atmospheres*, *120*(7), 2970–2989, doi:10.1002/2014JD022602.

Bony, S., C. Risi, and F. Vimeux (2008), Influence of convective processes on the isotopic composition (δ18O and δD) of precipitation and water vapor in the tropics: 1. Radiative-convective equilibrium and Tropical Ocean-Global Atmosphere-CCoupled Ocean-Atmosphere Response Experiment (TOGA-COARE) simulations, *Journal of Geophysical Research: Atmospheres*, *113*(D19), doi:10.1029/2008JD009942.

Braud, I., T. Bariac, J. P. Gaudet, and M. Vauclin (2005), SiSPAT-Isotope, a coupled heat, water and stable isotope (HDO and H218O) transport model for bare soil. Part I. Model description and first verifications, *Journal of Hydrology*, *309*(1?4), 277–300, doi:10.1016/j.jhydrol.2004.12.013.

Braud, I., P. Biron, T. Bariac, P. Richard, L. Canale, J. P. Gaudet, M. Vauclin, P. Biron, and M. Vauclin (2009a), Isotopic composition of bare soil evaporated water vapor. Part I: RUBIC IV experimental setup and results, *Journal of Hydrology*, *369*(1-2), 1–16, doi:10.1016/j.jhydrol.2009.01.034.

Braud, I., T. Bariac, P. Biron, and M. Vauclin (2009b), Isotopic composition of bare soil evaporated water vapor. Part ii: Modeling of RUBIC IV experimental results, *Journal of Hydrology*, *369*(1-2), 17–29, doi:10.1016/j.jhydrol.2009.01.038.

Brutsaert, W. (1982), *Evaporation into the Atmosphere: Theory, History and Applications*, Environmental Fluid Mechanics, Springer Netherlands.

Buenning, N. H., L. Stott, K. Yoshimura, and M. Berkelhammer (2012), The cause of the seasonal variation in the oxygen isotopic composition of precipitation along the

western U.S. coast, *Journal of Geophysical Research: Atmospheres*, *117*(D18), doi: 10.1029/2012JD018050.

Cappa, C. D., M. B. Hendricks, D. J. DePaolo, and R. C. Cohen (2003), Isotopic fractionation of water during evaporation, *Journal of Geophysical Research: Atmospheres.*, *108*(D16), doi:10.1029/2003jd003597.

Cavanaugh, M. L., S. A. Kurc, and R. L. Scott (2011), Evapotranspiration partitioning in semiarid shrubland ecosystems: a two-site evaluation of soil moisture control on transpiration, *Ecohydrology*, *4*(5), 671–681, doi:10.1002/eco.157.

Choi, H. I., and X.-Z. Liang (2010), Improved terrestrial hydrologic representation in mesoscale land surface models, *Journal of Hydrometeorology*, *11*(3), 797–809, doi:10. 1175/2010JHM1221.1.

Coenders-Gerrits, A. M. J., R. J. van der Ent, T. A. Bogaard, L. Wang-Erlandsson, M. Hrachowitz, and H. H. G. Savenije (2014), Uncertainties in transpiration estimates, *Nature*, *506*(7487), E1–E2, doi:10.1038/nature12925.

Cooper, P., J. Keatinge, and G. Hughes (1983), Crop evapotranspiration?a technique for calculation of its components by field measurements, *Field Crops Research*, *7*, 299–312.

Craig, H. (1961), Isotopic variations in Meteoric Waters, *Science*, *133*(3465), 1702–1703, doi:10.1126/science.133.3465.1702.

Craig, H., and L. I. Gordon (1965), *Deuterium and Oxygen 18 Variations in the Ocean and the Marine Atmosphere*, Consiglio nazionale delle richerche, Laboratorio de geologia nucleare.

Daikoku, K., S. Hattori, A. Deguchi, Y. Aoki, M. Miyashita, K. Matsumoto, J. Akiyama, S. Iida, T. Toba, Y. Fujita, and T. Ohta (2008), Influence of evaporation from the forest floor on evapotranspiration from the dry canopy, *Hydrological Processes*, *22*(20), 4083–4096, doi:10.1002/Hyp.7010.

Dansgaard, W. (1964), Stable isotopes in precipitation, *Tellus*, *16*(4), 436–468, doi:10.1111/j.2153-3490.1964.tb00181.x.

Diawara, A., D. Loustau, and P. Berbigier (1991), Comparison of two methods for estimating the evaporation of a Pinus pinaster (Ait.) stand: sap flow and energy balance with sensible heat flux measurements by an eddy covariance method, *Agricultural and Forest Meteorology*, *54*(1), 49–66, doi:http://dx.doi.org/10.1016/0168-1923(91)90040-W.

Ding, R., L. Tong, F. Li, Y. Zhang, X. Hao, and S. Kang (2015), Variations of crop coefficient and its influencing factors in an arid advective cropland of northwest china, *Hydrological Processes*, *29*(2), 239–249.

Dirmeyer, P. a., X. Gao, M. Zhao, Z. Guo, T. Oki, and N. Hanasaki (2006), GSWP-2: Multimodel analysis and implications for our perception of the land surface, *Bulletin of the American Meteorological Society*, *87*(10), 1381–1397, doi:10.1175/BAMS-87-10-1381.

Domec, J.-C., G. Sun, A. Noormets, M. J. Gavazzi, E. A. Treasure, E. Cohen, J. J. Swenson, S. G. McNulty, and J. S. King (2012), A comparison of three methods to estimate evapotranspiration in two contrasting loblolly pine plantations: age-related changes in water use and drought sensitivity of evapotranspiration components, *Forest Science*, *58*(5), 497–512.

Dongmann, G., H. W. Nurnberg, H. Forstel, and K. Wagener (1974), On the enrichment of H_2 ˆ18O in the leaves of transpiring plants, *Radiation and Environmental Biophysics*, *11*(1), 41–52, doi:10.1007/BF01323099.

Dubbert, M., M. Cuntz, A. Piayda, C. Maguas, and C. Werner (2013), Partitioning evapotranspiration - Testing the Craig and Gordon model with field measurements of oxygen isotope ratios of evaporative fluxes, *Journal of Hydrology*, *496*, 142–153, doi:10.1016/j.jhydrol.2013.05.033.

Dubbert, M., A. Piayda, M. Cuntz, A. C. Correia, F. e Silva, J. S. Pereira, and C. Werner (2014a), Stable oxygen isotope and flux partitioning demonstrates understory of an oak savanna contributes up to half of ecosystem carbon and water exchange, *Front. Plant Science*, *5*, 530, doi:10.3389/fpls.2014.00530.

Dubbert, M., M. Cuntz, A. Piayda, and C. Werner (2014b), Oxygen isotope signatures of transpired water vapor: the role of isotopic non-steady-state transpiration under natural conditions, *New Phytologist*, *203*(4), 1242–1252, doi:10.1111/nph.12878.

Dugas, W. A., R. A. Hicks, and R. P. Gibbens (1996), Structure and function of c 3 and c 4 chihuahuan desert plant communities. energy balance components, *Journal of Arid Environments*, *34*(1), 63–79.

Eastham, J., P. Gregory, D. Williamson, and G. Watson (1999), The influence of early sowing of wheat and lupin crops on evapotranspiration and evaporation from the soil surface in a mediterranean climate, *Agricultural Water Management*, *42*(2), 205–218.

Eberbach, P., and M. Pala (2005), Crop row spacing and its influence on the partitioning of evapotranspiration by winter-grown wheat in northern syria, *Plant and Soil*, *268*(1), 195–208.

Ek, M. B., K. E. Mitchell, Y. Lin, E. Rogers, P. Grunmann, V. Koren, G. Gayno, and J. D. Tarpley (2003), Implementation of Noah land surface model advances in the National Centers for Environmental Prediction operational mesoscale Eta model, *Journal of Geophysical Research: Atmospheres*, *108*(D22), doi:10.1029/2002JD003296.

Evaristo, J., S. Jasechko, and J. J. McDonnell (2015), Global separation of plant transpiration from groundwater and streamflow, *Nature*, *525*(7567), 91–94, doi:10.1038/nature1498310.1038/nature14983.

Farlin, J., C.-T. Lai, and K. Yoshimura (2013), Influence of synoptic weather events on the isotopic composition of atmospheric moisture in a coastal city of the western United States, *Water Resources Research*, *49*(6), 3685–3696, doi:10.1002/wrcr.20305.

Farquhar, G. D., and L. A. Cernusak (2005), On the isotopic composition of leaf water in the non-steady state, *Functional Plant Biology*, *32*(4), 293–303, doi:10.1071/Fp04232.

Fekete, B. M., C. J. Vorosmarty, and W. Grabs (2002), High-resolution fields of global runoff combining observed river discharge and simulated water balances, *Global Biogeochemical Cycles*, *16*(3), 15–1–15–10, doi:10.1029/1999GB001254.

Flanagan, L. B., J. P. Comstock, and J. R. Ehleringer (1991), Comparison of Modeled and Observed Environmental Influences on the Stable Oxygen and Hydrogen Isotope Composition of Leaf Water in Phaseolus vulgaris L, *Plant Physiology*, *96*(2), 588–596.

Frankenberg, C., K. Yoshimura, T. Warneke, I. Aben, A. Butz, N. Deutscher, D. Griffith, F. Hase, J. Notholt, M. Schneider, H. Schrijver, and T. R\ddotockmann (2009), Dynamic processes governing lower-tropospheric HDO/H2O ratios as observed from space and ground, *Science*, *325*(5946), 1374–1377, doi:10.1126/science.1173791.

Frankenberg, C., D. Wunch, G. Toon, C. Risi, R. Scheepmaker, J.-E. Lee, P. Wennberg, and J. Worden (2013), Water vapor isotopologue retrievals from high-resolution GOSAT shortwave infrared spectra, *Atmospheric Measurement Techniques*, *6*(2), 263–274, doi:10.5194/amt-6-263-2013.

Friedl, M., A. Strahler, and J. Hodges (2010), Islscp ii modis (collection 4) igbp land cover, 2000-2001, doi:10.3334/ORNLDAAC/968.

Galewsky, J., and K. Samuels-Crow (2014a), Summertime moisture transport to the southern south American Altiplano: Constraints from in situ measurements of water vapor isotopic composition, *Journal of Climate*, *28*(7), 2635–2649, doi:10.1175/JCLI-D-14-00511.1.

Galewsky, J., and K. Samuels-Crow (2014b), Water vapor isotopic composition of a stratospheric air intrusion: Measurements from the Chajnantor Plateau, Chile, *Journal of Geophysical Research: Atmospheres*, *119*(16), 9679–9691, doi:10.1002/2014JD022047.

Gat, J. R. (1996), Oxygen and hydrogen isotopes in the hydrologic cycle, *Annual Review of Earth and Planetary Sciences*, *24*(1), 225–262, doi:10.1146/annurev.earth.24.1.225.

Gibbens, R. P., R. A. Hicks, and W. A. Dugas (1996), Structure and function of c 3 and c 4 chihuahuan desert plant communities. standing crop and leaf area index, *Journal of Arid Environments*, *34*(1), 47–62.

Good, S. P., K. Soderberg, L. X. Wang, and K. K. Caylor (2012), Uncertainties in the assessment of the isotopic composition of surface fluxes: A direct comparison of techniques using laser-based water vapor isotope analyzers, *Journal of Geophysical Research: Atmospheres.*, *117*(D15), doi:10.1029/2011jd017168.

Good, S. P., K. Soderberg, K. Y. Guan, E. G. King, T. M. Scanlon, and K. K. Caylor (2014), δ2H isotopic flux partitioning of evapotranspiration over a grass field following a water pulse and subsequent dry down, *Water Resource Research*, *50*(2), 1410–1432, doi:10.1002/2013wr014333.

Good, S. P., D. Noone, N. Kurita, M. Benetti, and G. J. Bowen (2015a), D/H isotope ratios in the global hydrologic cycle, *Geophysical Research Letters*, *42*(12), 5042–5050, doi:10.1002/2015GL064117.

Good, S. P., D. Noone, and G. Bowen (2015b), Hydrologic connectivity constrains partitioning of global terrestrial water fluxes, *Science*, *349*(6244), 175–177, doi:10.1126/science.aaa5931.

Granier, A., P. Biron, and D. Lemoine (2000), Water balance, transpiration and canopy conductance in two beech stands, *Agricultural and Forest Meteorology*, *100*(4), 291 – 308, doi:10.1016/S0168-1923(99)00151-3.

Griffis, T. J., X. Lee, J. M. Baker, K. Billmark, N. Schultz, M. Erickson, X. Zhang, J. Fassbinder, W. Xiao, and N. Hu (2011), Oxygen isotope composition of evapotranspiration and its relation to C4 photosynthetic discrimination, *Journal of Geophysical Research*, *116*(G1), doi:10.1029/2010jg001514.

Gutiérrez, M. V., and F. C. Meinzer (1994), Energy balance and latent heat flux partitioning in coffee hedgerows at different stages of canopy development, *Agricultural and Forest Meteorology*, *68*(3-4), 173–186, doi:10.1016/0168-1923(94)90034-5.

Halder, J., S. Terzer, L. I. Wassenaar, L. J. Araguás-Araguás, and P. K. Aggarwal (2015), The Global Network of Isotopes in Rivers (GNIR): integration of water isotopes in watershed observation and riverine research, *Hydrology and Earth System Sciences*, *19*(8), 3419–3431, doi:10.5194/hess-19-3419-2015.

Hall, F. G., E. de Colstoun, G. J. Collatz, D. Landis, P. Dirmeyer, A. Betts, G. J. Huffman, L. Bounoua, and B. Meeson (2006), ISLSCP Initiative II global data sets: Surface boundary conditions and atmospheric forcings for land-atmosphere studies, *Journal of Geophysical Research: Atmospheres*, *111*(D22), n/a—-n/a, doi:10.1029/2006JD007366.

Ham, J. M., J. L. Heilman, and R. J. Lascano (1990), Determination of soil water evaporation and transpiration from energy balance and stem flow measurements, *Agricultural and Forest Meteorology*, *52*, 287–301, doi:10.1016/0168-1923(90)90087-M.

Harrold, L. L., D. B. Peters, F. R. Dreibelbis, and J. L. McGuinness (1959), Transpiration Evaluation of Corn Grown on a Plastic-Covered Lysimeter, *Soil Science Society of America Journal*, *23*, 174–178, doi:10.2136/sssaj1959.03615995002300020027x.

He, H., and R. B. Smith (1999), Stable isotope composition of water vapor in the atmospheric boundary layer above the forests of New England, *Journal of Geophysical Research: Atmospheres.*, *104*(D9), 11,657–11,673, doi:10.1029/1999jd900080.

He, X., H. Kim, P.-E. Kirstetter, K. Yoshimura, E.-C. Chang, C. R. Ferguson, J. M. Erlingis, Y. Hong, and T. Oki (2014), The Diurnal Cycle of Precipitation in Regional Spectral Model Simulations over West Africa: Sensitivities to Resolution and Cumulus Schemes, *Weather and Forecasting*, *30*(2), 424–445, doi:10.1175/WAF-D-14-00013.1.

Helliker, B. R., J. A. Berry, A. K. Betts, P. S. Bakwin, K. J. Davis, A. S. Denning, J. R. Ehleringer, J. B. Miller, M. P. Butler, and D. M. Ricciuto (2004), Estimates of

net CO2 flux by application of equilibrium boundary layer concepts to CO2 and water vapor measurements from a tall tower, *Journal of Geophysical Research: Atmospheres*, *109*(D20), doi:10.1029/2004JD004532.

Herbst, M., L. Kappen, F. Thamm, and R. Vanselow (1996), Simultaneous measurements of transpiration, soil evaporation and total evaporation in a maize field in northern Germany, *Journal of Experimental Botany*, *47*(305), 1957–1962.

Herbst, M., P. T. W. Rosier, D. D. McNeil, R. J. Harding, and D. J. Gowing (2008), Seasonal variability of interception evaporation from the canopy of a mixed deciduous forest, *Agricultural and Forest Meteorology*, *148*(11), 1655–1667, doi:10.1016/j.agrformet.2008.05.011.

Holdo, R. M., and J. B. Nippert (2015), Transpiration dynamics support resource partitioning in african savanna trees and grasses, *Ecology*, *96*(6), 1466–1472, doi:10.1890/14-1986.1.

Hu, Z. M., G. R. Yu, Y. L. Zhou, X. M. Sun, Y. N. Li, P. L. Shi, Y. F. Wang, X. Song, Z. M. Zheng, L. Zhang, and S. G. Li (2009), Partitioning of evapotranspiration and its controls in four grassland ecosystems: Application of a two-source model, *Agricultural and Forest Meteorology*, *149*(9), 1410–1420, doi:10.1016/j.agrformet.2009.03.014.

Hu, Z. M., X. F. Wen, X. M. Sun, L. H. Li, G. R. Yu, X. H. Lee, and S. G. Li (2014), Partitioning of evapotranspiration through oxygen isotopic measurements of water pools and fluxes in a temperate grassland, *Journal of Geophysical Research: Biogeosciences*, *119*(3), 358–371, doi:10.1002/2013jg002367.

Huang, L., and X. Wen (2014), Temporal variations of atmospheric water vapor δD and δ18O above an arid artificial oasis cropland in the Heihe River Basin, *Journal of Geophysical Research: Atmospheres*, *119*(19), 11,411–456,476, doi:10.1002/2014JD021891.

Jacob, H., and C. Sonntag (1991), An 8-year record of the seasonal variation of 2H and

18O in atmospheric water vapour and precipitation at Heidelberg, Germany, *Tellus B*, *43*(3).

Jansson, P.-E., E. Cienciala, A. Grelle, E. Kellner, A. Lindahl, and M. Lundblad (1999), Simulated evapotranspiration from the norunda forest stand during the growing season of a dry year, *Agricultural and forest meteorology*, *98*, 621–628.

Jara, J., C. O. Stockle, and J. Kjelgaard (1998), Measurement of evapotranspiration and its components in a corn (Zea Mays L.) field, *Agricultural and Forest Meteorology*, *92*(2), 131–145, doi:10.1016/S0168-1923(98)00083-5.

Jasechko, S., Z. D. Sharp, J. J. Gibson, S. J. Birks, Y. Yi, and P. J. Fawcett (2013), Terrestrial water fluxes dominated by transpiration, *Nature*, *496*(7445), 347–350, doi: 10.1038/nature11983.

Jian, S., C. Zhao, S. Fang, and K. Yu (2015), Effects of different vegetation restoration on soil water storage and water balance in the Chinese Loess Plateau, *Agricultural and Forest Meteorology*, *206*, 85–96, doi:http://dx.doi.org/10.1016/j.agrformet.2015.03.009.

Jouzel, J., and L. Merlivat (1984), Deuterium and oxygen 18 in precipitation: Modeling of the isotopic effects during snow formation, *Journal of Geophysical Research: Atmospheres*, *89*(D7), 11,749–11,757, doi:10.1029/JD089iD07p11749.

Keeling, C. D. (1958), The Concentration and Isotopic Abundances of Atmospheric Carbon Dioxide in Rural Areas, *Geochimica et Cosmochimica Acta*, *13*(4), 322–334, doi: 10.1016/0016-7037(58)90033-4.

Kelliher, F., B. Köstner, D. Hollinger, J. Byers, J. Hunt, T. McSeveny, R. Meserth, P. Weir, and E.-D. Schulze (1992), Evaporation, xylem sap flow, and tree transpiration in a new zealand broad-leaved forest, *Agricultural and Forest Meteorology*, *62*(1), 53 – 73, doi:10.1016/0168-1923(92)90005-O.

Kelliher, F., R. Leuning, and E. Schulze (1993), Evaporation and canopy characteristics of coniferous forests and grasslands, *Oecologia*, *95*(2), 153–163, doi:10.1007/BF00323485.

Kelliher, F., R. Leuning, M. Raupach, and E.-D. Schulze (1995), Maximum conductances for evaporation from global vegetation types, *Agricultural and Forest Meteorology*, *73*(1-2), 1–16, doi:10.1016/0168-1923(94)02178-M.

Kelliher, F., D. Hollinger, E.-D. Schulze, N. Vygodskaya, J. Byers, J. Hunt, T. McSeveny, I. Milukova, A. Sogatchev, A. Varlargin, W. Ziegler, A. Arneth, and G. Bauer (1997), Evaporation from an eastern siberian larch forest, *Agricultural and Forest Meteorology*, *85*(3-4), 135 – 147.

Kim, K., and X. Lee (2011), Isotopic enrichment of liquid water during evaporation from water surfaces, *Journal of Hydrology*, *399*(3-4), 364–375, doi:10.1016/j.jhydrol.2011.01.008.

Kondo, J., and T. Watanabe (1992), Studies on the Bulk Transfer Coefficients over a Vegetated Surface with a Multilayer Energy Budget Model, *Journal of the Atmospheric Sciences*, *49*(23), 2183–2199, doi:10.1175/1520-0469(1992)049<2183:SOTBTC>2.0.CO;2.

Kool, D., N. Agam, N. Lazarovitch, J. L. Heitman, T. J. Sauer, and A. Ben-Gal (2014), A review of approaches for evapotranspiration partitioning, *Agricultural and Forest Meteorology*, *184*, 56–70, doi:10.1016/j.agrformet.2013.09.003.

Kumagai, T., M. Tateishi, Y. Miyazawa, M. Kobayashi, N. Yoshifuji, H. Komatsu, and T. Shimizu (2014), Estimation of annual forest evapotranspiration from a coniferous plantation watershed in japan (1): Water use components in japanese cedar stands, *Journal of Hydrology*, *508*, 66–76, doi:10.1016/j.jhydrol.2013.10.047.

Lacour, J.-L., L. Clarisse, J. Worden, M. Schneider, S. Barthlott, F. Hase, C. Risi, C. Clerbaux, D. Hurtmans, and P.-F. Coheur (2015), Cross-validation of IASI/MetOp derived tropospheric δd with tes and ground-based FTIR observations, *Atmospheric Measurement Techniques*, *8*(3), 1447–1466, doi:10.5194/amt-8-1447-2015.

Lai, C.-T., and J. R. Ehleringer (2011), Deuterium excess reveals diurnal sources of water vapor in forest air, *Oecologia*, *165*(1), 213–223, doi:10.1007/s00442-010-1721-2.

Lai, C. T., J. R. Ehleringer, B. J. Bond, and K. T. P. U (2006), Contributions of evaporation, isotopic non-steady state transpiration and atmospheric mixing on the δˆ18O of water vapour in Pacific Northwest coniferous forests, *Plant Cell Environment*, *29*(1), 77–94, doi:10.1111/j.1365-3040.2005.01402.x.

Lai, C.-T. T., J. P. H. B. Ometto, J. A. Berry, L. A. Martinelli, T. F. Domingues, and J. R. Ehleringer (2008), Life form-specific variations in leaf water oxygen-18 enrichment in Amazonian vegetation, *Oecologia*, *157*(2), 197–210, doi:10.1007/s00442-008-1071-5.

Landerer, F. W., and S. C. Swenson (2012), Accuracy of scaled GRACE terrestrial water storage estimates, *Water Resources Research*, *48*(4), n/a—-n/a, doi:10.1029/2011WR011453.

Lascano, R. J., C. H. M. van Bavel, J. L. Hatfield, and D. R. Upchurch (1987), Energy and Water Balance of a Sparse Crop: Simulated and Measured Soil and Crop Evaporation, *Soil Science Society of America Journal*, *51*, 1113–1121, doi:10.2136/sssaj1987.03615995005100050004x.

Laskar, A. H., J.-C. Huang, S.-C. Hsu, S. K. Bhattacharya, C.-H. Wang, and M.-C. Liang (2014), Stable isotopic composition of near surface atmospheric water vapor and rain-vapor interaction in Taipei, Taiwan, *Journal of Hydrology*, *519*(0), 2091–2100, doi:10.1016/j.jhydrol.2014.10.017.

Lawrence, D. M., P. E. Thornton, K. W. Oleson, and G. B. Bonan (2007), The Partitioning of Evapotranspiration into Transpiration, Soil Evaporation, and Canopy Evaporation in a GCM: Impacts on Land–Atmosphere Interaction, *Journal of Hydrometeorology*, *8*(4), 862–880, doi:10.1175/JHM596.1.

Lawrence, D. M., K. W. Oleson, M. G. Flanner, P. E. Thornton, S. C. Swenson, P. J. Lawrence, X. Zeng, Z.-L. Yang, S. Levis, K. Sakaguchi, G. B. Bonan, and A. G. Slater

(2011), Parameterization improvements and functional and structural advances in Version 4 of the Community Land Model, *Journal of Advances in Modeling Earth Systems*, *3*(3), 1–27, doi:10.1029/2011MS000045.

Lawrence, J. R., S. D. Gedzelman, D. Dexheimer, H.-K. Cho, G. D. Carrie, R. Gasparini, C. R. Anderson, K. P. Bowman, and M. I. Biggerstaff (2004), Stable isotopic composition of water vapor in the tropics, *Journal of Geophysical Research: Atmospheres*, *109*(D6), doi:10.1029/2003JD004046.

Lee, D., J. Kim, K. Lee, and S. Kim (2010), Partitioning of catchment water budget and its implications for ecosystem carbon exchange, *Biogeosciences*, *7*, 1903–1914, doi:10.5194/bg-7-1903-2010.

Lee, J.-E., and I. Fung (2008), Amount effect of water isotopes and quantitative analysis of post-condensation processes, *Hydrological Processes*, *22*(1), 1–8, doi:10.1002/hyp.6637.

Lee, X., R. Smith, and J. WIlliams (2006), Water vapour 18O/16O isotope ratio in surface air in New England, USA, *Tellus B*, *58*(4), 293–304, doi:10.1111/j.1600-0889.2006.00191.x.

Lee, X. H., K. Kim, and R. Smith (2007), Temporal variations of the ˆ18O/ˆ16O signal of the whole-canopy transpiration in a temperate forest, *Global Biogeochemical Cycles*, *21*(3), doi:10.1029/2006gb002871.

Li, Y., J. Fan, Z. Hu, Q. Shao, L. Zhang, and H. Yu (2015), Influence of land use patterns on evapotranspiration and its components in a temperate grassland ecosystem, *Advances in Meteorology*.

Lin, Y., G. Wang, J. Guo, and X. Sun (2012), Quantifying evapotranspiration and its components in a coniferous subalpine forest in southwest china, *Hydrological Processes*, *26*(20), 3032–3040.

Liu, Y., and T. Yamanaka (2012), Tracing groundwater recharge sources in a mountain-plain transitional area using stable isotopes and hydrochemistry, *Journal of Hydrology*, *464- 465*, 116 – 126, doi:http://dx.doi.org/10.1016/j.jhydrol.2012.06.053.

Liu, Z., K. Yoshimura, G. J. Bowen, N. H. Buenning, C. Risi, J. M. Welker, and F. Yuan (2014), Paired oxygen isotope records reveal modern North American atmospheric dynamics during the Holocene., *Nature communications*, *5*, 3701, doi: 10.1038/ncomms4701.

Long, D., L. Longuevergne, and B. R. Scanlon (2014), Uncertainty in evapotranspiration from land surface modeling, remote sensing, and GRACE satellites, *Water Resources Research*, *50*(2), 1131–1151, doi:10.1002/2013WR014581.

Majoube, M. (1971), Fractionnement en oxygene-18 et en deuterium entre lfeau et sa vapeur, *Journal of Chemical Physics*, *68*(10), 1423–1436.

Maruyama, A., and T. Kuwagata (2008), Diurnal and seasonal variation in bulk stomatal conductance of the rice canopy and its dependence on developmental stage, *Agricultural and Forest Meteorology*, *148*(6-7), 1161–1173, doi:10.1016/j.agrformet.2008.03.001.

Maruyama, A., and T. Kuwagata (2010), Coupling land surface and crop growth models to estimate the effects of changes in the growing season on energy balance and water use of rice paddies, *Agricultural and Forest Meteorology*, *150*(7-8), 919–930, doi:10.1016/j.agrformet.2010.02.011.

Massman, W. J., and J. M. Ham (1994), An evaluation of a surface energy balance method for partitioning ET data into plant and soil components for a surface with partial canopy cover, *Agricultural and Forest Meteorology*, *67*(3-4), 253–267, doi:10.1016/0168-1923(94)90006-X.

Mathieu, R., and T. Bariac (1996), A numerical model for the simulation of stable isotope profiles in drying soils, *Journal of Geophysical Research: Atmospheres*, *101*(D7), 12,685–12,696, doi:10.1029/96JD00223.

Miralles, D. G., J. H. Gash, T. R. H. Holmes, R. A. M. de Jeu, and A. J. Dolman (2010), Global canopy interception from satellite observations, *Journal of Geophysical Research: Atmospheres*, *115*(D16), doi:10.1029/2009JD013530.

Miralles, D. G., T. R. H. Holmes, R. A. M. De Jeu, J. H. Gash, A. G. C. A. Meesters, and A. J. Dolman (2011a), Global land-surface evaporation estimated from satellite-based observations, *Hydrology and Earth System Sciences*, *15*(2), 453–469, doi:10.5194/hess-15-453-2011.

Miralles, D. G., R. A. M. De Jeu, J. H. Gash, T. R. H. Holmes, and A. J. Dolman (2011b), Magnitude and variability of land evaporation and its components at the global scale, *Hydrology and Earth System Sciences*, *15*(3), 967–981, doi:10.5194/hess-15-967-2011.

Mitchell, P. J., E. Veneklaas, H. Lambers, and S. S. O. Burgess (2009), Partitioning of evapotranspiration in a semi-arid eucalypt woodland in south-western Australia, *Agricultural and Forest Meteorology*, *149*(1), 25–37, doi:10.1016/j.agrformet.2008.07.008.

Mitchell, P. J., R. G. Benyon, and P. N. J. Lane (2012), Responses of evapotranspiration at different topographic positions and catchment water balance following a pronounced drought in a mixed species eucalypt forest, Australia, *Journal of Hydrology*, *440-441*, 62–74, doi:http://dx.doi.org/10.1016/j.jhydrol.2012.03.026.

Moreira, M. Z., L. D. L. Sternberg, L. A. Martinelli, R. L. Victoria, E. M. Barbosa, L. C. M. Bonates, and D. C. Nepstad (1997), Contribution of transpiration to forest ambient vapour based on isotopic measurements, *Global Change Biology*, *3*(5), doi:10.1046/j.1365-2486.1997.00082.x.

Mu, Q., M. Zhao, and S. W. Running (2011), Improvements to a {MODIS} global terrestrial evapotranspiration algorithm, *Remote Sensing of Environment*, *115*(8), 1781 – 1800, doi:http://dx.doi.org/10.1016/j.rse.2011.02.019.

Mueller, B., S. I. Seneviratne, C. Jimenez, T. Corti, M. Hirschi, G. Balsamo, P. Ciais, P. Dirmeyer, J. B. Fisher, Z. Guo, M. Jung, F. Maignan, M. F. McCabe, R. Re-

ichle, M. Reichstein, M. Rodell, J. Sheffield, A. J. Teuling, K. Wang, E. F. Wood, and Y. Zhang (2011), Evaluation of global observations-based evapotranspiration datasets and IPCC AR4 simulations, *Geophysical Research Letters*, *38*(6), 1–7, doi: 10.1029/2010GL046230.

Mueller, B., M. Hirschi, C. Jimenez, P. Ciais, P. a. Dirmeyer, a. J. Dolman, J. B. Fisher, M. Jung, F. Ludwig, F. Maignan, D. G. Miralles, M. F. McCabe, M. Reichstein, J. Sheffield, K. Wang, E. F. Wood, Y. Zhang, and S. I. Seneviratne (2013), Benchmark products for land evapotranspiration: Landflux-EVAL multi-data set synthesis, *Hydrology and Earth System Sciences*, *17*(10), 3707–3720, doi:10.5194/hess-17-3707-2013.

Nizinski, J. J., G. Galat, and A. Galat-Luong (2011), Water balance and sustainability of eucalyptus plantations in the Kouilou basin (Congo-Brazzaville), *Russian Journal of Ecology*, *42*(4), 305–314, doi:10.1134/S1067413611040126.

Noone, D. (2012), Pairing measurements of the water vapor isotope ratio with humidity to deduce atmospheric moistening and dehydration in the Tropical Midtroposphere, *Journal of Climate*, *25*(13), 4476–4494, doi:10.1175/JCLI-D-11-00582.1.

Noone, D., C. Risi, A. Bailey, M. Berkelhammer, D. P. Brown, N. Buenning, S. Gregory, J. Nusbaumer, D. Schneider, J. Sykes, B. Vanderwende, J. Wong, Y. Meillier, and D. Wolfe (2013), Determining water sources in the boundary layer from tall tower profiles of water vapor and surface water isotope ratios after a snowstorm in Colorado, *Atmospheric Chemistry and Physics*, *13*(3), 1607–1623, doi:10.5194/acp-13-1607-2013.

Oishi, A. C., R. Oren, and P. C. Stoy (2008), Estimating components of forest evapotranspiration: A footprint approach for scaling sap flux measurements, *Agricultural and Forest Meteorology*, *148*(11), 1719–1732, doi:http://dx.doi.org/10.1016/j.agrformet.2008.06.013.

Oki, T., and S. Kanae (2006), Global hydrological cycles and world water resources, *Science*, *313*(5790), 1068–1072, doi:10.1126/science.1128845.

Oleson, K., D. Lawrence, G. Bonan, B. Drewniak, M. Huang, C. Koven, S. Levis, F. Li, W. Riley, Z. Subin, et al. (2013), Technical description of version 4.5 of the community land model (clm). ncar tech, *Tech. rep.*, Note NCAR/TN-503+ STR. National Center for Atmospheric Research, Boulder, CO., doi:10.5065/D6RR1W7M.

Ono, K., A. Maruyama, T. Kuwagata, M. Mano, T. Takimoto, K. Hayashi, T. Hasegawa, and A. Miyata (2013), Canopy-scale relationships between stomatal conductance and photosynthesis in irrigated rice, *Global Change Biology*, *19*(7), 2209–2220, doi:10.1111/Gcb.12188.

Oren, R., N. Phillips, G. Katul, B. E. Ewers, and D. E. Pataki (1998), Scaling xylem sap flux and soil water balance and calculating variance: a method for partitioning water flux in forests, *Annals of Forest Science*, *55*(1-2), 191–216, doi:10.1051/forest:19980112.

Pangle, L. A., J. Klaus, E. S. F. Berman, M. Gupta, and J. J. McDonnell (2013), A new multisource and high-frequency approach to measuring δ^2H and δ^{18}O in hydrological field studies, *Water Resour. Res.*, *49*(11), 7797–7803, doi:10.1002/2013wr013743.

Penman, H. L. (1948), Natural Evaporation from Open Water, Bare Soil and Grass, *Proceedings of the Royal Society, Ser. A*, *193*(1032), 120–145, doi:10.1098/rspa.1948.0037.

Peters, L. I., and D. Yakir (2010), A rapid method for the sampling of atmospheric water vapour for isotopic analysis, *Rapid Communications in Mass Spectrometry*, *24*(1), 103–108, doi:10.1002/rcm.4359.

Phillips, D. L., and J. W. Gregg (2001), Uncertainty in source partitioning using stable isotopes, *Oecologia*, *127*(2), 171–179.

Priestley, C. H. B., and R. J. Taylor (1972), On the assessment of surface heat flux and evaporation using large-scale parameters, *Monthly Weather Review*, *100*(2), 81–92, doi:10.1175/1520-0493(1972)100<0081:OTAOSH>2.3.CO;2.

Ramillien, G., F. Frappart, A. G ntner, T. Ngo-Duc, A. Cazenave, and K. Laval (2006), Time variations of the regional evapotranspiration rate from gravity recovery and climate experiment (GRACE) satellite gravimetry, *Water Resources Research*, *42*(10), doi:10.1029/2005WR004331, w10403.

Raz-Yaseef, N., E. Rotenberg, and D. Yakir (2010), Effects of spatial variations in soil evaporation caused by tree shading on water flux partitioning in a semi-arid pine forest, *Agricultural and Forest Meteorology*, *150*(3), 454 – 462, doi:10.1016/j.agrformet.2010.01.010.

Raz-Yaseef, N., D. Yakir, G. Schiller, and S. Cohen (2012), Dynamics of evapotranspiration partitioning in a semi-arid forest as affected by temporal rainfall patterns, *Agricultural and Forest Meteorology*, *157*, 77–85, doi:10.1016/j.agrformet.2012.01.015.

Ringgaard, R., M. Herbst, and T. Friborg (2014), Partitioning forest evapotranspiration: interception evaporation and the impact of canopy structure , local and regional advection, *Journal of Hydrology*, *517*, 677–690, doi:10.1016/j.jhydrol.2014.06.007.

Risi, C., S. Bony, F. Vimeux, C. Frankenberg, D. Noone, and J. Worden (2010), Understanding the Sahelian water budget through the isotopic composition of water vapor and precipitation, *Journal of Geophysical Research: Atmospheres*, *115*(D24), doi:10.1029/2010JD014690.

Risi, C., D. Noone, C. Frankenberg, and J. Worden (2013), Role of continental recycling in intraseasonal variations of continental moisture as deduced from model simulations and water vapor isotopic measurements, *Water Resources Research*, *49*, doi:10.1002/wrcr.20312.

Rothfuss, Y., P. Biron, I. Braud, L. Canale, J.-L. Durand, J.-P. Gaudet, P. Richard, M. Vauclin, and T. Bariac (2010), Partitioning evapotranspiration fluxes into soil evaporation and plant transpiration using water stable isotopes under controlled conditions, *Hydrological Process*, *24*(22), 3177–3194, doi:10.1002/hyp.7743.

Rothfuss, Y., I. Braud, N. Le Moine, P. Biron, J.-L. Durand, M. Vauclin, and T. Bariac (2012), Factors controlling the isotopic partitioning between soil evaporation and plant transpiration: Assessment using a multi-objective calibration of SiSPAT-Isotope under controlled conditions, *Journal of Hydrology*, *442-443*, 75–88, doi:10.1016/j.jhydrol.2012.03.041.

Rothfuss, Y., H. Vereecken, and N. Brüggemann (2013), Monitoring water stable isotopic composition in soils using gas-permeable tubing and infrared laser absorption spectroscopy, *Water Resourcde Research*, *49*(6), 3747–3755, doi:10.1002/wrcr.20311.

Roupsard, O., J.-M. Bonnefond, M. Irvine, P. Berbigier, Y. Nouvellon, J. Dauzat, S. Taga, O. Hamel, C. Jourdan, L. Saint-Andr , I. Mialet-Serra, J.-P. Labouisse, D. Epron, R. Joffre, S. Braconnier, A. Rouzière, M. Navarro, and J.-P. Bouillet (2006), Partitioning energy and evapotranspiration above and below a tropical palm canopy, *Agricultural and Forest Meteorology*, *139*(3-4), 252–268, doi:10.1016/j.agrformet.2006.07.006.

Sadras, V., D. Whitfield, and D. Connor (1991), Regulation of evapotranspiration, and its partitioning between transpiration and soil evaporation by sunflower crops: a comparison between hybrids of different stature, *Field Crops Research*, *28*(1), 17–37.

Sahoo, A. K., M. Pan, T. J. Troy, R. K. Vinukollu, J. Sheffield, and E. F. Wood (2011), Reconciling the global terrestrial water budget using satellite remote sensing, *Remote Sensing of Environment*, *115*(8), 1850–1865, doi:10.1016/j.rse.2011.03.009.

Saito, M., A. Miyata, H. Nagai, and T. Yamada (2005), Seasonal variation of carbon dioxide exchange in rice paddy field in Japan, *Agricultural and Forest Meteorology*, *135*(1-4), 93–109, doi:10.1016/j.agrformet.2005.10.007.

Sakuratani, T. (1987), Studies of evaporation from crops. II. Separate estimation of transpiration and evaporation from a soybean field without water shortage., *Journal of Agricultural Meteorology*, *42*(4), 309–317.

Samuels-Crow, K. E., J. Galewsky, D. R. Hardy, Z. D. Sharp, J. Worden, and C. Braun (2014a), Upwind convective influences on the isotopic composition of atmospheric water vapor over the tropical Andes, *Journal of Geophysical Research: Atmospheres*, *119*(12), 7051–7063, doi:10.1002/2014JD021487.

Samuels-Crow, K. E., J. Galewsky, Z. D. Sharp, and K. J. Dennis (2014b), Deuterium excess in subtropical free troposphere water vapor: Continuous measurements from the Chajnantor plateau, northern Chile, *Geophysical Research Letters*, *41*(23), 8652–8659, doi:10.1002/2014GL062302.

Sauer, T. J., J. W. Singer, J. H. Prueger, T. M. DeSutter, and J. L. Hatfield (2007), Radiation balance and evaporation partitioning in a narrow-row soybean canopy, *Agricultural and Forest Meteorology*, *145*, 206–214, doi:10.1016/j.agrformet.2007.04.015.

Scanlon, T. M., and W. P. Kustas (2012), Partitioning Evapotranspiration Using an Eddy Covariance-Based Technique: Improved Assessment of Soil Moisture and Land-Atmosphere Exchange Dynamics, *Vadose Zone Journal*, *11*(3), doi:10.2136/Vzj2012.0025.

Schlaepfer, D. R., B. E. Ewers, B. N. Shuman, D. G. Williams, J. M. Frank, W. J. Massman, and W. K. Lauenroth (2014), Terrestrial water fluxes dominated by transpiration: Comment, *Ecosphere*, *5*(5), art61, doi:10.1890/ES13-00391.1.

Schlesinger, W. H., and S. Jasechko (2014), Transpiration in the global water cycle, *Agricultural and Forest Meteorology*, *189-190*(0), 115–117, doi:10.1016/j.agrformet.2014.01.011.

Schlesinger, W. H., P. J. Fonteyn, and G. M. Marion (1987), Soil moisture content and plant transpiration in the chihuahuan desert of new mexico, *Journal of Arid Environments*, *12*(2), 119–126.

Schneider, U., A. Becker, P. Finger, A. Meyer-Christoffer, M. Ziese, and B. Rudolf (2014), Gpcc's new land surface precipitation climatology based on quality-controlled in situ

data and its role in quantifying the global water cycle, *Theoretical and Applied Climatology*, *115*(1-2), 15–40, doi:10.1007/s00704-013-0860-x.

Sepaskhah, A. R., and S. Ilampour (1995), Effects of soil moisture stress on evapotranspiration partitioning, *Agricultural Water Management*, *28*(4), 311–323, doi:10.1016/0378-3774(95)01176-5.

Sheffield, J., C. R. Ferguson, T. J. Troy, E. F. Wood, and M. F. McCabe (2009), Closing the terrestrial water budget from satellite remote sensing, *Geophysical Research Letters*, *36*(7), doi:10.1029/2009GL037338.

Simonin, K., T. Kolb, M. Montes-Helu, and G. Koch (2007), The influence of thinning on components of stand water balance in a ponderosa pine forest stand during and after extreme drought, *Agricultural and Forest Meteorology*, *143*(3- 4), 266 – 276, doi:10.1016/j.agrformet.2007.01.003.

Simpson, H. J., A. L. Herczeg, and W. S. Meyer (1992), Stable Isotope Ratios in Irrigation Water Can Estimate Rice Crop Evaporation, *Geophysical Research Letters*, *19*(4), 377–380, doi:10.1029/91gl02952.

Soegaard, H., and E. Boegh (1995), Estimation of evapotranspiration from a millet crop in the Sahel combining sap flow, leaf area index and eddy correlation technique, *Journal of Hydrology*, *166*, 265–282.

Stannard, D. I., and M. A. Weltz (2006), Partitioning evapotranspiration in sparsely vegetated rangeland using a portable chamber, *Water resources research*, *42*(2).

Steen-Larsen, H. C., S. J. Johnsen, V. Masson-Delmotte, B. Stenni, C. Risi, H. Sodemann, D. Balslev-Clausen, T. Blunier, D. Dahl-Jensen, M. D. Ellehøj, S. Falourd, A. Grindsted, V. Gkinis, J. Jouzel, T. Popp, S. Sheldon, S. B. Simonsen, J. Sjolte, J. P. Steffensen, P. Sperlich, A. E. Sveinbj\ddotornsdóttir, B. M. Vinther, and J. W. C. White (2013), Continuous monitoring of summer surface water vapor isotopic composition above the

Greenland ice sheet, *Atmospheric Chemistry and Physics*, *13*(9), 4815–4828, doi:10.5194/acp-13-4815-2013.

Steen-Larsen, H. C., A. E. Sveinbj\ddotornsdottir, A. J. Peters, V. Masson-Delmotte, M. P. Guishard, G. Hsiao, J. Jouzel, D. Noone, J. K. Warren, and J. W. C. White (2014a), Climatic controls on water vapor deuterium excess in the marine boundary layer of the North Atlantic based on 500 days of in situ, continuous measurements, *Atmospheric Chemistry and Physics*, *14*(15), 7741–7756, doi:10.5194/acp-14-7741-2014.

Steen-Larsen, H. C., V. Masson-Delmotte, M. Hirabayashi, R. Winkler, K. Satow, F. Prié, N. Bayou, E. Brun, K. M. Cuffey, D. Dahl-Jensen, M. Dumont, M. Guillevic, S. Kipfstuhl, A. Landais, T. Popp, C. Risi, K. Steffen, B. Stenni, and A. E. Sveinbjörnsdott\'ir (2014b), What controls the isotopic composition of Greenland surface snow?, *Climate of the Past*, *10*(1), 377–392, doi:10.5194/cp-10-377-2014.

Steen-Larsen, H. C., A. E. Sveinbj\ddotornsdottir, T. Jonsson, F. Ritter, J.-L. Bonne, V. Masson-Delmotte, H. Sodemann, T. Blunier, D. Dahl-Jensen, and B. M. Vinther (2015), Moisture sources and synoptic to seasonal variability of North Atlantic water vapor isotopic composition, *Journal of Geophysical Research: Atmospheres*, *120*(12), 5757–5774, doi:10.1002/2015JD023234.

Strong, M., Z. D. Sharp, and D. S. Gutzler (2007), Diagnosing moisture transport using D/H ratios of water vapor, *Geophysical Research Letters*, *34*(3), doi:10.1029/2006GL028307.

Sun, X., Y. Onda, H. Kato, K. Otsuki, and T. Gomi (2013), Partitioning of the total evapotranspiration in a Japanese cypress plantation during the growing season, *Ecohydrology*, doi:10.1002/eco.1428.

Sutanto, S. J., J. Wenninger, A. M. J. Coenders-Gerrits, and S. Uhlenbrook (2012), Partitioning of evaporation into transpiration, soil evaporation and interception: a com-

parison between isotope measurements and a hydrus-1d model, *Hydrology and Earth System Sciences*, *16*(8), 2605–2616, doi:10.5194/hess-16-2605-2012.

Sutanto, S. J., B. van den Hurk, P. A. Dirmeyer, S. I. Seneviratne, T. R ckmann, K. E. Trenberth, E. M. Blyth, J. Wenninger, and G. Hoffmann (2014), HESS opinions "a perspective on isotope versus non-isotope approaches to determine the contribution of transpiration to total evaporation", *Hydrology and Earth System Sciences*, *18*(8), 2815–2827, doi:10.5194/hess-18-2815-2014.

Tang, J., P. V. Bolstad, B. E. Ewers, A. R. Desai, K. J. Davis, and E. V. Carey (2006), Sap flux upscaled canopy transpiration, stomatal conductance, and water use efficiency in an old growth forest in the Great Lakes region of the United States, *Journal of Geophysical Research: Biogeosciences*, *111*(G2), n/a—-n/a, doi:10.1029/2005JG000083.

Tremoy, G., F. Vimeux, S. Mayaki, I. Souley, O. Cattani, C. Risi, G. Favreau, and M. O\ddotI (2012), A 1-year long δ18O record of water vapor in Niamey (Niger) reveals insightful atmospheric processes at different timescales, *Geophysical Research Letters*, *39*(8), doi:10.1029/2012GL051298.

Tremoy, G., F. Vimeux, S. Soumana, I. Souley, C. Risi, G. Favreau, and O. Monique (2014), Clustering mesoscale convective systems with laser-based water vapor δ18O monitoring in Niamey (Niger), *Journal of Geophysical Research: Atmospheres*, *119*(9), 5079–5103, doi:10.1002/2013JD020968.

Tsujimura, M., L. Sasaki, T. Yamanaka, A. Sugimoto, S.-G. Li, D. Matsushima, A. Kotani, and M. Saandar (2007), Vertical distribution of stable isotopic composition in atmospheric water vapor and subsurface water in grassland and forest sites, eastern Mongolia, *Journal of Hydrology*, *333*(1), 35–46, doi:10.1016/j.jhydrol.2006.07.025.

Uemura, R., Y. Matsui, K. Yoshimura, H. Motoyama, and N. Yoshida (2008), Evidence of deuterium excess in water vapor as an indicator of ocean surface conditions, *Journal of Geophysical Research: Atmospheres*, *113*(D19), doi:10.1029/2008JD010209.

Uemura, R., N. Yonezawa, K. Yoshimura, R. Asami, H. Kadena, K. Yamada, and N. Yoshida (2012), Factors controlling isotopic composition of precipitation on Okinawa Island, Japan: Implications for paleoclimate reconstruction in the East Asian Monsoon region, *Journal of Hydrology*, *475*(0), 314–322, doi:10.1016/j.jhydrol.2012.10.014.

Unsworth, M., N. Phillips, T. Link, B. Bond, M. Falk, M. Harmon, T. Hinckley, D. Marks, and K. Paw U (2004), Components and Controls of Water Flux in an Old-growth Douglas-fir-Western Hemlock Ecosystem, *Ecosystems*, *7*(5), 468–481, doi: 10.1007/s10021-004-0138-3.

van Geldern, R., and J. A. C. Barth (2012), Optimization of instrument setup and post-run corrections for oxygen and hydrogen stable isotope measurements of water by isotope ratio infrared spectroscopy (IRIS), *Limnology and Oceanography: Methods*, *10*(12), 1024–1036, doi:10.4319/lom.2012.10.1024.

Verstraeten, W., B. Muys, J. Feyen, F. Veroustraete, M. Minnaert, and A. De Schrijver (2005), Comparative analysis of the actual evapotranspiration of Flemish forest and cropland , using the soil water balance model WAVE, *Hydrology and Earth System Sciences*, *9*, 225–241.

Villegas, J. C., F. Dominguez, G. A. Barron-Gafford, H. D. Adams, M. Guardiola-Claramonte, E. D. Sommer, A. W. Selvey, J. F. Espeleta, C. B. Zou, D. D. Breshears, et al. (2015), Sensitivity of regional evapotranspiration partitioning to variation in woody plant cover: insights from experimental dryland tree mosaics, *Global Ecology and Biogeography*, *24*(9), 1040–1048.

Wallace, J., C. Lloyd, and M. Sivakumar (1993), Measurements of soil, plant and total evaporation from millet in niger, *Agricultural and Forest Meteorology*, *63*(3), 149–169.

Wang, L., K. K. Caylor, J. C. Villegas, G. A. Barron-Gafford, D. D. Breshears, and T. E. Huxman (2010), Partitioning evapotranspiration across gradients of woody plant

cover: Assessment of a stable isotope technique, *Geophy. Res. Let.*, *37*(9), doi:10.1029/2010GL043228.

Wang, L., S. P. Good, K. K. Caylor, and L. A. Cernusak (2012), Direct quantification of leaf transpiration isotopic composition, *Agricultural and Forest Meteorology*, *154-155*, 127–135, doi:10.1016/j.agrformet.2011.10.018.

Wang, L., S. Niu, S. P. Good, K. Soderberg, M. F. McCabe, R. A. Sherry, Y. Luo, X. Zhou, J. Xia, and K. K. Caylor (2013), The effect of warming on grassland evapotranspiration partitioning using laser-based isotope monitoring techniques, *Geochimica et Cosmochimica Acta*, *111*, 28–38, doi:10.1016/j.gca.2012.12.047.

Wang, L., S. P. Good, and K. K. Caylor (2014), Global synthesis of vegetation control on evapotranspiration partitioning, *Geophy. Res. Let.*, doi:10.1002/2014GL061439.

Wang, P., and T. Yamanaka (2014), Application of a two-source model for partitioning evapotranspiration and assessing its controls in temperate grasslands in central Japan, *Ecohydrology*, *7*(2), 345–353, doi:10.1002/eco.1352.

Wang, P., T. Yamanaka, X.-Y. Li, and Z. Wei (2015), Partitioning evapotranspiration in a temperate grassland ecosystem: Numerical modeling with isotopic tracers, *Agricultural and Forest Meteorology*, *208*, 16–31, doi:10.1016/j.agrformet.2015.04.006.

Wang, X. F., and D. Yakir (2000), Using stable isotopes of water in evapotranspiration studies, *Hydrol. Process*, *14*(8), 1407–1421, doi:10.1002/1099-1085(20000615)14:8--<1407::Aid-Hyp992-->textgreater3.0.Co;2-K.

Wang-Erlandsson, L., R. J. van der Ent, L. J. Gordon, and H. H. G. Savenije (2014), Contrasting roles of interception and transpiration in the hydrological cycle Part 1: Simple Terrestrial Evaporation to Atmosphere Model, *Earth System Dynamics Discussions*, *5*(1), 203–279, doi:10.5194/esdd-5-203-2014.

Watkins, M. M., D. N. Wiese, D.-N. Yuan, C. Boening, and F. W. Landerer (2015), Improved methods for observing Earth's time variable mass distribution with GRACE using spherical cap mascons, *Journal of Geophysical Research: Solid Earth*, *120*(4), 2648–2671, doi:10.1002/2014JB011547.

Wei, Z., and K. Yoshimura (2016), Is terrestrial evaporation flux dominated by transpiration ?, *In preparation*.

Wei, Z., A. OKAZAKI, H. MAEDA, Y. SATOH, M. KIGUCHI, K. NODA, M. KOIKE, W. KIM, Z. LIU, and K. YOSHIMURA (2014), Investigating vegetation-atmosphere water exchange by using high frequency spectroscopy vapor isotope observations, *Journal of Japan Society of Civil Engineers, Ser. B1 (Hydraulic Engineering)*, *70*(4), 181–186, doi:10.2208/jscejhe.70.I_181.

Wei, Z., K. Yoshimura, A. Okazaki, W. Kim, Z. Liu, and M. Yokoi (2015), Partitioning of evapotranspiration using high-frequency water vapor isotopic measurement over a rice paddy field, *Water Resources Research*, doi:10.1002/2014WR016737.

Wei, Z., K. Yoshimura, A. Okazaki, K. Ono, W. Kim, M. Yokoi, and C.-T. Lai (2016), Understanding the variability of water isotopologues in near-surface atmospheric moisture over a humid subtropical rice paddy in tsukuba, japan, *Journal of Hydrology*, *533* , 91–102, doi:10.1016/j.jhydrol.2015.11.044.

Welp, L. R., X. Lee, K. Kim, T. J. Griffis, K. A. Billmark, and J. M. Baker (2008), δ^{18}O of water vapour, evapotranspiration and the sites of leaf water evaporation in a soybean canopy, *Plant, Cell and Environment*, *31*(9), 1214–1228, doi:10.1111/j.1365-3040.2008.01826.x.

Welp, L. R., X. Lee, T. J. Griffis, X.-F. Wen, W. Xiao, S. Li, X. Sun, Z. Hu, M. Val Martin, and J. Huang (2012), A meta-analysis of water vapor deuterium-excess in the midlatitude atmospheric surface layer, *Global Biogeochemical Cycles*, *26*(3), doi:10.1029/2011GB004246.

Wen, X., B. Yang, X. Sun, and X. Lee (2016), Evapotranspiration partitioning through in-situ oxygen isotope measurements in an oasis cropland, *Agricultural and Forest Meteorology, in press*(-), –, doi:-.

Wen, X.-F., S.-C. Zhang, X.-M. Sun, G.-R. Yu, and X. Lee (2010), Water vapor and precipitation isotope ratios in Beijing, China, *Journal of Geophysical Research: Atmospheres*, *115*(D1), doi:10.1029/2009JD012408.

Wiese, D. N. (2015), Grace monthly global water mass grids netcdf release 5.0. ver. 5.0., pp. n/a—-n/a, doi:10.5067/TEMSC-OCL05.

Williams, D. G., W. Cable, K. Hultine, J. C. B. Hoedjes, E. A. Yepez, V. Simonneaux, S. Er-Raki, G. Boulet, H. A. R. de Bruin, A. Chehbouni, O. K. Hartogensis, and F. Timouk (2004), Evapotranspiration components determined by stable isotope, sap flow and eddy covariance techniques, *Agricultural and Forest Meteorology*, *125*(3-4), 241–258, doi:10.1016/j.agrformet.2004.04.008.

Wilson, K. B., P. J. Hanson, and D. D. Baldocchi (2000), Factors controlling evaporation and energy partitioning beneath a deciduous forest over an annual cycle, *Agricultural and Forest Meteorology*, *102*(2-3), 83–103, doi:10.1016/S0168-1923(00)00124-6.

Wilson, K. B., P. J. Hanson, P. J. Mulholland, D. D. Baldocchi, and S. D. Wullschleger (2001), A comparison of methods for determining forest evapotranspiration and its components: sap-flow, soil water budget, eddy covariance and catchment water balance, *Agricultural and forest Meteorology*, *106*(2), 153–168.

Worden, H. M., J. A. Logan, J. R. Worden, R. Beer, K. Bowman, S. A. Clough, A. Eldering, B. M. Fisher, M. R. Gunson, R. L. Herman, S. S. Kulawik, M. C. Lampel, M. Luo, I. A. Megretskaia, G. B. Osterman, and M. W. Shephard (2007), Comparisons of Tropospheric Emission Spectrometer (TES) ozone profiles to ozonesondes: Methods and initial results, *Journal of Geophysical Research: Atmospheres*, *112*(D3), doi:10.1029/2006JD007258.

Xu, Z., H.-B. Yang, F.-D. Liu, S.-Q. An, J. Cui, Z.-S. Wang, and S.-R. Liu (2008), Partitioning evapotranspiration flux components in a subalpine shrubland based on stable isotopic measurements, *Botanical Studies*, *49*(4), 351–361.

Yakir, D., and L. D. L. Sternberg (2000), The use of stable isotopes to study ecosystem gas exchange, *Oecologia*, *123*(3), 297–311, doi:10.1007/s004420051016.

Yakir, D., and X. F. Wang (1996), Fluxes of CO2 and water between terrestrial vegetation and the atmosphere estimated from isotope measurements, *Nature*, *380*(6574), 515–517, doi:10.1038/380515a0.

Yang, Y., D. Long, H. Guan, W. Liang, C. Simmons, and O. Batelaan (2015), Comparison of three dual-source remote sensing evapotranspiration models during the musoexe-12 campaign: Revisit of model physics, *Water Resources Research*, *51*(5), 3145–3165, doi: 10.1002/2014WR015619.

Yepez, E. A., D. G. Williams, R. L. Scott, and G. H. Lin (2003), Partitioning overstory and understory evapotranspiration in a semiarid savanna woodland from the isotopic composition of water vapor, *Agricultural and Forest Meteorology*, *119*(1-2), 53–68, doi: 10.1016/S0168-1923(03)00116-3.

Yepez, E. A., T. E. Huxman, D. D. Ignace, N. B. English, J. F. Weltzin, A. E. Castellanos, and D. G. Williams (2005), Dynamics of transpiration and evaporation following a moisture pulse in semiarid grassland: A chamber-based isotope method for partitioning flux components, *Agricultural and Forest Meteorology*, *132*(3-4), 359–376, doi:10.1016/j.agrformet.2005.09.006.

Yimam, Y. T., T. E. Ochsner, and V. G. Kakani (2015), Evapotranspiration partitioning and water use efficiency of switchgrass and biomass sorghum managed for biofuel, *Agricultural Water Management*, *155*, 40–47, doi:10.1016/j.agwat.2015.03.018.

Yoshimura, K. (2015), Stable water isotopes in climatology, meteorology, and hydrology:

A review, *Journal of the Meteorological Society of Japan*, *333*(1), 35–46, doi:10.2151/jmsj.2015-036.

Yoshimura, K., and M. Kanamitsu (2009), Specification of External Forcing for Regional Model Integrations, *Monthly Weather Review*, *137*(4), 1409–1421, doi:10.1175/2008MWR2654.1.

Yoshimura, K., T. Oki, N. Ohte, and S. Kanae (2004), Colored Moisture analysis estimates of variations in 1998 Asian monsoon water sources, *Journal of the Meteorological Society of Japan. Ser. II*, *82*(5), 1315–1329, doi:10.2151/jmsj.2004.1315.

Yoshimura, K., M. Shin, K. Shinjiro, and O. Taikan (2006), Iso-matsiro, a land surface model that incorporates stable water isotopes, *Global and Planetary Change*, *51*(1- 2), 90 – 107, doi:10.1016/j.gloplacha.2005.12.007.

Yoshimura, K., M. Kanamitsu, D. Noone, and T. Oki (2008), Historical isotope simulation using Reanalysis atmospheric data, *Journal of Geophysical Research: Atmospheres*, *113*(D19), doi:10.1029/2008JD010074.

Yoshimura, K., T. Miyoshi, and M. Kanamitsu (2014), Observation system simulation experiments using water vapor isotope information, *Journal of Geophysical Research: Atmospheres*, *119*(13), 7842–7862, doi:10.1002/2014JD021662.

Yuan, H., Y. Dai, Z. Xiao, D. Ji, and W. Shangguan (2011), Reprocessing the MODIS Leaf Area Index products for land surface and climate modelling, *Remote Sensing of Environment*, *115*(5), 1171–1187, doi:http://dx.doi.org/10.1016/j.rse.2011.01.001.

Yunusa, I., R. Walker, and D. Blackmore (1997), Characterisation of water use by sultana grapevines (vitis vinifera l.) on their own roots or on ramsey rootstock drip-irrigated with water of different salinities, *Irrigation Science*, *17*(2), 77–86.

Yunusa, I. a. M., R. R. Walker, and P. Lu (2004), Evapotranspiration components from energy balance, sapflow and microlysimetry techniques for an irrigated vineyard in

inland Australia, *Agricultural and Forest Meteorology*, *127*(1-2), 93–107, doi:10.1016/j.agrformet.2004.07.001.

Zhang, L., W. R. Dawes, and G. R. Walker (2001), Response of mean annual evapotranspiration to vegetation changes at catchment scale, *Water Resources Research*, *37*(3), 701–708, doi:10.1029/2000WR900325.

Zhang, Y., C. Liu, Y. Shen, A. Kondoh, C. Tang, T. Tanaka, and J. Shimada (2002), Measurement of evapotranspiration in a winter wheat field, *Hydrological Processes*, *16*(14), 2805–2817, doi:10.1002/hyp.1072.